UNIVERSITAT POLITÈCNICA DE CATALUNYA

DOCTORAL THESIS

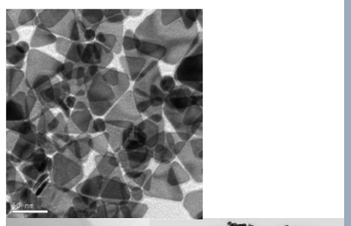

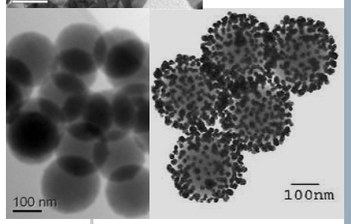

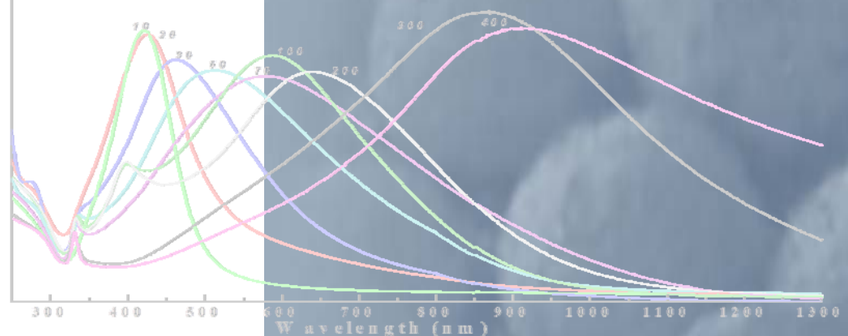

Silver Nanostructures: Chemical Synthesis of colloids and composites nanoparticles, plasmon resonance properties and silver nanoparticles monolayer films prepared by spin-coating.

Victor Elias Torres Heredia
Universidad Politécnica de Catalunya

November 2011

Table of Contents

RESUMEN 1

ABSTRACT 2

LITERATURE REVIEW 3

***Chapter 1** : Silver Nanoparticles Synthesis*

1. Overview 8
1.1. Metallic nanostructures 8
1.2. Stabilization of Colloidal Metal Particles in Liquids 9
1.3. Synthesis chemical methods for the preparation of colloidal metal nanoparticle 11
1.4. Characterization and Properties of Metal nanoparticles 13
1.5. Plasmon Optical properties 19
1.5.1. Surface plasmon resonance (SPR) 19
1.6. Metal nanoparticles applications 20
1.7. Experimental description 21
1.7.1. Synthesis of Silver nanoparticles in different systems 21
1.7.2. Optical absorption and Morphological studies 22
1.8. Result and Discussion 23
1.8.1. Formation of spherical colloid in different solvent 23
1.8.2. Study of silver nanoparticles stability in different aqueous medium 26
1.8.3. Silver nanoparticles homogenize in H_2O using SC-$NaBH_4$ 27
1.9. Summary 30

***Chapter 2** Silver Nanoprisms Synthesis*

2. Overview 32
2.1. Silver nanoprisms 32
2.2. Experimental Description 33
2.2.1. Silver nanoprisms colloid preparation 33
2.3. Results and discussion 34
2.3.1. Formation of triangular silver nanoprisms 34
2.3.2. Influence of different parameters of the solution on silver nanoprisms growth 34
2.4. Effect oxidizing of H_2O_2 (oxidizing H_2O_2 - reducing PVP effect) 41
2.5. Colloidal solutions stable with time 44
2.6. Dynamic Light Scattering Analysis (Photon correlation spectroscopy) 46
2.7. Summary 48

Chapter 3 *: Films*

3. Overview 51
3.1. Spin Coating 51
3.2. Coatings preparations 52
3.3. Results and discussion 53
3.4. Summary 55

Chapter 4 *: Composites materials synthesis*

4. Overview 57
4.1. Core-shell nanoparticles 57
4.2. Composites materials 57
4.3. Experimental Section 59
4.3.1. Synthesis of bare SiO_2 particle 59
4.3.2. Synthesis of SiO_2@Ag core–shells particles 59
4.3.3. Synthesis of TiO_2 and TiO_2-Ag composites in solution 60
4.3.4. Synthesis of SiO_2-TiO_2-Ag nanocomposites 61
4.4. Result and Discussion 61
4.4.1. SiO_2@Ag core–shells particles 61
4.4.2. TiO_2 composites 64
4.5. Summary 70

Chapter 5 *: General Conclusion-Highlight*

General Conclusion 71

Bibliography 75

Annex A. Electron diffraction pattern (ED) of Silver nanoparticles 86
Annex B. Analysis of PVP effect in the silver nanoparticles formation 87
Annex C. Reaction mechanism of PVP-Ag 88
Annex D. Oxidative effect of the hydrogen peroxide (H_2O_2) 89
Annex E. Precursors, reducing agents and polymeric stabilizers used in the metal nanoparticles synthesis 90

Publications 91

LITERATURE REVIEW

Background

Synthesis and processing of nanomaterials and nanostructures are the essential aspects of nanotechnology. Studies on new physical properties and applications of nanomaterials and nanostructures are possible only when nanostructured materials are made available with desired size, morphology, crystal and microstructure and chemical composition. However, nanoparticles of noble metals have an especially long tradition, and fundamental synthetic strategies have therefore been known for some decades. A huge number of synthetic pathways to metal nanoparticles have been developed. The advancement of the understanding of small-particle science and the potential for new materials science based on the chemistry and physics of nanoscale metal clusters rests on the measurement and application of useful size-dependent properties of small metal nanoparticles. Ideally this requires the preparation and isolation of monodisperse metal particles with a great degree of control over size, structure and composition. Metals in varying levels of dispersion have a long history in many technological applications, but the methods of preparation used are usually determined by the intended use for the metal and are not necessarily developed with the aim of preparing well-defined metal particles.

With these considerations in mind, the researchers have begun to address the needs of metal particle research by developing the synthetic chemistry of colloidal metals. Nanoparticles with diameters ranging from 1 to 10 nm with consistent crystal structure, surface area, and a high degree of monodispersity have been processed by various techniques. One of the most challenging problems in synthesis is the controlled generation of monodispersed nanoparticles with size variance so small that size selection by centrifugal precipitation or mobility classification is not necessary. Among all the synthesis techniques, gas-phase synthesis is one of the best techniques with respect to size monodispersity by using a combination of rigorous control of nucleation-condensation and growth, as well as by the effective collection of nanoparticles and their handling afterwards. The stability of the collected nanoparticles against agglomeration, sintering, and compositional changes can be ensured by redispersion the nanoparticles in liquid suspension. For semiconducting particles, stabilization of the liquid suspension has been demonstrated by the addition of polar solvent [1]; surfactant molecules have been used to stabilize the liquid suspension of metallic nanoparticles. In the synthesis and processing of nanomaterials, organic materials often play an indispensable role, such as surfactants in the synthesis of ordered mesoporous materials, and polymers in the synthesis of monodispersed nanoparticles.

New approaches need to be developed for the generation of monodisperse nanoparticles that do not require the use of a size classification procedure. An example of this is a process developed in Japan where well monodispersed gold colloidal nanoparticles with diameters of about 1 nm have been prepared by reduction of metallic salts with UV irradiation in the presence of dendrimers[2]. Poly (amidoamine) dendrimers with surface amino groups of higher generations have spherical 3-D structures, which may have an effective protective action for the formation of gold nanoparticles.

Although the specific role of dendrimers for the formation of monodispersed nanoparticles has yet to be defined, good monodispersity is thought to come from the complex reaction accompanying the decomposition of dendrimers, which eventually leads to the conversion of solution ions to gold nanoparticles.

The chemical reduction of transition metal salt in the presence of stabilizing agents to generate zerovalent metal colloids in aqueous or organic media was first published in 1857 by Faraday [3]. More recently, Turkevich [4] synthesized gold nanoparticles of 20 nm size by reduction of $[AuCl_4]^-$ with sodium citrate and he proposed a mechanism for the stepwise formation of nano-clusters based on nucleation, growth and agglomeration. The used protective agents (polymer, solvents as THF, MeOH, and propylene carbonate, long chain alcohols, surfactant and organometallic) are necessary to stabilize nanostructured colloidal metal and to prevent agglomeration. In the case of silver, it has been verified that stronger reducing agents produce smaller nuclei to yield colloidal metal particles in the size range 1-50 nm.

The objectives of this thesis were focused on the synthesis of nanoparticles through thermodynamical approach based on the formation of mono-sized metallic silver by a combination of a solute ($AgNO_3$) and the use of a low concentration of polymeric monolayer stabilizers as polyvinyl-pyrrolidone (PVP) adhered onto the growth surfaces. The nanoparticles were prepared on different reactions medium as water, propanediol, methoxyethanol, ethylene glycol and polyvinyl alcohol with and without PVP and heated up to 90ºC. Silver nanoprisms have been synthesized via chemical process using sodium borohydride as strong reducing agent, sodium citrate and hydrogen peroxide as stabilizer and surface control. Controlling the size, shape and structure of metal nanoparticles and nanoprisms is technically important because of strong correlation between these parameters and theirs physical-chemistry properties.

Here in this work, the size, structure, optical properties, and composition distribution of the resultant nanostructures were characterized by transmission electron microscopy (TEM), X-ray diffraction (XRD), Dynamic Light Scatter (DLS) and UV-vis spectroscopy.

In the first chapter, we present an approach to the study of surfactant assisted preparation of silver nanoparticles at room temperature using a simple methodology (*chemical reduction metallic salt*). Both polar and non-polar surfactants were used in this study in order to distinguish the role their nature can play. The poly(vinylpyrrolidone) (PVP) is a polymer capable of complexing and stabilizing Ag nanoparticles formed through the reduction of Ag^+ ions with 1,2-propanediol, 2-methoxyethanol, water, polyvinyl alcohol and ethylene glycol. The reduction can be efficiently performed heating the solution into 90º during 30 minutes. Experimental spectra observed by UV-Vis spectroscopy and average particle size determinations from TEM micrographs are also presented.

Less is known with respect to solution synthetic methods for non-spherical particles such as triangles or prisms. Recently, much effort has been devoted to the synthesis of Ag nanoparticles with different shapes (nanorods, disks, wires, nanoplates, triangles and nanoprisms), specially focused on triangular silver nanoprisms, because of their unusual optical properties (lithography, vacuum deposition, chemical reduction of metal salts, and photoinduced aggregation of small nanoparticle seeds)[5].

In chapter two, silver structures has been prepared as triangular nanoprisms with sharp corners by continuous stirring of an aqueous dispersion of spherical colloids of silver with an average diameter of 10 nm. Colloidal suspension of triangular silver nanoprisms were prepared in water by the reduction of silver nitrate at room temperature in the presence of poly (vinyl-pyrrolidone), sodium citrate, sodium borohydride and hydrogen peroxide. Non-spherical shapes are evidenced by three different resonance frequencies, determined by UV-Vis spectroscopy and observed by TEM microscopy. We also studied the effects of sodium citrate, hydrogen peroxide and sodium borohydride on the reaction.

Dispersions and coatings present a wide range of new and enhanced functionalities which are now becoming available by means of nanostructuring. They cover the whole set of properties that are of interest in optical, thermal, and electrical applications. This is the most natural area of nanoscale science and technology. Many current commercial applications include printing, sunscreens, photography, and pharmaceuticals. Some examples of the present technological impact of nanostructuring are thermal and optical barriers, imaging enhancement, ink-jet materials, coated abrasive and information-recording layers. From our point of view at present, there appears to be a very strong potential impact in the areas of targeted drug delivery, gene therapy, and multifunctional coatings. Successful nanoscale dispersions and coatings require freedom from agglomeration and surface control. Process controls are required to ensure reproducibility, reliability, and scalability. Chapter 3 presents the preparation of nanoparticle coatings. In this chapter, we discuss the thermal treatment and dielectric surrounding effects on the optical properties of silver nano-particles and prisms films. We prepared a metallic coating in a conventional process such as spin-coating and the samples were characterized by UV-Vis spectroscopy.

The potential application in optics, catalysis, chemical, pharmaceutics and biology, of the coated silver nanoparticles on a silica substrate provide a high surface area and chemical and physical properties that are distinct from those of both the bulk phase and individual molecules. In the fourth chapter, we describe an additional method, that is, a via sol-gel modified synthesis for coating nanosized silver nanoparticles on silica spheres. This method involves the preparation of homogeneous silica spheres at room temperature, combined with the deposition of silver nanoparticles from one solution, by using water/ethanol mixtures, tetraethylorthosilicate as Si source and silver nitrate as Ag source in a single-pot wet chemical route without an added coupling agent or surface modification, which leads to the formation of core@shell homogeneous nanospheres. We present the preparation and characterization of the SiO_2@Ag core–shell nanospheres and also of bare silica spheres in the absence of silver, and different silver nanoshell morphology are produced on silica spheres, and propose a reaction mechanism for the formation of the core–shell structure. This work was realized in collaboration with the student J. Carlos Flores G. as part of his doctoral thesis. Only we discuss the more important results obtained.

Another particular objective of this thesis is to develop materials in solution and nanosize with photo-catalytic activity on visible region and they can to be characterized by Ultraviolet-Visible spectroscopy. This last chapter is devoted to the synthesis of composites nanoparticles of TiO_2-Ag, SiO_2-Ag-TiO_2 in solution and powders. The purpose of this synthesis is to develop hybrid systems heterogeneous with photo-catalytic activity or as protect monolayer. For the synthesis of these materials, we employed the

sol-gel method. The flexibility of the sol-gel method allow to work in both polar and non-polar (solvent) medium, as well as acid, basic or acid↔basic medium for to produce different particle size and morphology.

First, the TiO_2 nanoparticles with chemically modified surface were synthesized from tetra-butyl orthotitanate in presence of absolute ethanol, water and using different reaction medium (NH_4OH, HCl, HCl-NH_4OH). The final solution was centrifuged and washed several times and then was heated until 800ºC in air oven by 2 hours. The initial resulting powder was white, and amorphous. After the heat treatment anatase TiO_2 nanoparticles were obtained, as shown by the peaks of X-ray diffraction. Subsequently, silver nanoparticles prepared in methoxyethanol were deposited over TiO_2.

Chapter I

Silver Nanoparticles Synthesis

I. OVERVIEW

1.1. Metallic nanostructures

Nanostructured materials derived from nanoparticles have evolved as a separate class of materials over the past decade. Currently, the most remarkable feature has been the way in which completely disparate disciplines have come together with nanomaterials as the theme and therefore it requires formation of and contribution from multidisciplinary groups (physicists, chemists, engineers, molecular biologists, pharmacologists, etc.) to work together on i) synthesis and processing of nanomaterial and nanostructures, ii) understanding the physical properties related to the nanometer scale, iii) design and fabrication of nano-devices or devices with nanomaterial, and iv) design and construction of novel tools for characterization of nanostructures and nanomaterial.

Currently, metal nanoparticles are great interest by their electronic, catalytic, magnetic and optical properties to technological and nanometer level. In the last few years, has paid greater attention to their preparation, determination of structure and applications. Metal nanoparticles [20] are defined as isolated particles between 1-100 nm diameters that do not represent a chemical compound with a metal-metal bond and a particular nuclearism. The nanoparticles represent cluster of atoms that are involved in a protective layer to prevent or stabilizing agglomeration [21].

Due to this small size, nanoparticles have a large fraction of surface atoms, i.e. a high surface-to-volume ratio. This increases the surface energy compared with that of bulk material. The high surface-to-volume ratio together with size effects (quantum effects) gives nanoparticles distinctively different properties (chemical, electronic, optical, magnetic and mechanical) from those of bulk material. In particular, the optical properties of metal nanoparticles rely on a strong absorption in the visible spectrum, called the Plasmon band, which is directly related to the size and shape of the particle [22][23][24][25], the metal species [26] and the surrounding medium [27], scattered [28], absorbed substance [29][26][30][31][32][33][34][35] and agglomerations [36][37]. For example, Au nanoparticles in solution show a yellow color, but Au coatings on optical glass substrates show a blue color. This characteristic blue color steadily change to orange, through several tones of purple and red, as the particle size is reduced down to ~ 3 nm. These effects are the result of changes in the surface plasmon resonance [[38]], defined as the frequency at which conduction electrons oscillate in phase with the electric field under electromagnetic radiation (light incident). Metal particles with free electrons possess surface plasmon resonance, essentially Au, Ag, Cu, and alkali metals and can be observed in the visible spectrum, which gives rise to these colors. As a result, a variety of optical properties such as absorption bands in the visible spectrum, intensity of Raman scattering and nonlinear properties can be found by varying the particle shape [39][40].

Different synthesis methods have been reported for the preparation of silver nanoparticles with different shapes, sizes and size distribution control. Within silver geometric shapes that have been prepared are: spherical [41][42][43][44][45][46][47][48][49][50][51][29], octahedral [52], tetrahedral [52], hexagonal [28], cubic [52][53], fibers (wires) [54][55][56], disks [57][58][59], triangular prisms [52][57][9][10][18], Shell [[60]], among others [61][62]. Overall, there are relatively few methods that allow one to systematically make such structures in high yield with control over their architectural parameters. The simplest and the most commonly used solution synthetic method for metal nanoparticles is the chemical reduction of metal salts.

1.2. Stabilization of Colloidal Metal Particles in Liquids

Before beginning a description of synthetic methods, a general and crucial aspect of colloid chemistry should be considered, and that is the means by which the metal particles are stabilized in the dispersing medium. At short interparticle distances, two particles would be attracted to each other by van der Waals forces and in the absence of repulsive forces to counteract this attraction an unprotected sol would coagulate or agglomerate. In this aspect, two stabilization methods can be achieved: electrostatic stabilization and steric stabilization [63][64].

Electrostatic Stabilization

When two particles are far apart or the distance between the surfaces of two particles is larger than the combined thickness of two electric double layers of two particles, there would be no overlap of diffusion double layers, and thus there would be no interaction between two particles (***Figure 1a***). However, when two particles move closer and the two electric double layers overlap, a repulsion force is developed. As the distance reduces, the repulsion increases and reaches the maximum when the distance between two particle surfaces equals the distance between the repulsive barrier and the surface (***Figure 2b***).

If the electric potential associated with the double layer is sufficiently high, electrostatic repulsion will prevent particle agglomeration. This stabilization method is generally effective in dilute aqueous or polar organic media systems with high dielectric constant. Because, one electrolytic medium can destroy the electronic cloud due to a change in ion concentration, which would result in agglomerated particles.

The DLVO (Derjaguin, Landau, Venvey and Overbeek) theory has been widely applied in practice to demonstrate the small particle stability in diffusive medium and has been verified by the Turkevich work [4]. DLVO theory describes the interaction between two particles in dispersion as the potential combination of Van der Waals attraction and repulsion magnetic field. The Figure X, show the Van der Waals attraction potential, electrostatic repulsion potential and the combination of the two opposite potentials as a function of distance from the surface of a spherical particle [65].

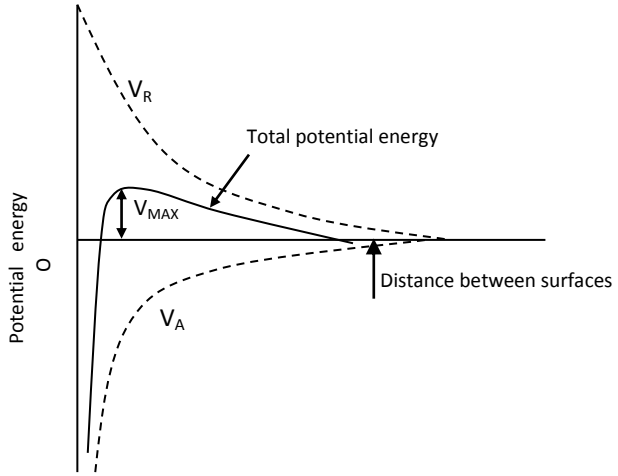

Figure 1. Schematic of DLVO potential: VA=attractive Van der Waals potential, VR=repulsive electrostatic potential.

At a distance far from the solid surface, both van der Waals attraction potential and electrostatic repulsion potential reduce to zero. Near the surface is a deep minimum in the potential energy produced by the van der Waals attraction. A maximum in the potential energy is located a little farther away from the surface, as the electric repulsion potential dominates the van der Waals attraction potential. This maximum is known as repulsive barrier, and dependent of Boltzmann (k) constant and temperature (T). If the repulsive barrier is greater than ~10kT, the collisions of two particles produced by Brownian motion will not overcome the barrier and agglomeration will not occur.

Steric Stabilization

Steric stabilization, also called polymeric stabilization has been method widely applied in stabilization of colloidal solution. Polymeric stabilization offers an additional advantage in the synthesis of nanoparticles, particularly when narrow size distribution is required. This process occurs when the metal particle is covered with a layer of a voluminous material (polymer). Polymeric layer absorbed on the surface of nanoparticles serves as a diffusion barrier, resulting in a diffusion-limited growth in the subsequent growth of nuclei and keep up the metal centers separated from each other, preventing possible agglomeration. In this process are used donor ligands as P, N, S (amines, thioethers, phosphines, thiols, etc.)

Another type of stabilization also used within the steric category is by trapping of nanoparticles in a polymeric material (PVP poly (vinyl pyrrolidone), PVA poly (vinyl alcohol), PMVE poly(methyl vinyl ether)) [66][67], blocks co- polymers [68], b-ciclodextrins [69], dendrimers [70]. In general, lipophilic stabilizers agents produce colloids or solution that are soluble in organic solvents and are called “organosol”; while when stabilizer agent is hydrophilic the colloid is soluble in water and are called “hydrosols”. These solutions are stable by long time without precipitation of metal, or loss of physic and chemical properties of metal particles [71].

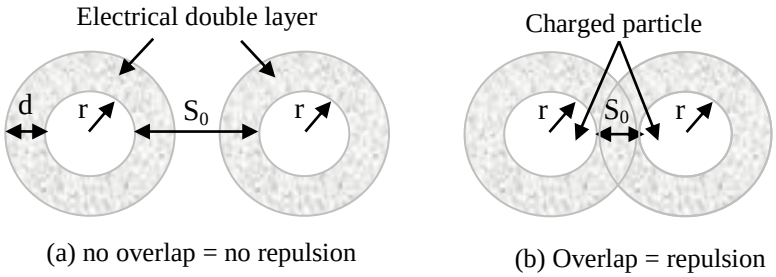

Figure 2. Schematic illustrating the conditions for the occurrence of electrostatic repulsion between two particles.

1.3. Synthesis chemical methods for the preparation of colloidal metal nanoparticle

A variety of methods have been employed to synthesize metal nanoparticles, including [72]: (i) chemical reduction of metal salts, (ii) thermal, sonochemical o photochemical decomposition of a complex organometallic, (iii) reduction and displacement of ligands in organometallic compounds, (iv) metal deposition in vapor phase, and (v) electrochemical synthesis [73][74].

The final size of metal particle reflects in the formation kinetic complexity, therefore, the extent of the reaction depends on the kind and concentration of surfactant, while the time need for its completion mainly depends on metal initial concentration and on temperature.

Chemical Reduction of metal salts

The reduction of transition metal salts in stabilizer solution is the most widely practiced method of generating colloidal suspensions of the metals. This methods was presented by Faraday at 1857 [3] and has become the most effective methods in the nanomaterials field. Later, a protocol for the Ag nanoparticles synthesis based on a nucleation, growth and agglomeration mechanism, from $(AuCl4)^-$ and sodium citrate was developed by Turkevih [4]. Hirai and Toshima [66][75] developed the so-called ‘‘alcohol reduction process’ which is a very general process for the production of metal nanoparticles, stabilized by organic polymers such as poly(vinylpyrrolidone), poly(vinyl alcohol), and poly(methyl vinyl ether). Henglein, observed the Ag^{3+} and Ag^{4+} cluster formation between 1-50nm by spectroscopy [76]. Therefore, the salt reduction advantage in a liquid medium is your reproducibility and facility to produce nanoparticles with controlled size and large quantities. Moreover, the use of this methods to silver triangular nanoprisms synthesize [25] with flat surface and without aggregates has been one the most interesting finding in this area. Although, controlling the size and shape are still being investigated.

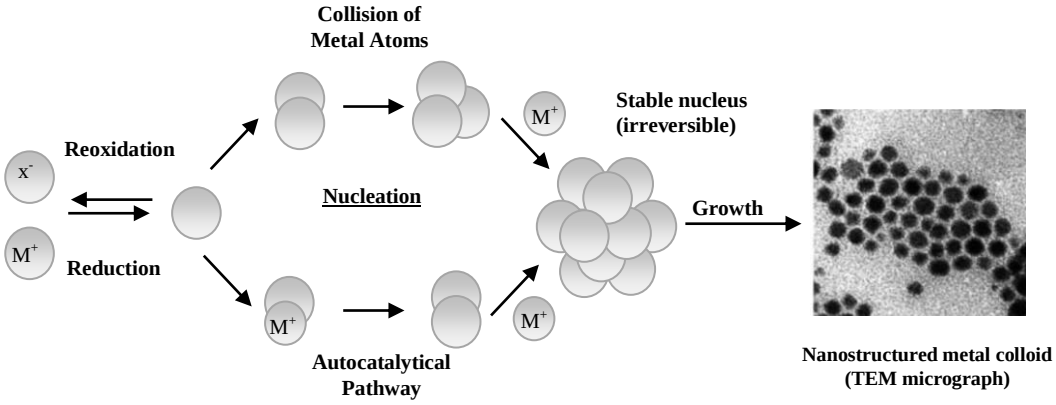

Figure 3. **Formation of nanostructured metal colloids by the ''salt reduction'' method** [77]

Thermal, Sonochemical or Photochemical Decomposition of a Complex Organometallic

Organometallic complexes and metal in zero oxidation state are decomposed by light, heat or ultrasonic radiation effect, to produce stabilized metallic particles in solution. In the literature we find that Ag nanoparticles with average particle size of 7nm can be prepared by ultraviolet light radiation the aqueous solution of AgClO4, acetone, 2-propanol and stabilizers polymer [31][67]. Ag amorphous nanoparticles (~20 nm) were prepared by sonochemical reduction from AgNO3 to 10ºC in Argon and Hydrogen atmosphere [78][79]. The sonochemical reduction advantage is the fast reaction rate and ability to form very small nanoparticle [80].

Ligands Reduction and Ligands Displacement from Organometallic

Reduction of the metal can be carried out prior to colloid preparation, giving a zero- valent metal complex as the intermediate colloid precursor. This synthesis is an approach of the organometallic decomposition [81]. In a further refinement, the supporting ligands in the zero-valent complex can be removed by ligands displacement with an excess of a weakly bound ligand or by ligand reduction, thus generating metal particles at low temperatures. Synthesis report over metal nanoparticles have been made from the ligands hydrogenation in organometallic compounds, using hydrogen as source reducer, alcohols and organic solvents [82][83], amines or thiols [84], polymers, organ-Silanols [85], meso-structured silica [86] or alumina membranes [87] Also, platinum [88][89], cobalt [90], Nickel [91] and bimetallic system (Co-Pt, Ru-Pt) [92][93] colloidal solution have been prepared from complex organometallic.

Metal Chemical Vapor Deposition

Nanoparticles can also be synthesized by vapor reaction, following the same mechanism discussed in the synthesis of nanoparticles in liquid medium. The preparation of colloidal metals by this method is the most simple technique to obtain material in a particular medium. In addition, vapor deposition has provided a route to prepare different metal colloid type [64][94]. However, this technique has certain limitations which prevent the obtaining of nanoparticles disperse.

Electrochemical Synthesis

Metal nanoparticles can be prepared by electrochemical deposition method developed by Reetz [95][96] on 1994. An electrochemical synthesis is achieved by passing an electric current between two or more electrodes (metallic anode and cathode of carbon/metal) separated by an electrolyte. The synthesis takes place in 6 elementary steps:

1. Oxidative dissolution of metal anode.
2. Migration of metal ions Mn^{+} to the cathode.
3. Reduction and formation of metal atoms M^{0} at the cathode.
4. Nucleation and growth of metal particles in solution.
5. Stabilization of metal nanoparticles by colloidal protecting agents.
6. Precipitation of metal colloids.

This synthesis method presents a one advantage respect to chemical reduction which is the absence of secondary pollutants generated during the reaction. On the other hand, different parameters as current density, time, temperature, distance between electrodes and solvent polarity can be controlled during the reaction, resulting in great control of the particle size.

1.4. Characterization and Properties of Metal nanoparticles

The discussion in this section is focused mainly on the fundamentals and basic principles of the characterization methods. Technical details, operation procedures and instrumentations are not the subjects of discussion here. The intention of this section is to provide readers with the basic information on the fundamentals that the characterization methods are based on. For technique details are recommended to relevant literature [97][98].

Structural Characterization

Regard to the metal core and specifically the particle size determination, often the Electron Microscopy (***TEM, Transmission Electron Microscopy*** [99]) is the most used technique. TEM allows direct observation of the image formed by electrons during their passage through the specimen and is projected on a fluorescent surface. This technique offers a unique capability to determinate exactly the metal core diameter, as well as information of form, structure and morphology of nanoparticle. The metallic colloids, especially the heavy metal have high electron density, which produce a great contrast in TEM analysis. For this reason the samples are coating with carbon on a grip.

The TEM, although is widely used have some limitations such as: the samples must be dried and examined under high vacuum, avoid getting any information about state in solution. A complementary technique to electron microscopy is the ***STM*** (***Scanning Tunneling Microscopy***), through which one can measure the particle diameter, ie, the sum of the metallic core diameter and stabilizing layer thickness.

In the ***High Resolution Transmission Electron Microscopy*** (***HRTEM***) the opening of the diaphragm of the microscope is larger and the images are formed from a number of diffracted beams; this multi-beam approach is known as phase-contrast imaging, and is necessary to construct an image of the crystal lattice. HRTEM provides access to much information about the sample, such as analysis crystalline defects and interfaces at the atomic scale, and observing and verifying devices, multilayers, nanoscrystals and nanostructures. The technique typically requires very thin TEM specimens free of preparation artefacts. By contrast, the limiting factor of this technique is to analyze particle size, while smaller particle the resolution is lower, limiting the number of atomic planes to study the different periodicities.

Another technique for determining the structure of nanoparticles is ***Electron Diffraction*** [100] (***ED***), which is related with electron microscopy techniques that allow us to obtain the crystal structure, crystalline spaces and exact composition of the material (d_{hkl}, ASTM tables for most common metals and minerals). Electron diffraction of solids is usually performed in a Transmission Electron Microscope (TEM) where the electrons pass through a thin film of the material to be studied (***Figure 4*****).** Amorphous materials do not consist of atoms arranged in ordered lattices, but in hodgepodge random sites. Amorphous materials are completely disordered. The electron diffraction pattern will consist of fuzzy rings of light on the fluorescent screen. The diameters of these rings of light are related to average nearest neighbor distances in the material.

The samples crystals consist of atoms arranged in an orderly lattice. Some types of crystal lattices are simple cubic, face centre cubic (f.c.c.), and body centre cubic (b.c.c). In general, single crystals with different crystal structures will cleave into their own characteristic geometry. Single crystals are the most ordered of the three structures. An electron beam passing through a single crystal will produce a pattern of spots. From the diffraction spots one can determine the type of crystal structure (f.c.c., b.c.c.) and the "lattice parameter" (i.e., the distance between adjacent (100) planes). Also, the orientation of the single crystal can be determined: if the single crystal is turned or flipped, the spot diffraction pattern will rotate around the centre beam spot in a predictable way. Polycrystalline materials are made up of many tiny single crystals. Most common metal materials (copper pipes, nickel coins, stainless steel forks) are polycrystalline. Also, a

ground-up powder sample appears polycrystalline. Any small single crystal "grain" will not in general have the same orientation as its neighbors. The single crystal grains in a polycrystal will have a random distribution of all the possible orientations. A polycrystal, therefore, is not as ordered as a single crystal. The diffraction pattern will therefore look like a superposition of single crystal spot patterns: a series of concentric rings resulting from many spots very close together at various rotations around the centre beam spot. From the diffraction rings one can also determine the type of crystal structure and the "lattice parameter". One cannot determine the orientation of a polycrystal, since there is no single orientation and flipping or turning the polycrystal will yield the same ring pattern.

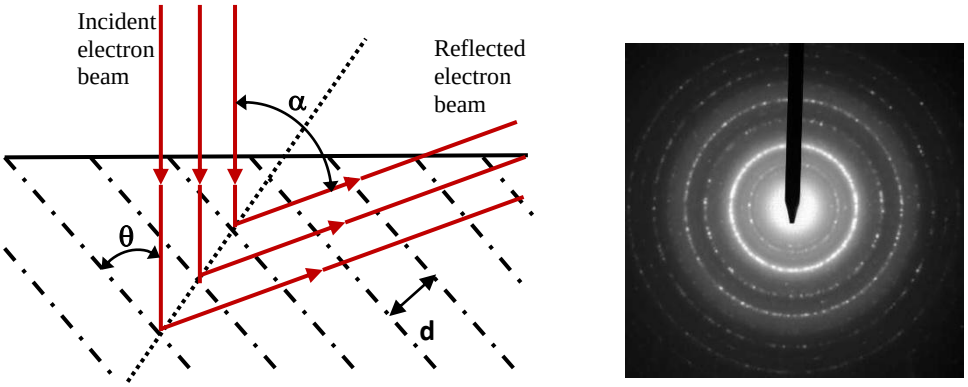

Figure 4. Schematic of a beam incident on a pair of planes separated by a distance d, and Electron diffraction pattern of a polycrystalline sample

In the other case, the X-ray diffraction [101] (***XRD***) can be used as a secondary or complementary technique to determine particle size, by analyzing the diffraction peaks. X-ray diffraction has been in use in two main areas, for the characterization of crystalline materials and the determination of their structure. Once the material has been identified, X-ray crystallography may be used to determine its structure, i.e. how are the atoms packed in the crystalline state, the interatomic distance and angle, etc; which is useful to identify the oxidation state of metal in nanoparticle systems.

Both XRD and ED, the incident beam interacts (diffraction or scattering) with different atomic planes of the sample, following Bragg's law, where θ is the angle between the incident beam and scattering planes, d_{hkl} is the spacing between the planes in the atomic lattice, n is an integer determined by the order give, and λ is the wavelength of the incident X-ray beam.

$$n * \lambda = 2d_{hkl} \sin\theta$$

Although Bragg's law used the interference pattern of X-ray scattered by crystal. The X-ray scattering experiments has been developed to study the structure and texture of all states of matter to atomic and nanometer scale. This analysis is complementary technique to TEM, with the advantage that can be performed both on powder nanoparticles as in colloidal solutions. Information in situ of the reaction medium during the for-

mation of nanoparticles can be obtained. The X-ray diffraction is a non-destructive technique and requires no elaborate preparation of samples, which makes to these materials characterization technique the most used.

Moreover, another technique that allows visualization of samples with high resolution is called ***Scanning Electron Microscopy*** (***SEM***), and is a type of electron microscope that images the sample surface by scanning it with a high-energy beam of electrons in a raster scan pattern. The electrons interact with the atoms that make up the sample producing signals that contain information about the sample's surface topography, morphology, composition and other properties such as electrical conductivity.

One advantage of SEM is that majority samples can be examined without any preparation (except biological materials). For conventional imaging, specimens must be electrically conductive, at least at the surface, and electrically grounded to prevent the accumulation of electrostatic charge at the surface. Nonconductive specimens tend to charge when scanned by the electron beam, and especially in secondary electron imaging mode, this causes scanning faults and other image artifacts. They are therefore usually coated with an ultrathin coating of electrically-conducting material, commonly gold, deposited on the sample either by low vacuum sputter coating or by high vacuum evaporation. Conductive materials in current use for specimen coating include gold, gold/palladium alloy, platinum, iridium, tungsten, chromium and graphite. Coating prevents the accumulation of static electric charge on the specimen during electron irradiation.

Chemical Characterization

The overall composition of the colloids is studied by conventional techniques: Nuclear Magnetic Resonance, Infrared Spectroscopy, Elemental analysis (determines the % metal), UV-Visible spectroscopy. The latter is particularly effective in cases where the surface plasmon of metal nanoparticle is in the visible spectrum. UV-Vis spectroscopy is a very useful technique which allows estimation of nanoparticles size, concentration, and aggregation level.

In the case of bimetallic nanoparticles is necessary know if all particles have the same composition or as two materials are distributed inside the particle. The techniques need to be sensitive to local difference in composition at the nanoscale. The ***Energy Dispersive X-Ray Spectroscopy*** (***EDS***) is an analytical technique used for the elemental analysis or chemical characterization of a sample used in conjunction with scanning electron microscopy (SEM). EDS works by detecting X-rays that are produced by a sample placed in an electron beam. The electron beam excites the atoms in the sample that subsequently produce X-rays to discharge the excess energy. The energy of the X-rays is characteristic of the atoms that produced them, forming peaks in the spectrum. EDS Spectroscopy studies the loss of excitation energy of the atoms in the sample by X-ray emission. This energy is characteristic of the excited atom and the emission intensity is proportional to the concentration of the elements in the particle.

Optical Spectroscopy

Optical spectroscopy has been widely used for the characterization of nanomaterials (Au, Ag and Pt). UV-Vis spectroscopy determines the electronic structures of atoms, ions, molecules or crystal through exciting electrons from the ground to excited states (absorption) and relaxing from the excited to ground states (emission). The metal nanoparticles exhibit an intense absorption band in the ultraviolet-visible region, known as the surface plasmon absorption band (SPAB) [46] [102][42][103][104][105][106]. This technique measures the intensity of light passing through a sample (I), and compares it to the intensity of light before it passes through the sample (I_0). ϵ is the wavelenght-dependent molar absorbity coefficient, b is the path length, and c is the concentration. The method is most often used in a quantitative way to determine concentrations of an absorbing species in solution, using the Beer-Lambert law:

$$A(\lambda) = -\log(\%T) = \epsilon * b * c$$

Materials researchers are often working not with liquids, but with solid materials. Some solid materials can be analyzed via UV-Vis spectroscopy by dissolving the solid in a solvent, but this process is labor intensive and can introduce many sources of error into the measurement. It is also a destructive technique so the sample cannot be recovered for other measurements. These factors make dissolution methods for UV-Vis absorption spectroscopy generally undesirable for most solid materials. The containers for the sample and reference solution must be transparent to the radiation which will pass through them. Quartz or fused silica cuvettes are required for spectroscopy in the UV region. These cells are also transparent in the visible region. The cuvettes are rectangular and 1 cm of interior width. This width is the path length (L) in the Beer-Lambert law.

Dynamic Light Scattering (DLS or Photon correlation spectroscopy)

This technique can be used to determine the size distribution profile of small particles in suspension or polymers in solution [107]. It can also be used to probe the behaviour of complex fluids such as concentrated polymer solutions. When light hits small particles the light scatters in all directions (Rayleigh scattering) so long as the particles are small compared to the wavelength (below 250 nm). If the light source is a laser, and thus is monochromatic and coherent, then one observes a time-dependent fluctuation in the scattering intensity. These fluctuations are due to the fact that the small molecules in solutions are undergoing Brownian motion and so the distance between the scatters in the solution is constantly changing with time. This scattered light then undergoes either constructive or destructive interference by the surrounding particles and within this intensity fluctuation, information is contained about the time scale of movement of the scatters.

A typical dynamic light scattering system comprises of six main components (see ***Figure 5***). Firstly, a laser (1) provides a light source to illuminate the sample contained in a cell (2). For dilute concentrations, most of the laser beam passes through the sample, but some is scattered by the particles within the sample at all angles. A detector (3) is used to measure the scattered light.

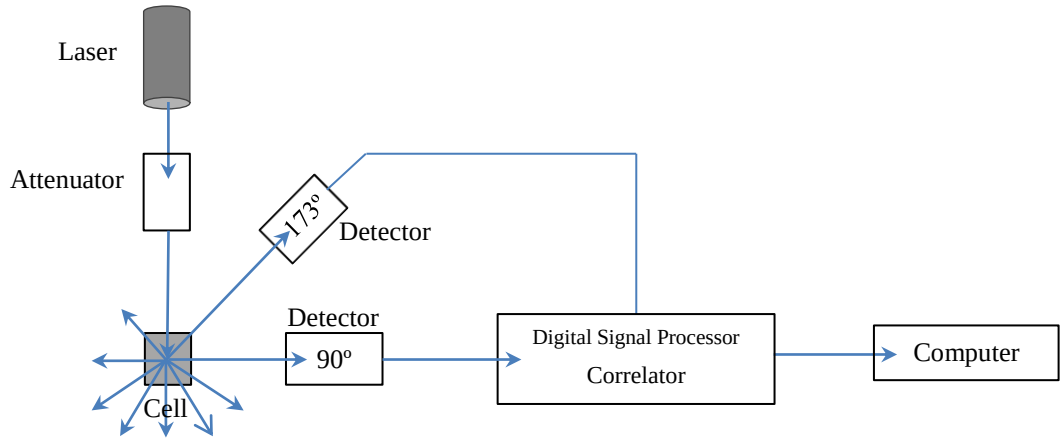

Figure 5. Optical configurations of the Malvern instruments for dynamic light scattering measurements

The intensity of scattered light must be within a specific range for the detector to successfully measure it. If too much light is detected, then the detector will become saturated. To overcome this, an attenuator (4) is used to reduce the intensity of the laser source and hence reduce the intensity of scattering. For samples that do not scatter much light, such as very small particles or samples of low concentration, the amount of scattered light must be increased. In this situation, the attenuator will allow more laser light through to the sample. The scattering intensity signal from the detector is passed to a digital processing board called a Correlator (5). The correlator compares the scattering intensity at successive time intervals to derive the rate at which the intensity is varying. This Correlator information is then passed to a computer (6), where the Nano software will analyze the data and derive size information.

Dynamic light scattering provides insight into the dynamic properties of soft materials by measuring single scattering events, meaning that each detected photon has been scattered by the sample exactly once. However, the application for many systems of scientific and industrial relevance has been limited due to often encountered multiple scattering, wherein photons are scattered multiple times by the sample before being detected. Accurate interpretation becomes exceedingly difficult for systems with non negligible contributions from multiple scattering. Particularly for larger particles and those with high refractive index, this limits the technique to very low particle concentrations, and a large variety of systems are, therefore, excluded from investigations with dynamic light scattering. However, as shown by Schaetzel [108], it is possible to suppress multiple scattering in dynamic light scattering experiments via a cross-correlation approach. The general idea is to isolate singly scattered light and suppress undesired contributions from multiple scattering in a dynamic light scattering experiment. Different implementations of cross-correlation light scattering have been developed and applied. Currently the most widely used scheme is the so called 3D-dynamic light scattering method [109][110].

1.5. Plasmon Optical properties

Recently, optical activity has been observed in a new class of metallic materials at the nanometric scale. Specifically, CD signals have been measured in monolayer-protected metal clusters and nanoparticles. Monolayer-protected metal nanoclusters are composed of a metallic cluster core surrounded by organic molecules or organometallic compounds. In particular, the capability for self-assembly and the study of quantum-size effects of protected silver nanoparticles have received special attention due to important applications in biology, catalysis and nanotechnology. In this section, we provide an overview the study of plasmonic optical properties of metal nanostructures with emphasis on understanding the relation between surface plasmon absorption and structure.

1.5.1. Surface plasmon resonance (SPR)

Optical properties of small metal nanoparticles have been of great interest for a long time, not only because of the beautiful colors of stained glass but also because of other aspects as materials properties with applications. When a particle is subject to an electromagnetic (EM) filed, its electrons start to oscillate under resonant conditions, transforming energy from the incident EM wave into, for example, thermal energy in an absorption process. When conduction electrons oscillate coherently, the electron cloud is displaced from the nuclei giving rise to a surface charge distribution (***see Figure 5***). The Coulomb attraction between positive and negative charges results in restoring forces, characterized by oscillation frequencies of the electron cloud with respect to the positive background. Each collective oscillation associated to different surface charge distributions is known as Surface plasmon resonance (SPR). When the size of a metal nanocrystal is smaller than the wavelength of incident radiation, a surface plasmon resonance is generated. The electron density, effective mass, particle shape, size, dielectric function, and its environment determine the number, frequency, and width of SPRs. The ***Figure 6*** shows schematically how a surface plasmon oscillation of a spherical metal nanoparticle is created in a simple manner.

While the color and surface plasmon absorption band are somewhat dependent on the size of spherical nanostructures, they strongly depend on the shape of the nanostructures. For a metal such as silver or gold, almost any color or absorption in any part of the visible spectrum can be produced by controlling the shape or structure of the nanomaterial. In principle, almost any shape can be produced. These different-shape nanostructures possess vastly different absorption spectra or color. The rich color or diverse absorption is the result of multiple resonances in the complex structures. More complex structures such as nanocages, aggregates, and nanoprisms usually have more nondegenerate resonances and thereby broad overall absorption spectrum. Therefore, the optical properties of metal nanomaterials can be altered at will by manipulating the details of the structure in a controllable manner.

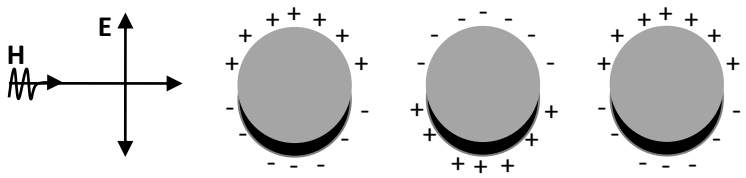

Figure 6. Schematic illustrating the excitation of the dipole surface plasmon oscillation. The electric field of an incoming light wave induces a polarization of the (free) conduction electrons with respect to the much heavier ionic core of a spherical metal nanoparticle.

The electric field of an incoming light induces a polarization of the free electrons in the nanoparticle. The net charge difference occurs at the nanoparticle boundaries (the surface), which in turn acts as a restoring force; resulting in a dipolar oscillation of electrons with a certain single resonant wavelength (frequency) [111]. The surface plasmon resonance is a dipolar excitation of the entire particle between the negatively charged free electrons and its positively charged lattice [112][113][114][115]. Because spherical particles are in principle completely symmetrical, there is only one dipolar plasmon resonance, or, in other words, all the possible dipolar modes are degenerate. As particles become more complex, many more nondegenerate dipolar modes arise and their optical absorption becomes more complex with many bands over a broad spectral region. Furthermore, as the particle becomes less symmetric, the induced electronic cloud on nonspherical nanoparticles is not distributed homogeneously on the surface such that the induced charge distribution on the surface can result in not only dipolar modes with different resonant frequencies but also higher multipolar charge distributions.

The high multipolar SPRs are always located at shorter wavelengths with respect to the dipolar ones, which, additionally, are always red-shifted by the presence of the electric field generated by the higher multipolar charge distributions. Examples include nanorods, nanoprisms, nanocages, aggregates, and hollow nanospheres [116][117][118][119]. When nanoparticles are dispersed in a matrix, their random orientation leads to an average absorption spectrum containing all SPRs associated to the corresponding geometry.

1.6. Metal nanoparticles application

Metal nanoparticles have an extremely broad range of potential applications in physical, chemical and biology field. They can serve as a model system to experimentally probe the effects of quantum confinement on electronic, magnetic and other related properties [120][121][122]. They have also been widely exploited for use in photography [123], catalysis [20], biological labeling [124],as molecular receptor [125], biosensors [126][127], and to diagnose certain diseases [128]; In physical system as photonics [129], optoelectronics [130], surface enhanced Raman scattering (SERS) [131][132], magnetic [133], semiconductors [134][135][136], nano-capacitors [137], and materials [138]. In the chemistry area, the nanoparticles are used in fuel cells [139][140][141][142][143] as electro-catalysts. One of the major interesting areas in the use of nanoparticle is the catalysis [20][144][145][146], where the colloids show a series of unique opportunities both in homogeneous (solutions) and heterogeneous (coating) catalysis, due to its large surface area and high concentration of atoms on the surface.

1.7. Experimental description

1.7.1. Synthesis of Silver nanoparticles in different systems

Silver nanoparticles were prepared by chemical reduction process. In a typical synthesis of silver nanoparticles, AgNO3 (Normapur Prolabo) were mixed with an amount of poly(vinyl-pyrrolidone) (PVP, average molecular weight 40,000, Calbiochem) in 100 ml of solvent/surfactants at room temperature under vigorous magnetic stirring until complete dissolution of the silver nitrate. The silver nanoparticles were synthesized with PVP/AgNO3 molar ratio of 0.5:1. The reaction mixture was then heated at different temperature (60, 90, 120º C) during 30 min. Then samples taken at each temperature were stored in tinted glass bottles. The obtained nanoparticles were diluted with ethanol and separated from dissolvent by centrifugation at 15000 rpm for 10 min. The scheme in ***Figure 6*** display the general experimental procedure followed to produce silver spherical nanoparticles colloidal suspension in different solvents. ***Table 1*** show the concentrations used to prepare silver nanoparticles in different systems. The samples were prepared with and without PVP.

During this process, the formation of uniform Ag nanoparticles is revealed by a pale yellow, implying the formation of the silver nanoparticles. After 30 min of heating, the colloid darkened to a deep yellow color.

Table 1. Reaction conditions for the silver nanoparticles synthesis.

Solvents	***Concentrations [mol]***					
	Buffer system	**T [ºK]**	**AgNO3**	**PVP/AgNO3**	**SC**	***NaBH4***
1	Propanediol	298, 363	30 mmol	0, 0.5:1	0	0
2	Methoxyethanol	298, 363	30 mmol	0, 0.5:1	0.2 mmol	0
3	Ethylene glycol	298, 363	30 mmol	0, 0.5:1	0	0
4	Polyvinyl alcohol	298, 363	30 mmol	0	0	0
5	H2O	298, 363	*30 mmol*	0, 0,5:1	0, 0.2 mmol	5-100 µmol

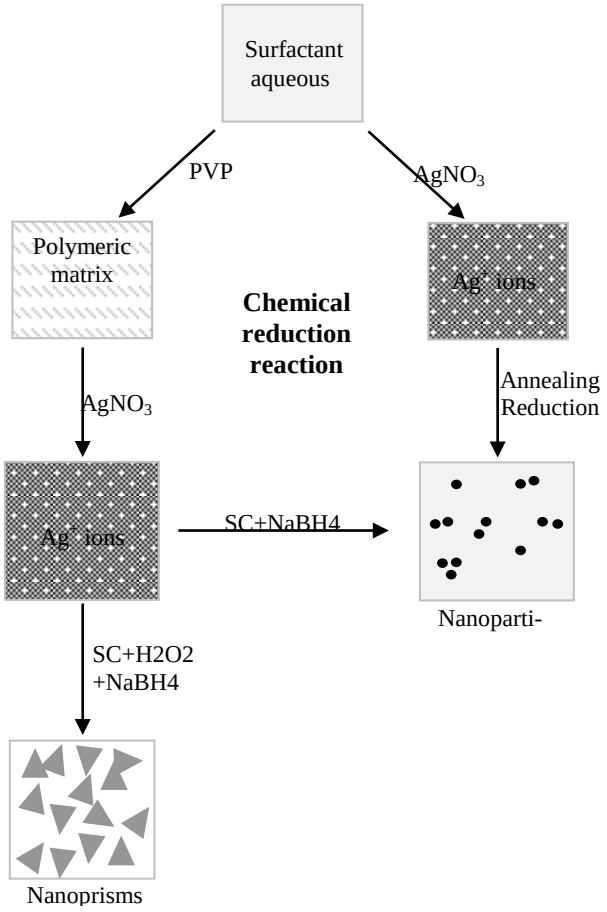

Figure 7. General experimental procedure followed to prepare silver nano- particles and prisms colloidal solutions.

1.7.2. Optical absorption and Morphological studies

The optical absorption features of Ag colloids in the UV-Vis range from 200 nm to 800 nm wavelength were measured using a spectrophotometer UV-Vis Shimadzu UV-2101. Samples for transmission electron microscopy (TEM) were prepared as follows: silver nanoparticles solutions were centrifuged at 20,000 rpm during 10 minutes and washed with ethanol. This process was made three consecutive times to eliminate the excessive polymer of the nanoparticles. The precipitate was dissolved in ethanol and deposited by dripping on a carbon coated grid and allowed to dry for TEM analysis in a Hitachi 800 operating at 200 kV. The solution could be diluted with ethanol without affecting their stability. The samples for XRD analysis were made by taking a small amount of the solution from the bottle and drying it on a quartz plate.

1.8. Result and Discussion

1.8.1. Formation of spherical colloid in different solvent

The addition of AgNO3 to initial solution of PVP produces a colorless precursor solution. Its UV-Vis spectrum shows a sharp peak at 280 nm which is associated with Ag^+ ions in the solution. This is the first stage of the AgNO3 reduction reaction, which is dissociated into Ag^+ and $NO3^-$ ions. Agglomerates of Ag^+ ions formed are called "clusters". We know that the preparation of polymer-stabilized nanoparticles in solution consists of reduction of the metal ions and polymer stabilization of the metal. These processes the reduction can take place before or after interaction between the metal ion and polymer. If the reduction precedes the interaction, the polymer may not properly control the nanoparticle growth; therefore, the second case is more favourable. This way, a yellow clear solution was obtained, increasing the intensity of the yellow color slowly over time. The samples prepared in 1,2-propanediol and 2-Methoxyethanol were heated at 60º, 90º and 120º C, with a rate of heating of 5 ºC/min (***Figure 8***) until reaching the wanted temperature and remaining in this temperature 30 min being observed a fast increment in the coloration when the temperature was increased until obtaining a dark yellow. The dispersions were stable for weeks and they presented the appearance of a single peak and the variation of intensity indicates the degree of advance of the reaction (reduction of Ag^+ at Ag^o) with the increase of the number of nanoparticles. Also, we shown that the rate of reduction of Ag^+ ions in both surfactants (1,2-propanediol and 2-Methoxyethanol) is strongly temperature dependent, although the reduction can take place at room temperature, the rate of reduction is much higher when the temperature is increased.

In the ***Figure 9,*** the experimental UV-Visible spectra of colloidal silver samples in different solvents during the formation nanoparticles are shown. Initially, only one band is present, centered at 410 nm, corresponding to the dipole resonance of silver nanospheres and reflecting spherical shape uniformity. This spectrum reveals that silver spherical nanoparticles give a strong surface plasmon band in the visible region. We can observe that the maximum absorbance of these bands increases as the particle radius increases. The nanospheres spectra were stable with temperature, up to the higher temperature used. The observed resonance peak position is in agreement with previous results and predictions for spherical silver nanoparticles with a mean particle size below 20 nm, [147][148] those which were observed in the TEM measurements. The colloidal silver nanoparticles prepared in 2-Methoxiethanol and H2O employs sodium citrate, which serves the dual role of a reductant and stabilizer. This particles formed have relatively large sized (10-50 nm) crystallites with well-defined facets. The two samples showed a wide dispersity of the particle size and shape, observed in the broad surface plasmon absorption with a maximum around 420 nm.

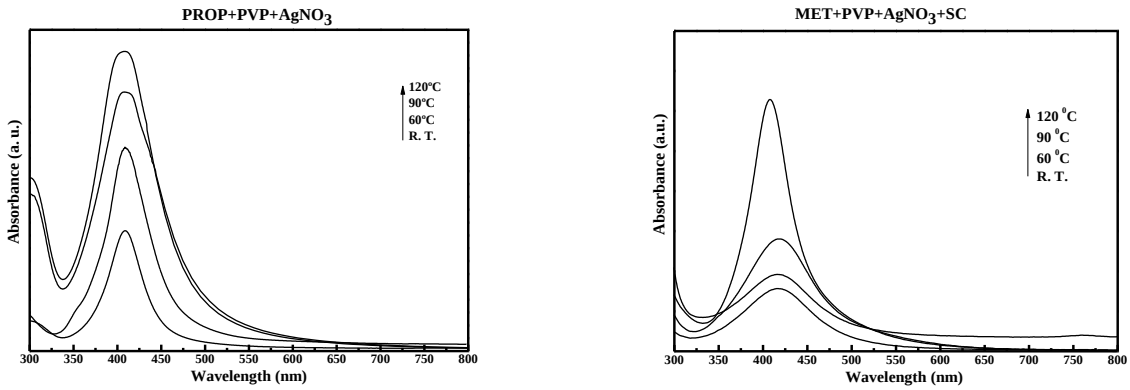

Figure 8. Evolution of UV-Vis absorption spectra after addition of ration PVP/$AgNO_3$ (24:1) in 1, 2-propanediol (*right*), 2-Methoxyethanol (*left*) and heating at different temperature.

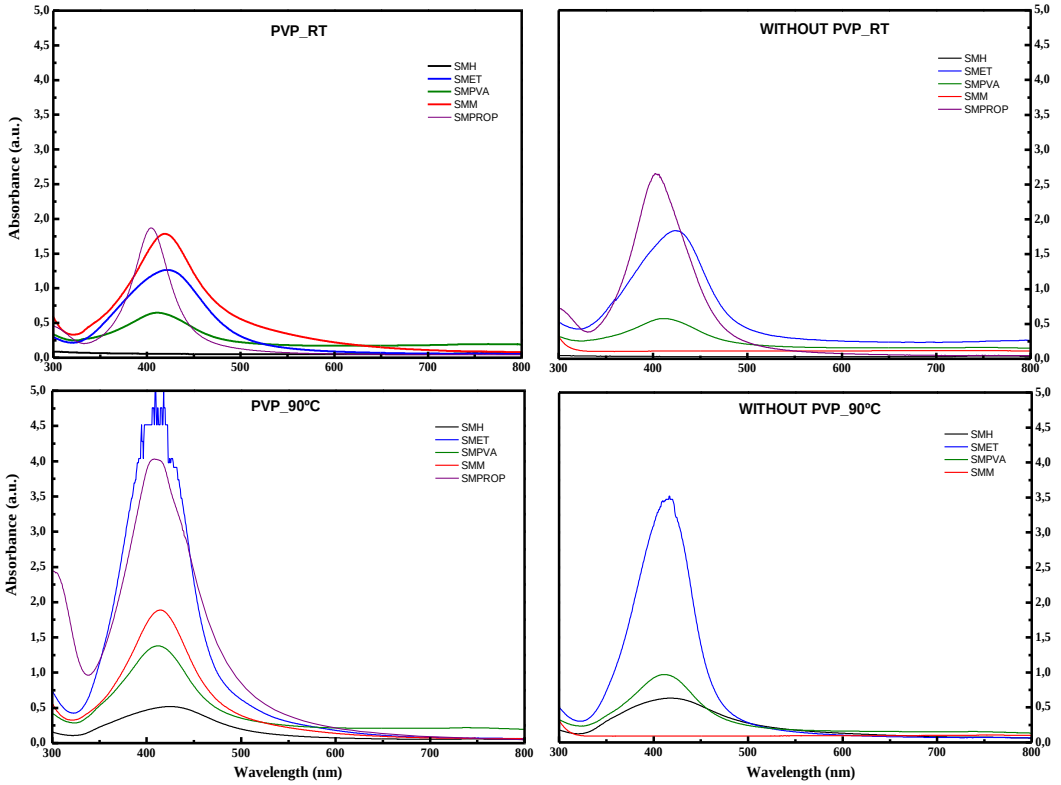

Figure 9. UV-visible spectral of silver nanoparticles prepared in different solvents. *SMH (water), SMET (Ethylene glycol), SMPVA (Polyvinyl alcohol), SMM (2-Methoxyethanol), SMPROP (1, 2-Propanediol).*

The morphological study of the solutions by transmission electron microscopy (TEM) and high resolution transmission electron microscopy (HRTEM) to determine shape and size (***Figure 10***) clearly reveals that the presence of PVP during the reduction of silver ions results in the growth of isolated nanoparticles and not agglomerates. The results of UV-Vis confirmed that shape and size did not change after several month of your preparation. In this works we confirmed that it is possible to obtain stable Ag nanoparticles in colloids using a quite low concentration of PVP [149], much lower than the usual concentrations previously reported in the literature.

The XRD and ED measurements indicate that the nanoparticles have good crystallinity (annex A). The electron diffraction (ED) pattern showed the (111), (200), and (220) reflections of metallic silver particles crystallized in the face centered cubic (fcc) structure with the characteristic peaks in accordance with the JCPDS file no. 4-0862. The mean crystalline particle size, determined using the Scherrer method on the main (111) diffraction peak of the X-ray diffraction pattern, is 20 ± 2 nm, in good agreement with the size of the isolated nanoparticles observed in TEM. Samples kept in dark and samples submitted to normal laboratory light and also to direct sunlight did not show any change in the appearance of the UV-Vis spectra after several month. TEM confirmed that size, shape did not change and the absence of agglomerates after one time aging exposed to sunlight. Analysis of EDX by TEM showed that the colloidal nanoparticles were only silver, the other peak corresponding of the substrate of Cu.

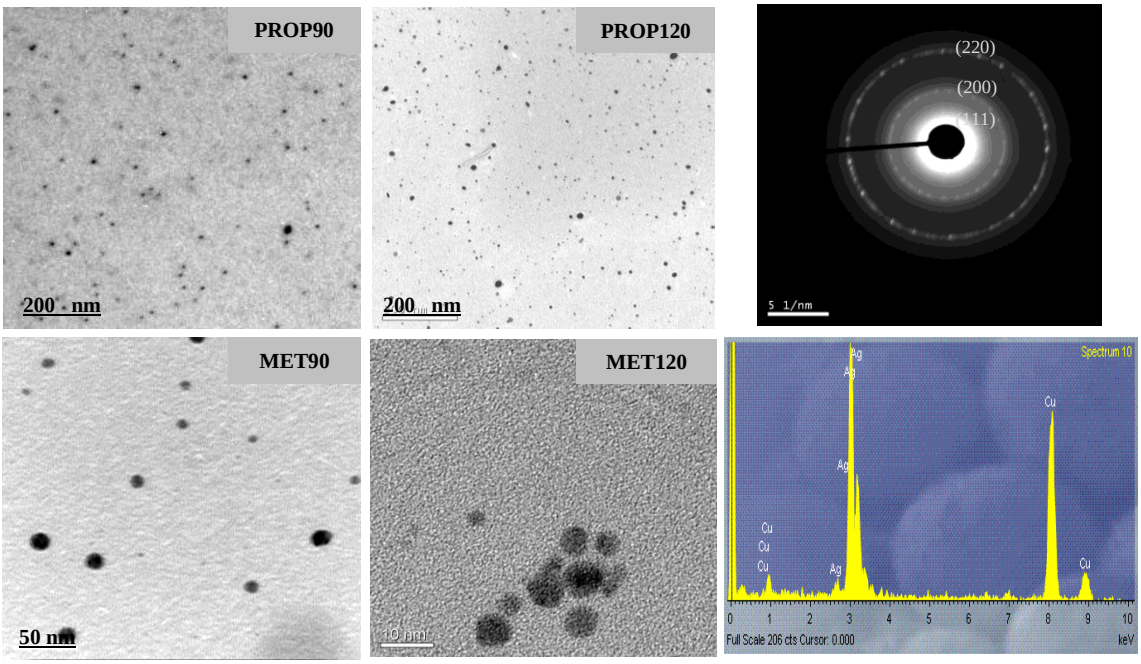

Figure 10. TEM and HRTEM micrographs showing silver nanoparticles in 1, 2-propanediol (*top left*) and 2-Methoxyethanol (*bottom left*). Selected area electron diffraction pattern (*top right*) and EDX (*bottom right*).

1.8.2. Study of silver nanoparticles stability in different aqueous medium

Since for a number of applications it is necessary to use different solvent which are less aggressive. We tested the stability of silver nanoparticles in different reaction medium, to explore the influence of the PVP on the optical response of the colloidal suspensions; we study the intensity of absorption band obtained by UV-Vis spectrometer. The samples showed a shift of the absorption peak between 400-424 nm for different solvent (***Figure 11***). The particle size could to be related with the full width half maximum (FWHM) of peak, as shown the data in the ***Table 2***. Little intensity variation was observed when the PVP was added to the reaction and was kept to room temperature. The silver nanoparticles were in general stable in all solvents used when the reaction was preceded with PVP, whereas without the polymer the nanoparticle formation was not observed by Ultraviolet-visible spectroscopy for any solvents. The temperature has an important role in the nanoparticle growth, because the formation rate of nanoparticles is accelerated resulting in larger particles. Variation in the peaks intensity were observed by UV-vis spectroscopy, which indicates that of increase in the full width half maximum should be related with the particle growth (see graphic of ***annex B***). Solutions with particle sizes more stable were observed in Ethylene Glycol and 1,2-Propanediol, which are consistent with previously published result [149], in which show a narrow particle size distribution and uniform absorption peak as shown in ***Figure 11b***.

Table 2. Effect of PVP on the chemical reduction and agglomeration of silver nanoparticles in different solvent to room temperature and 90ºC.

	PVP = 80 mg (rt)			PVP = 80 mg (90ºC)			PVP = 0 mg (rt)			PVP = 0 mg (90ºC)		
[Co] solvente	λ (nm)	I λmax (a.u.)	FWHM (nm)	λ (nm)	I λmax (a.u.)	FWHM (nm)	λ (nm)	I λmax (a.u.)	FWHM (nm)	λ (nm)	I λmax (a.u.)	FWHM (nm)
PROP	404,3	1,562	47,07	411,7	3,221	71,14	406,2	2,192	63	411,1	4,032	49,868
MM	419,2	1,324	79,64	413,9	1,496	73,4	--	--	--	--	--	--
H2O	--	--	--	421,7	0,428	109,2	--	--	--	418,3	0,485	107,6
EG	417,8	1,108	96,74	410,1	4,256	73,85	417	1,458	85,18	410,6	3,151	66,76
PVA	411,4	0,384	70,3	411,1	1,063	79,43	411,2	0,32	69,95	410,3	0,73	75,93

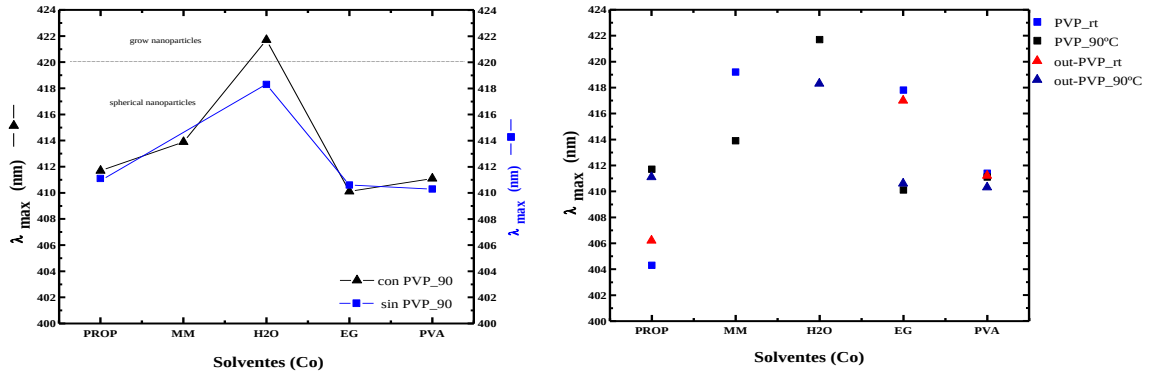

Figure 11. PVP effect over the silver nanoparticles formation using different solvents.

The environment in which one nanoparticle is embedded also affects the optical response of the same. The ***Figure 9***, show the absorbance band of spherical silver nanoparticles solution embedded in different media, with refractive indices η_{med} different. The increase in the refractive index of the host material induces a red shift in the plasmon $\lambda_{PROP} < \lambda_{PVA} < \lambda_{EG} < \lambda_{MM} < \lambda_{H2O}$ (displacement toward longer wavelength as shown in the ***Table 2***), the subscript indicates the refraction indices of the medium and the dipole resonance position to room temperature and 90ºC. The intensity is also affected as the η_{med} value increase, for example, to η_{PROP} the intensity is close to 1.6 when the solution is prepared at room temperature; while η_{MM}, η_{PVA}, η_{H2O} are lower at room temperature. However, when the solutions were prepared to 90ºC the η_{med} changed inducing to change in the plasmon position $\lambda_{EG} < \lambda_{PVA} \approx \lambda_{PROP} < \lambda_{MM} < \lambda_{H2O}$ and the intensity $I_{EG} > I_{PROP} > I_{MM} > I_{PVA} > I_{H2O}$ for the different medium. Finally, when the η_{med} increase, the spectrum intensity decreases a room temperature, while increase a 90ºC as shown in the graphic of the ***annex B***. The changes caused by the reaction medium in the optical response of the silver nanoparticles, are mainly due to the medium is able to absorb and disperse the electromagnetic field and the effect of PVP capping, so what we see is a reflection of the light interaction with particle-medium system [150].

1.8.3. Silver nanoparticles homogenize in H2O using SC-NaBH4

The preparation of a silver nanoparticles precursor solution takes place according to the following method: silver nitrate was dissolved in an aqueous solution the poly (vinyl pyrrolidone) powder, continued by addition sodium citrate; the process was accompanied by vigorous stirring at room temperature during all time. After this step the solution was stored in tinted glass bottle. Then sodium borohydride in different concentrations was quickly mixed in the solution in ambient condition. Formation of silver spherical nanoparticles was observed during this process by transmission microscopy and UV-visible spectroscopy. Because the color of light scattered (yellow) by nanoparticles depends upon their size, it is possible to estimate that these particles have sizes around 20 nm. In good agreement with results obtained by ED and XRD measurement pattern showing the 111, 200, and 220 reflections of metallic silver particles crystallized in the face centered cubic (fcc) structure (see annex A). Absorption spectra of colloidal solutions of Ag nanoparticles are shown in ***0***. The silver particles have a narrow size distribution as can to be seen in the figure, with an absorption band around 410 nm. The spectrum of the nanoparticles exhibits decreasing absorption intensity when the sodium borohydride concentrations increase. The growth of silver nanoparticles was observable within a few minutes of the addition of sodium borohydride and no apparent change was seen after 30 min. However, the mixture was kept at room temperature all night to complete the growth of nanoparticles. UV-visible absorption spectroscopy carried out during and after the reaction showed the appearance of only one surface plasmon peak. The color solution was yellow, indicating the formation of nanoparticles.

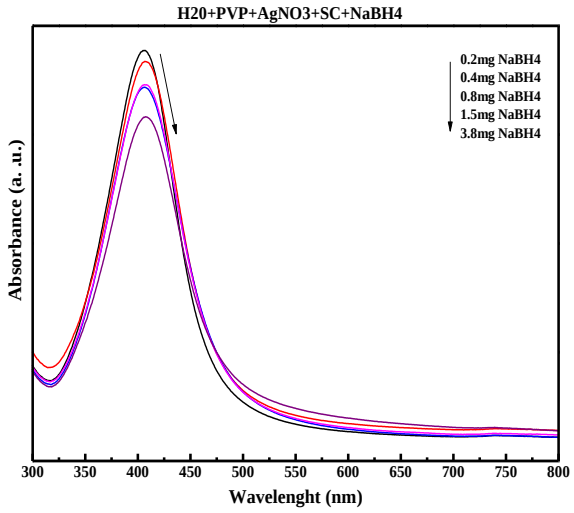

Figure 12. UV-Vis spectrum of silver spherical nanoparticles colloidal suspension with different concentrations of NaBH4 [0.2-3.8 mg] to room temperature.

The aspect ratio can be tuned by varying the concentration of NaBH4 added to the growth solution. It was observed that the aspect ratio increase with decrease in the concentration of sodium borohydride used, forming a well-defined nanoparticle in the presence of surface stabilizing as PVP and Sodium Citrate (SC) (***Table 3***). We considerate that the sodium citrate acts as a buffer to maintain neutral or weakly basic pH of the solution by reaction with the nitric acid as it is generated. Besides, citrate complexes silver and then associates with Ag^+ ions on a surface of a growing nanoparticle, covering the surface negatively charged and electrostatically preventing nanoparticles from agglomerating. Other role of citrate is the possible stabilization of close packed (111) planes in silver nanoparticles.

Table 3. Kinetic growth of silver nanoparticles mediate by SC-NaBH4

[NaBH4]	SC = 0 mg			SC = 60 mg		
	$I_{\lambda max}$	λ max	FWHM	$I_{\lambda max}$	λ max	FWHM
0,2	0,716	414,50	87,514	1,649	402,90	86,014
0,4	0,873	405,90	71,022	1,559	405,10	91,009
0,8	0,853	409,50	64,762	1,492	405,90	93,453
1,5	0,753	401,50	76,936	1,491	406,50	92,471
3,8	0,576	394,60	98,991	1,312	407,00	91,473

A plot of maximum absorbance intensity and full width half maximum (FWHM) of the set of the prepared silver nanoparticles in water with or without sodium citrate as a function of sodium borohydride concentration is presented in ***Figure 13***. The solutions prepared with sodium citrate shown a full width half maximum most narrow that the samples without this, indicating spherical silver nanoparticles well defined, while the other samples shown anisotropy.

Citrate plays the dual role of reductant and stabilizer, reducing silver to colloidal silver clusters, where virtually all of the silver starting material is converted to product, demonstrating excellent atom economy. The addition of an amount of sodium citrate increased the reduction reaction especially the nucleation. Thus, a larger number of silver nuclei were achieved and possibly more polycrystals formed, which lacked the potential to grow into particles. After nucleation, high-efficiency citrate was almost consumed and sodium borohydride continued to reduce silver salt, leading to subsequent growth spherical particles. The stability of colloidal and nanoparticles solutions is attributed to the collective effects of van der Waals interactions, electrostatics, and steric forces [151].

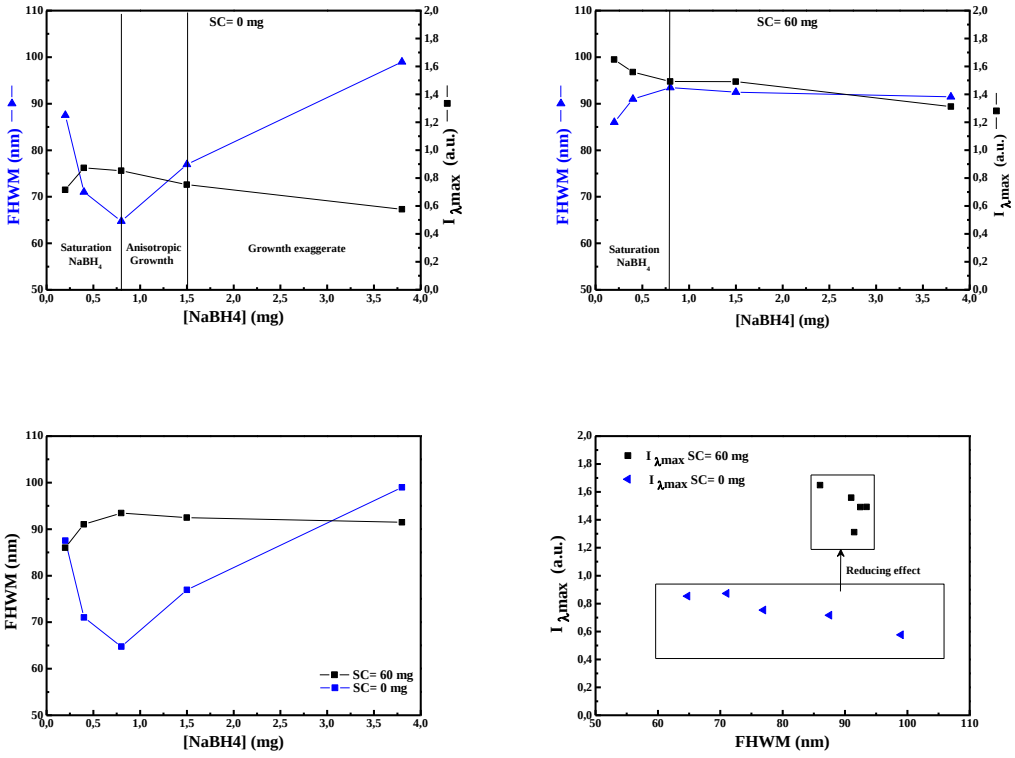

Figure 13. Maximum absorbance intensity and FWHM versus NaBH4 concentration of colloidal silver nanoparticles prepared in water with or without sodium citrate.

1.9. Summary

Silver nanoparticles possess unique and fascinating optical properties that are useful for fundamental research as well as for various technological applications. Besides size, shape is an important parameter that can be used to easily manipulate the optical properties and functionalities. Many properties of silver particles do not change significantly from their bulk counterparts; certain properties are sensitive to the atomic details that require further theoretical and experimental studies.

Stable colloids of Ag spherical nanoparticles were obtained in different reaction media using a simple wet-chemical route. The non-ionic surfactants (Propanediol, Methoxyethanol, Ethylene-Glycol, Polyvinyl Alcohol) form a shield-like layer on the surface of the silver nanoparticles, which lets only the first formed nuclei to grow up to the final silver nanoparticles. After the initial stage there are not produced any other new nuclei because of the inhibiting effect of the formed protecting layer formed by the surfactant molecules. Therefore the polydispersity of the prepared silver nanoparticles has been significantly changed especially in contrast to the surfactant-free system. The non-ionic surfactants can thus be considered suitable for the preparation of monodisperse silver nanoparticles. However, still great attention must be paid to the initial concentrations of the reaction components.

We have studied the general behavior of the surface plasmon resonance on silver nanoparticles prepared in different reaction media in terms of their shape and surfactant used. UV-VIS spectra indicate that the position of the surface plasmon absorption peak of silver colloids shifts between 400-424 nm for the different solvents and temperatures used. This red or blue shift in the optical spectra of silver nanoparticles is related to an increase in particle size, a process that may involve reduction of silver ions adsorbed at the silver particle-solution interface. In conclusion, we found that the intensity and width of the surface plasmon resonance are sensitive to the nanoparticle morphology and temperature used during the synthesis. We also found that when the nanoparticles become anisotropic, the main resonance is blue shifted, overlapping other resonance, and increasing its full width half maximum. UV-VIS spectra showed that the location of surface plasmon resonance is sensitive to the dielectric environment and medium refractive index.

Silver nanoparticle were synthesized in water by means of borohydride method that involved the reduction of silver nitrate with sodium borohydride in presence of poly (vinyl pyrrolidone) and sodium citrate as stabilizing and surface modification respectively. The nanoparticles were stable when the sodium citrate was added, while anisotropic nanoparticles were observed without sodium citrate. Citrate complexes silver and then associates with Ag^{+} ions on a surface of a growing nanoparticle, covering the surface negatively charged and electrostatically preventing nanoparticles from agglomerating. The role of citrate is the possible stabilization of close packed (111) planes in silver nanoparticles.

Chapter II

Silver Nanoprisms Synthesis

II. OVERVIEW

2.1. Silver nanoprisms

Metal nanoparticles are among the most promising systems for applications mainly because of their characteristic large electric-field enhancement. The plasmon-resonance conditions depend on a number of parameters, such as particle size, surface charge, the nature of the dielectric environment, and inter-particle coupling, but the particle morphology has been shown to play a fundamental role. [152][153][154][155][156] Applications of metal nanoparticles are already well established. Since the formation of anisotropic nanoparticles also provides a convenient tool to control the optical response, mainly through variation of the aspect ratio, [153][154][155][156][157] new methods to produce disks, [158][159] rods and wires, [160][161][162][163] and prisms [5][6][7][8][9][10][11][12][13][14][15][16][17][18][19] have been rapidly developed in the last few years.

Recent publications have focused on the synthesis and optical characterization of gold [5][6][7][8] and silver nanoprisms [9][10][11][12][13][14][15][16][17][18][19] because of their unusual optical properties, which result in surface-plasmon resonance (SPR) peaks at relatively long wavelengths [14]. Focusing on silver, various physical and chemical procedures have been devised to fabricate nanoprisms. Example of physical technique to prepare Ag nanoprisms is nanosphere lithography (NSL) [166][167] or vacuum deposition [168][169][170]. Although these nanofabrication techniques have been demonstrated to be an alternative to solution-phase methods, the chemical methods are more versatile. So far, two main chemical approaches can be identified: chemical reduction of metal salts [9][10][11][12][13][164] and photoinduced aggregation of small nanoparticle seeds [14][15][16][17][18][19][165]. The photochemical routes provide more monodisperse samples and greater control over structural parameters through judicious selection of irradiation wavelengths. In contrast, the thermal routes involve the gradual conversion of colloidal silver nanoparticles into silver nanoprisms. None of the synthesis methods developed thus far provides a study on the agent's effect in the silver nanoprisms formation, and low aspect ratio PVP: $AgNO_3$ or the area to pattern or coat is substantially limited.

In this section, we present the preparation of triangular silver nanoprisms using a room temperature route that allows the growth of nearly unimodal distributions, so that the in-plane dipole plasmon resonance is shifted to wavelengths above 600 nm. We discuss the structural and optical properties of the obtained Ag nanoprisms using (scanning and transmission) electron microscopy techniques and UV-visible spectroscopy. Finally, we propose a mechanism for the formation of the nanoprisms on the basis of optical measurements.

2.2. Experimental Description

2.2.1. Silver nanoprisms colloid preparation

An PVP:AgNO3 precursor solution prepared initially by chemical reduction method, which consist of reduction the silver nitrate (AgNO3, 3.9 mg, 23 µmol) in 200 ml deionized water in the presence of poly(vinyl-pyrrolidone) (PVP, 80 mg, 2 µmol), which acts a capping reagent. The solution was stirred at room temperature until silver nitrate dissolved. Then, sodium citrate and hydrogen peroxide were added to solution under constant stirring at 400 rpm. Sodium borohydride, which acts as reducing agent, was injected to form silver nanoprisms at room temperature in air. The solution was prepared in a glass beaker-200 ml, using mass ratio of PVP to $AgNO_3$ from 0.2:1 to 10:1. Sodium citrate, hydrogen peroxide and sodium borohydride concentrations were 10-100 mg (0.034-0.34 mmol), 10-1000 µL (0.0971-9.71 mmol), and 0.2-3.8 mg (5.28-100.4 µmol) respectively. The ***Table 4*** summary the concentration used during the synthesis of silver nanoprisms.

Table 4. Summary of different synthesis conditions

Experim.	[PVP]	[AgNO3]	[SC]	[H2O2][1]	[NaBH4][1]
A	80 mg (2 µmol)	3.9 mg (23 µmol)	10-1001[1] (0.034-0.34 mmol)	0	0
B	80 mg	3.9 mg	0	10-70 µL (0.0971-0.679 mmol)	0
C	80 mg	3.9 mg	60 mg (0.204 mmol)	10-70 µL (0.0971-0.679 mmol)	0
D	80 mg	3.9 mg	0	0	0.2-3.8 mg (5.28-100.4 µmol)
E	80 mg	3.9 mg	60 mg (0.204 mmol)	0	0.2-3.8 mg (5.28-100.4 µmol)
F	80 mg	3.9 mg	0	10-70 µL (0.0971-0.679 mmol)	0.2-3.8 mg (5.28-100.4 µmol)
G	80 mg	3.9 mg	60 mg (0.204 mmol)	10-70 µL (0.0971-0.679 mmol)	0.2-3.8 mg (5.28-100.4 µmol)
H	80 mg	3.9 mg	0	10-1000 µL (0.0971-9.71 mmol)	8 mg[2] (0.211 mmol)
I	80 mg	3.9 mg	60 mg (0.204 mmol)	10-1000 µL (0.0971-9.71 mmol)	8 mg[2] (0.211 mmol)

The base reaction was carried out in 200 ml water. [1]This concentrations were added to 10 ml of solution. [2]Solution prepared in 24 ml of water and 2.7 ml were added to 10 ml.

Finally, samples of the colloid were stored in transparent and tinted glass bottles, exposed to normal laboratory light, to direct sunlight and kept in the dark, to study their stability at different storage conditions.

The optical absorption features of Ag colloids in the UV-Vis range from 200 nm to 800 nm wavelength were measured using a spectrophotometer UV-Vis Shimadzu UV-2101 and the morphology of the silver nanoprisms was studied using a Hitachi 800 transmission electron microscope operating at 200 KV. For electron microscopy, portions of each colloid were centrifuged at 20,000 rpm for 10 min, in order to concentrate the silver nanoprisms in the liquid. A drop of the solution was dispersed in ethanol and place onto a carbon coated grid and allowed to dry. The solutions could be diluted with ethanol without affecting their stability.

2.3. Results and discussion

2.3.1. Formation of triangular silver nanoprisms

Silver nanoprisms are synthesized via chemical reduction of silver nitrate. Following the above synthesis, the concentrations of silver nitrate, poly (vinyl pyrrolidone) and trisodium citrate were set as show in the ***Table 4***, and the concentration of hydrogen peroxide and sodium borohydride was changed from 0 to 486 mM and 0 to 10.04 mM for different experiments. First, the solutions of silver nitrate, poly (vinyl pyrrolidone) and trisodium citrate were mixed in the flask at room temperature, and then different amounts of hydrogen peroxide and sodium borohydride solution was added dropwise into 10 mL of the base mixture.

When the sodium citrate and hydrogen peroxide are added before NaBH4 (sodium borohydride) were observed shape silver triangular nanoprisms as it is show in the representative micrograph of ***Figure 15*** obtained by Transmission electron microscopy (high resolution). The solution acquires first a yellow color, but immediately after changed to blue, violet, purple and brown when were combined with varying amounts of hydrogen peroxide as shown in the digital photography of the ***Figure 14***. The UV–Vis measurements of the colloidal nanoprisms clearly reflect their anisotropic shape. Because of three peaks appear at 682 nm, 480 nm and 333 nm and the characteristic peak for spherical nanoparticles at 410 nm. The next ***Table 5*** shows the conversion process of colloidal silver nanoparticles toward silver nanoprisms and the color observed in the solution during the reaction, so as the pH of the solutions before/after of the addition the hydrogen peroxide and sodium borohydride.

Table 5. Conversion process of nanoparticles toward nanoprisms from AgNO3 by a H2O2 oxidative process

SAMPLES	VOLUME (mL)	BASE SOLUTION	[H2O2] (mL)	pH=9,332 [NaBH4] (mL)	COLOR SOLUCION	pH after [H2O2] add.	pH after [NaBH4] add.
REF	20	H2O+PVP+AgNO3+SC	0	0	s/color		
SS	20	H2O+PVP+AgNO3+SC	0	2,7	amarillo	6,908	9,012
S1	20	H2O+PVP+AgNO3+SC	10	2,7	amarillo	6,912	9,099-9,1
S2	20	H2O+PVP+AgNO3+SC	20	2,7	amarillo-ambar	6,914	9,118-9,089
S3	20	H2O+PVP+AgNO3+SC	30	2,7	ambar claro	6,919	9,021-9,09
S4	20	H2O+PVP+AgNO3+SC	50	2,7	ambar oscuro	6,902	9,068-9,071
S6	20	H2O+PVP+AgNO3+SC	60	2,7	color tierra	6,912	8,665-8,659
S11	20	H2O+PVP+AgNO3+SC	62	2,7	verde-azul	6,869-6,873	9,16-9,18
S12	20	H2O+PVP+AgNO3+SC	65	2,7	azul-violeta	6,855-6,858	9,17-9,18
S5	20	H2O+PVP+AgNO3+SC	70	2,7	violeta oscuro	6,908-6,891	9,0-9,1
S7	20	H2O+PVP+AgNO3+SC	100	2,7	azul-violeta oscu.	6,908-6,930	9,13-9,20
S0	20	H2O+PVP+AgNO3+SC	200	2,7	azul oscuro	6,908-6,872	9,04-9,09
S14	20	H2O+PVP+AgNO3+SC	300	2,7	azul fuerte	6,860-6,922	9,145-9,141
S13	20	H2O+PVP+AgNO3+SC	400	2,7	azul claro	6,850-6,854	8,961-8,871
S9	20	H2O+PVP+AgNO3+SC	500	2,7	violeta palido	6,785-6,771	8,896-8,872
S10	20	H2O+PVP+AgNO3+SC	1000	2,7	s/color	6,632-6,635	7,765-7,767

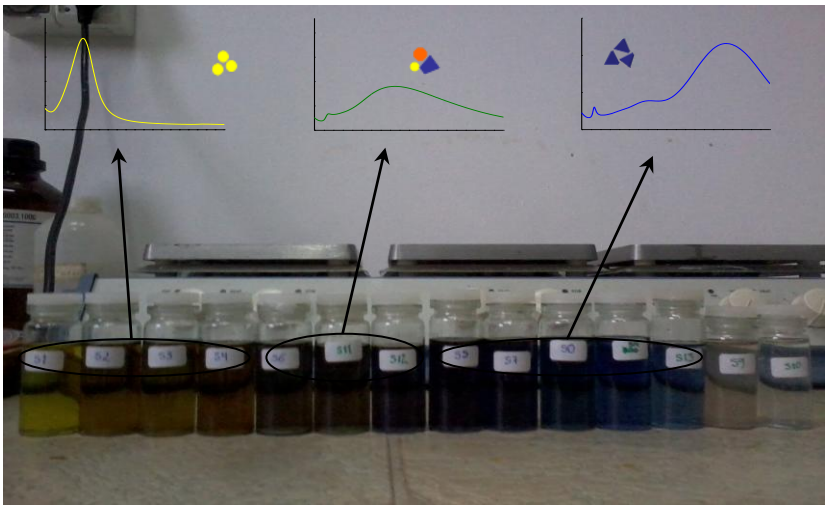

Figure 14. Digital photography of Silver nanoprisms colloid suspensions.

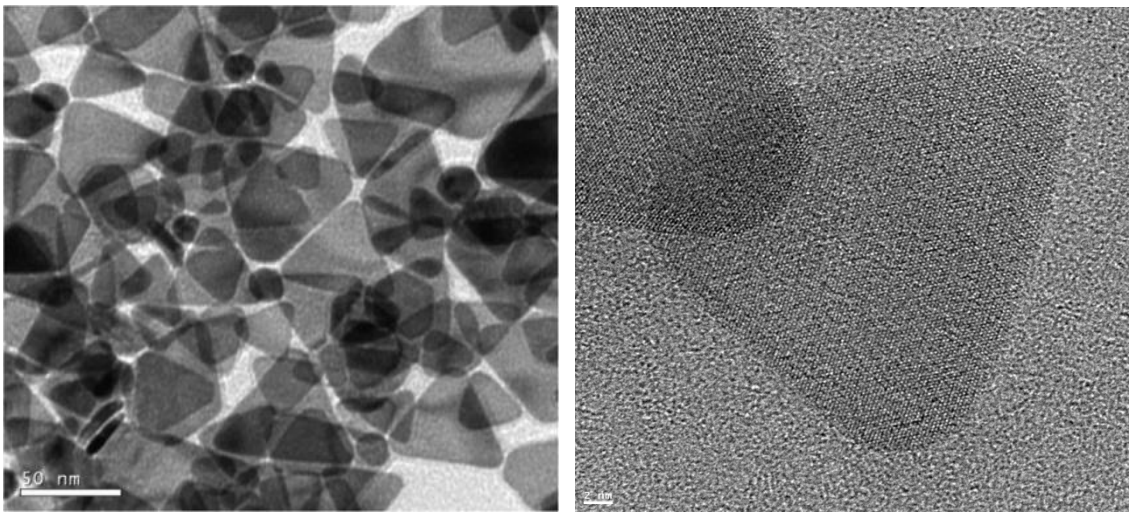

Figure 15. TEM micrograph showing triangular silver nanoprisms obtained in solution by reduction of silver ions at room temperature.

2.3.2. Influence of different parameters of the solution on silver nanoprisms growth

A study focused on the effect of PVP, sodium citrate, hydrogen peroxide and sodium borohydride concentration on the synthesis of nanoprisms provided insight into their roles in this process. The reactions were followed by UV-visible spectra to further understand the shape evolution from silver nanoparticles to nanoprisms. First, unstable silver anisotropic particles were observed when the PVP was no added or a low concentration (0.1 mg) was used; requiring the presence of one PVP amount appropriate, as was describe in the next experiment. On other hand, the sodium citrate concentration was varied with a fixed PVP concentration and without change the silver nitrate concentration. The solution was completely transparent without formation of nanoparticles and only weak absorbance was detected (*gray line*, ***Figure 16b***). By other hand, when the sodium citrate was omitted from reaction mixture, various hydrogen peroxide concentration had no effect in the nanoprisms formation when is incorporate immediately after the $AgNO_3$. Neither, change some was observed when the SC (Sodium Citrate) was added before/after the hydrogen peroxide; as be observed in the graphs of the ***Figure 16 (a, b)***, only one increase in Ag+ ions concentrations was detected.

In our study over aqueous $AgNO_3$ solutions, we determinate that metal ions may be complexed as larger units of anions, ligands, or solvent molecules and their presence can influence reaction outcomes. We considerate than a high amount of Ag clusters as Ag^+, $[Ag_2(NO_3)]^+$, Ag_3^+, $[Ag_3(NO_3)_2]^+$ are formed when the $AgNO_3$ powders are dissolved in water [171]. All these clusters have a stronger affinity for electrons than Ag^+, making them more favorable sites for nucleation and growth once a reductant is introduced, according to electron microscopy studies where the reduction of these $AgNO_3$ solutions with a reducing agent and poly (vinyl-pyrrolidone) (PVP), yields triangular nanoplates [172].

The samples with sodium borohydride before and after sodium citrate are shown in the graphs of the ***Figure 17***. When we sodium borohydride added after other reagents (sodium citrate) the liquid acquires a yellow color. The yellow colour is caused by well crystallized spherical silver nanoparticles with diameters around 20 nm, the which are formed by the reduction the silver ions to different sodium borohydride concentrations (***Figure 17b***). The UV-Vis measurements of the Ag nanoparticles of the ***Figure 17*** exhibited a single peak at 410 nm, independent of the nanoparticles concentration, in good agreement with result and predictions for spherical silver nanoparticles of size between 3 nm and 20 nm [147][148]. When sodium borohydride was added immediately after the silver salt as is shown in the spectra of the ***Figure 17a***, the sodium borohydride reduced the silver ions producing anisotropic particles without one well defined shape.

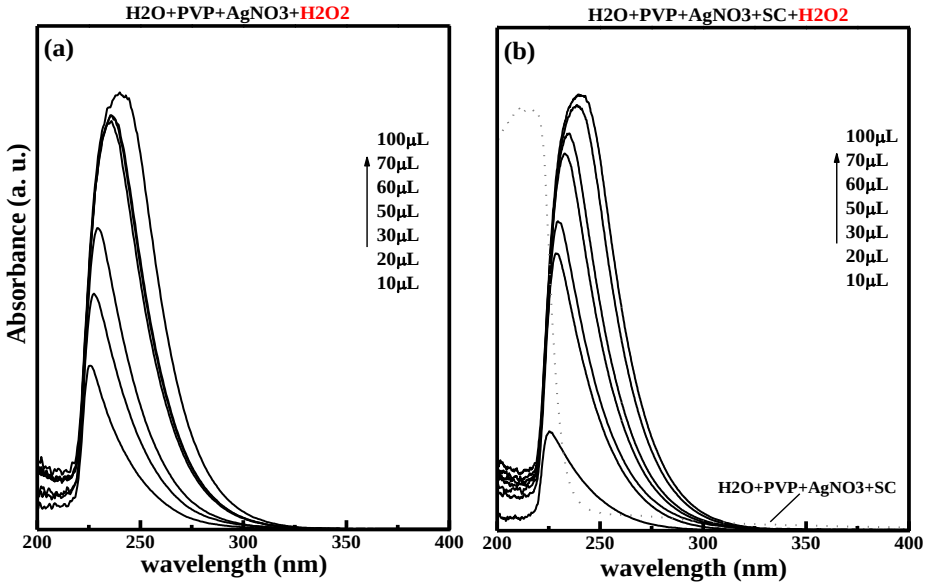

Figure 16. UV-Vis spectrum of colloidal suspensions with different concentrations of H2O2 [70-100 *µL*].

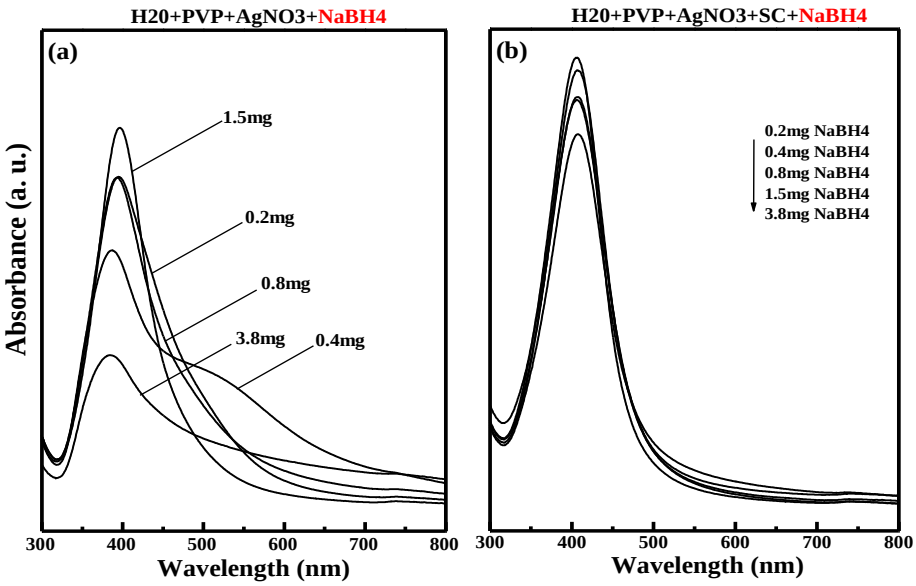

Figure 17. UV-Vis spectrum of anisotropic silver nanoparticles formed with increasing amount of NaBH4 [0.2-3.8 mg]: (a) without sodium citrate, (b) with sodium citrate.

The effects of the hydrogen peroxide and sodium borohydride were observed when they were added immediately after the SC (Sodium Citrate). We determinate that to high concentrations of hydrogen peroxide and low sodium borohydride concentrations, silver nanoprisms are obtained like it are shown in the graph of the ***Figure 18b***. The band absorption to 0.4 mg of sodium borohydride and 70 µL of hydrogen peroxide show that the peak at longer wavelength became dominant. This bands in the region of 600-700 nm as well in the one 340 nm approximately, correspond to the in-plane dipole plasmon and out-of-plane quadrupole resonance, suggested the formation of silver nanoparticles with triangular nanoprisms structure at the end of the reaction. Only, for-

mation silver nanoparticles were observed for solutions that contained sodium citrate before hydrogen peroxide and sodium borohydride, but with a low concentration of hydrogen peroxide as those that are shown in the ***Figure 18c***. The broad absorbance peak could be associated with increase of the particle size. The graph **(*a*)** shows the formation of silver nanoparticles when the sodium borohydride concentration was increasing, indicating the precursor was consumed gradually and simultaneously, the intensity of the absorbance around 400 nm increased.

Then we can deduce that the sodium citrate no has a direct effect on the conversion of Ag spherical nanoparticles to prisms. Therefore, the sodium citrate controls the oxidative and reducer effect when the hydrogen peroxide and sodium borohydride are incorporate after the sodium citrate in order, resulting in a controlled microstructure the silver nanoprisms. In the UV-VIS spectrum of the ***Figure 19b*** can be observed that with concentrations of 10 µL and 70 µL of hydrogen peroxide (H2O2) [fixing the other concentrations], silver nanoprisms were obtained with very good microstructure in accordance with measurement realized by transmission electron Microscopy.

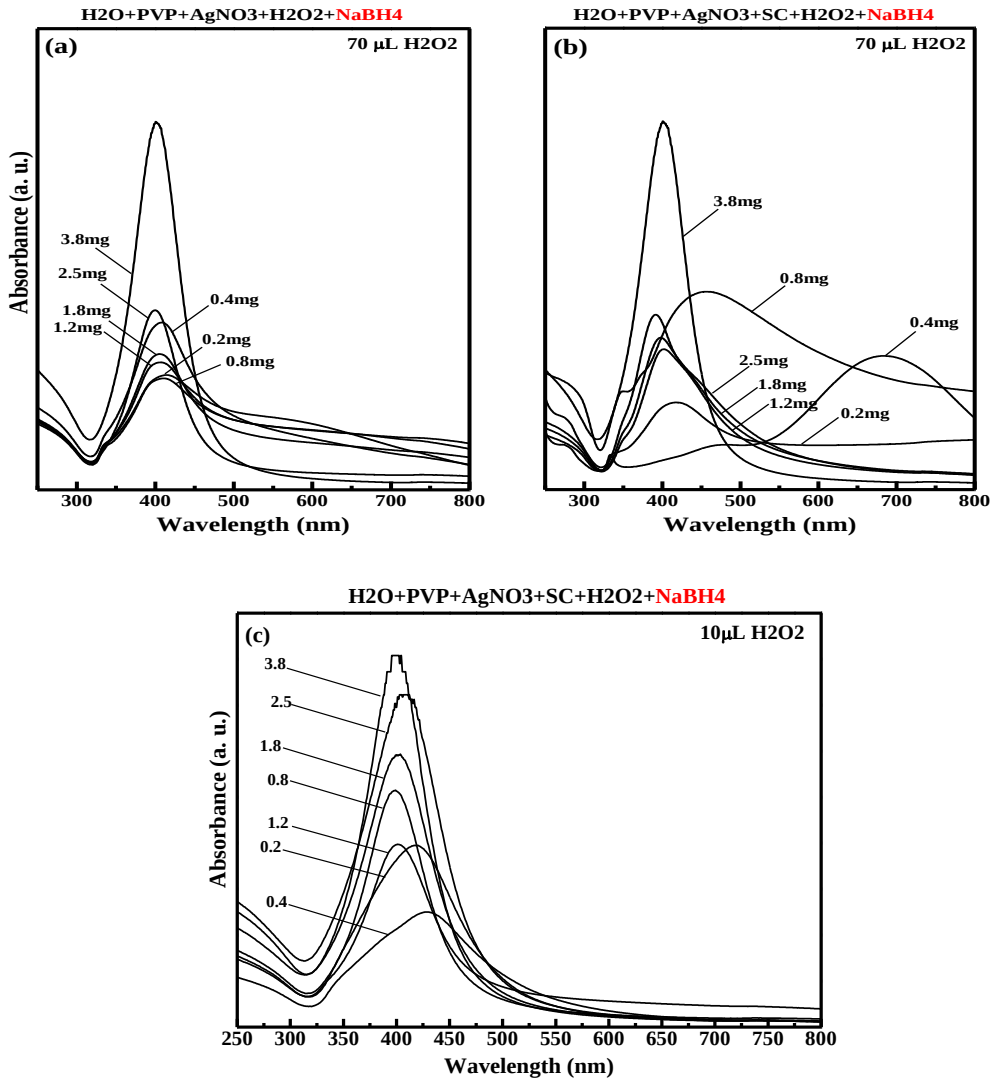

Figure 18. UV-Vis spectrum of anisotropic shape silver nanoparticles prepared using (a), (b) 70 *µL* of H2O2, (c) 10 *µL* of H2O2. To different NaBH4 concentrations [0.2-3.8 mg].

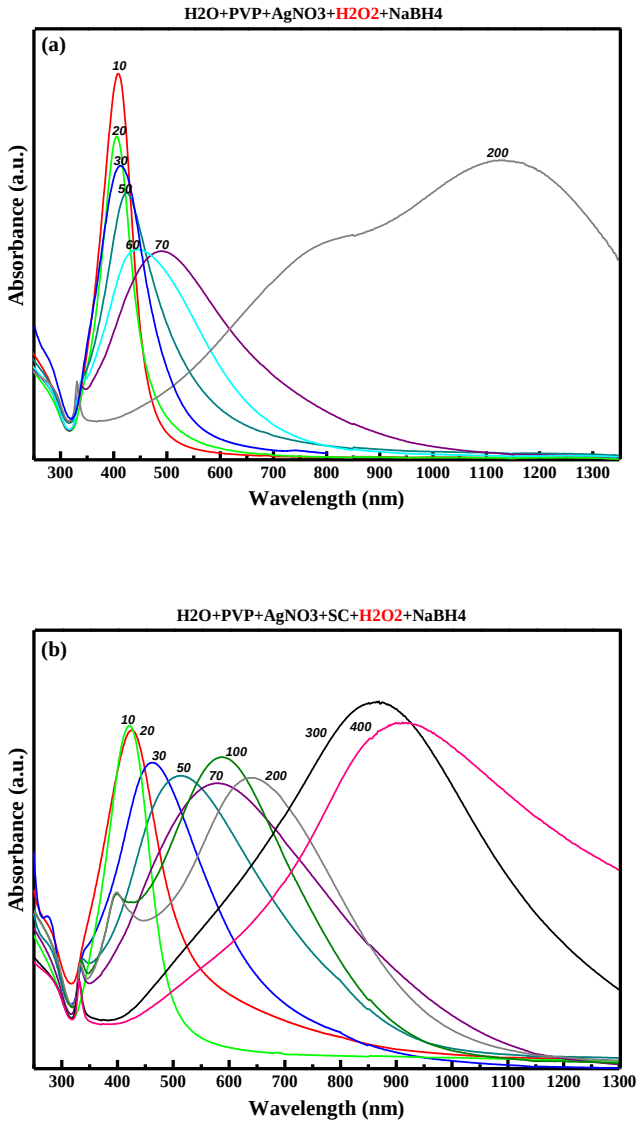

Figure 19.H2O2 concentration-dependent UV-Vis spectra showing the conversion of silver nanospheres to nanoprisms, (a) without sodium citrate, (b) with sodium citrate.

When the sodium citrate and hydrogen peroxide are added before sodium borohydride, the solution acquires first a yellow colour, but after one hour, the colour had change to different shades for the interval of concentration of hydrogen peroxide, as show in ***Figure 19b***. The morphological study of the nanoparticles by TEM clearly reveals that the presence of sodium citrate and hydrogen peroxide during the reduction of silver ions results in growth of triangular silver crystallites (***Figure 15***). However, without the use of citrate (***Figure 19a***), the formation and excessive growth of silver nanoparticles with anisotropic structure were detected in the absorbance spectra due to rapid reduction of silver ions. The absorption peak experienced a shift to longer wavelength when the hydrogen peroxide concentration was increased, indicating the growth or agglomeration of the anisotropic particles.

The UV-Vis measurements of the colloidal nanoprisms clearly reflect their anisotropic shape. Instead of a single peak at 410 nm characteristic of spherical particles, three peaks appear at 682 nm, 480 nm and 333 nm and the peak characteristic for spherical nanoparticles at 410 nm is hardly distinguishable as a very weak shoulder. The same three peaks have been described in previous experimental and theoretical works [14] as characteristic of triangular nanoprisms and have been attributed to the in-plane dipole, in-plane quadrupole and out-of-plane quadrupole plasmon resonances. This interpretation of the UV-Vis measurements agrees with the TEM measurements showing only nanoprisms and no spherical particle. The results of image analysis of these micrographs indicate that the average particle size increases from 30 nm to 100 nm for different samples of reaction. For this interval of hydrogen peroxide concentration, the peak position of the SPAB shifts from 420 nm to 680 nm, thus confirming the dependence of the SPAB position on the average particle size, this can be observed clearer in the graph ***(b)*** of the ***Figure 19*** where the variation the hydrogen peroxide concentration produces a SPAB shift toward longer wavelength. The final product obtained, shown in ***Figure 15***, is composed of triangular silver nanoprisms with a very narrow size distribution.

The concentration of sodium borohydride employed in this reaction had a dramatic effect on the degree of conversion of silver nanoparticles to nanoprisms. The in-plane dipole surface plasmon band has been shown to be a good indicator of general nanoprisms architecture. Therefore, one can quickly assess the effect of different reaction parameters on the type of nanoprisms formed by evaluating the UV-Vis spectra of the colloids. For the concentrations studied over the 10-1000 μL range, different types of nanoparticles with anisotropic shape were obtained.

These observations supports our hypothesis that these clusters likely serve as nuclei for the addition and reduction of Ag^{+}, with the triangular shape being largely retained during the growth process. Also, we considerate that when the decomposition or reduction becomes considerably slow, the atoms tend to form nuclei and seeds through random hexagonal close packing (rhcp), together with the inclusion of stacking faults as have been reported in other works [173]. This type of synthesis has been known as kinetically controlled and the seed typically takes a shape derivate from those favored by thermodynamics. In first place, inclusion of stacking faults and/or twin planes can lead to the formation of a plate-like seed (***0***). A plate-like seed is covered by (111) facets at the top and bottom surfaces (plane A), together with stacking faults and/or twin defects along the vertical direction (plane B).

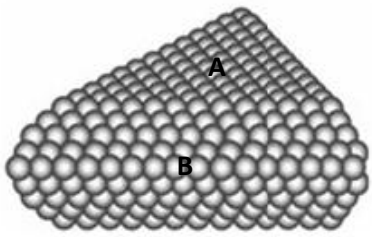

Figure 20. Schematic of a plate-like seed with a random hexagonal close-packed (rhcp) structure. Note that stacking faults and/or lamellar twins are introduced into the crystal lattice (B).

2.4. Effect oxidizing of H2O2 (oxidizing H2O2 - reducing PVP effect)

Analysis over the stability and the hydrogen peroxide effect on the formation of silver nanoprisms is described to continuation; so as a discussion on the possible mechanism of evolution or formation of the nanoprisms. Also we discuss the effect of different reducing agents (SC, H2O2 and NaBH4) on silver nanoprisms through intensity, FHWM and change in wavelength of absorption peaks of the UV-visible spectral. First, we analyze the silver nanoparticles formation and their conversion into silver nanoprisms, changing the sodium borohydride concentration as summarized in the ***Table 6***. These data were obtained from UV-visible spectra of the ***0*** described above. Where only silver nanoparticles formation was observed when the hydrogen peroxide concentration was very low. While structures as nanoprisms shape were found in colloidal solutions with higher hydrogen peroxide concentration (70 µL) and a low sodium borohydride concentration.

Table 6. Analysis of Intensity, λ max, and FHWM for anisotropic silver nanoparticles prepared using H2O2, and different NaBH4 concentrations

[NaBH4]	10 µL H2O2			70 µL H2O2					
	SC= 60 mg			SC= 0 mg			SC= 60 mg		
	$I_{\lambda max}$	λ max	FHWH	$I_{\lambda max}$	λ max	FHWH	$I_{\lambda max}$	λ max	FHWH
0,2	1,976	414,7	113,56	0,996	410,9	284,67	0,957	412,5	240,84
0,4	1,056	430,0	289,58	1,231	408,0	123,65	1,076	687,5	238,04
0,8	2,574	399,2	70,65	0,997	410,0	303,23	1,419	455,8	436,08
1,2	1,988	403,6	80,54	1,106	407,5	190,78	1,217	417,9	106,22
1,8	2,957	400,5	81,50	1,178	405,0	120,56	1,317	398,5	114,93
2,5	3,613	405,0	89,32	1,558	400,4	76,59	1,516	391,0	112,66
3,8	4,039	399,2	73,33	3,194	401,2	72,42	3,194	401,2	71,48

In our first analysis we took two critical concentrations of hydrogen peroxide and observed its effect on the formation of anisotropic particles. From UV-vis spectra we observe a clear increase in the intensity of the absorption peak when the concentration of reducing agent (NaBH4) increased, indicating reduction of silver salt and formation of silver particles. A low hydrogen peroxide concentration (10 µL) showed no effect during the reaction, we believe that only contributes to the rapid oxidation of the silver particles smaller towards Ag^{+} ions and then be reabsorbed by larger particles. However, the FHWM was higher only for a sample with 0.4 mg of sodium borohydride as seen in ***Figure 21c***, only a small region of low concentrations (between 0.2 to 0.8 mg of NaBH4) and a high hydrogen peroxide concentration (70 µL) showed a change in the FHWM of the absorption bands as observed in the graphs in ***Figure 21b***.

On the other hand, colloidal solutions prepared with sodium citrate and hydrogen peroxide concentration of 70 µL showed significant changes in UV-vis spectra. Formation of anisotropic silver nanoparticles (truncated prisms, triangular prisms) were observed in the solutions prepared with concentrations between 0.2-0.8 mg of sodium borohydride. In the graph in ***Figure 21a*** we see that the maximum absorption peak for samples prepared without sodium citrate and various sodium borohydride concentrations remained around 400 nm (black plot). While that the samples prepared in the presence of sodium citrate showed a shift of the maximum absorption peak toward longer wavelengths (blue plot). This shift observed in the range of 0.2-0.4 mg of sodium borohydride corresponds to anisotropic particles as shown in ***Figure 21***. Only truncated sil-

ver nanoprisms were produced without the presence of nanoparticles. This indicates that all starting material was converted to silver triangular prism or truncated. The presence of sodium citrate in the reaction plays a crucial role in the formation of silver nanoprisms, and various anisotropic shapes are obtained without sodium citrate (nanoparticles, oblate and prisms). ***Figure 21d*** shows the position of maximum absorption peak for samples prepared with two hydrogen peroxide concentrations. Therefore, we can say that only a small region of sodium borohydride concentration there is formation of stable silver nanoprisms, where particle formation were not observed.

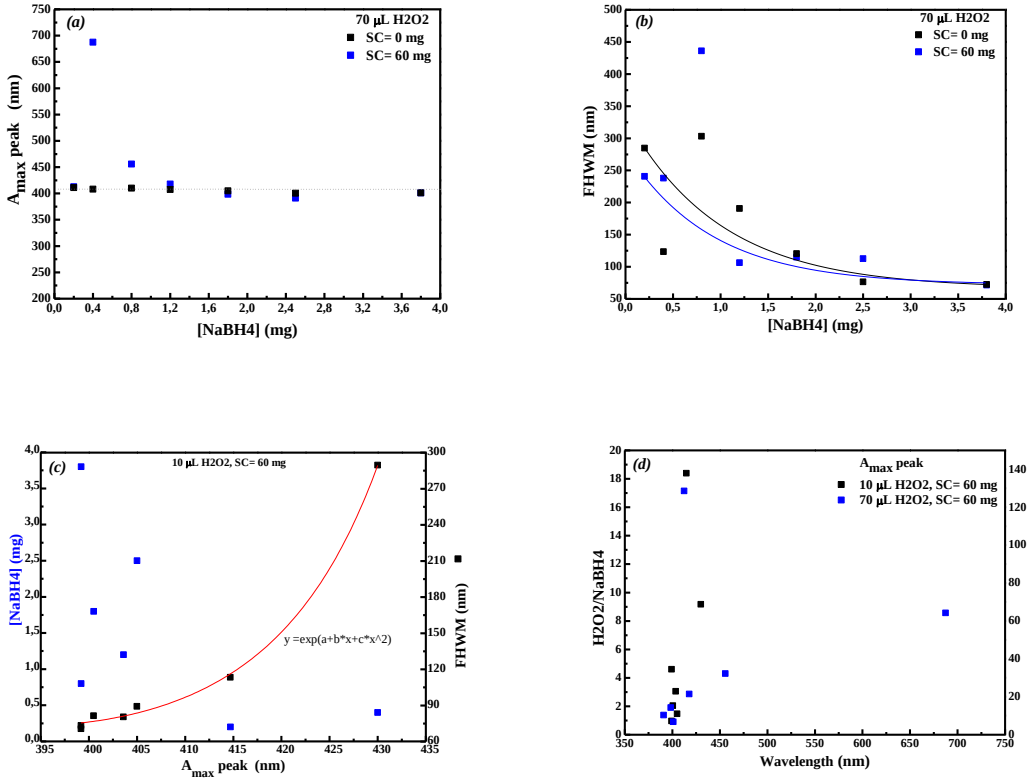

Figure 21. Correlation between FHWM, maximum Absorbance peak and NaBH4 concentration during the formation of silver nanoparticles and their evolution into anisotropic silver nanoparticles.

Having identified this area of concentration for the formation of stable nanoprisms, we analyzed the oxidative effect of hydrogen peroxide when was increased as summarized in ***Table 7***, where the sodium borohydride concentration remained constant. The oxidative effect of hydrogen peroxide has been studied due to the role that plays in the conversion of silver nanoparticles to nanoprisms.

Table 7. Analysis of λ_{max}, and FHWM of silver nanoprisms by reduction oxidative of the H2O2

[H2O2]	SC= 0 mg			SC=60 mg		
	$I_{\lambda max}$	λ max	FHWH	$I_{\lambda max}$	λ max	FHWH
10	1,2101	409,0	70,582	0,8118	421,0	95,328
20	1,0121	405,0	70,409	0,7213	425,5	103,758
30	1,5505	411,5	120,355	0,9421	463,0	213,498
50	0,8338	423,0	126,866	0,9018	514,5	305,105
60	0,6542	447,0	215,444	0,2706	418,3	137,885
60				0,3743	574,6	306,185
70	0,6494	489,0	270,603	0,5696	575,0	347,444
100				0,7371	590,6	362,360
200	0,9279	1147,8	758,706	0,6881	639,0	444,646
300				1,1303	863,8	544,049
400				0,2135	503,7	325,723

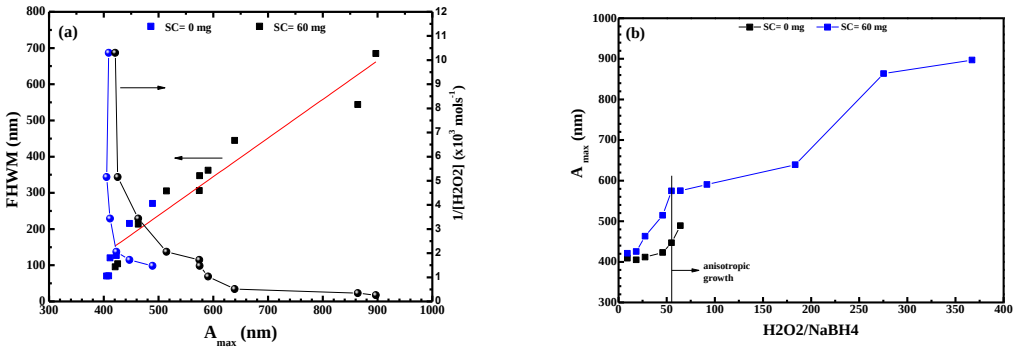

Figure 22. Maximum Absorbance band position versus H2O2 concentration and oxidative effect during their evolution into anisotropic silver nanoparticles.

The ***Figure 22*** shows the formation of prisms due to the oxidative effect of hydrogen peroxide has on smaller silver nanoparticles. The smaller nanoparticles were dissolved into Ag^{+} ions as the hydrogen peroxide concentration increased. The Ag^{+} ions were deposited on the surface of larger particles, contributing to the growth of silver nanoprisms as shown in ***Figure 22a***.

The Complexation and oxidation of Ag^{0} surface atoms of the nanoparticle due to H2O2 and $HO2^{-}$ should be the determining step in the reaction rate. However, the PVP used in the solution plays a dual role, acting as a stabilizer in the metal nanoparticles synthesis and has a retarding effect on the reaction rate (dissolution reaction). The Ag^{0} surface atoms are oxidized into Ag^{+} due to OH^{-} ions generated by the decomposition of hydrogen peroxide, and then quickly complexed (Ag^{+} cations) with molecular ligands or solvents present in the solution. Hydrogen peroxide is employed to facilitate formation of shape-selected nanoparticles, in our case the formation of silver triangular nanoprisms.

Silver nanoprisms were not formed in the solutions without sodium citrate, indicating that the reaction rate of the solution is much faster when the sodium citrate is not present in the solution; this is shown in the graph b of ***Figure 22***. The increase of hydrogen peroxide caused the complete oxidation of the silver ions, preventing the formation of small silver particles or prisms.

2.5. Colloidal solutions stable with time

Three samples of silver nanoprisms colloidal solutions were taken to analyze their stability over time. The UV-visible spectra shown in ***Figure 23*** correspond to three samples measured by UV-visible spectroscopy after preparation (M_1) and three years after preparation (M_2). The samples not showed any important change after the 3 years of they have been synthesized. The shift observed in all samples is attributed to possible agglomeration of nanoprisms at the solution by the time. These results show the effectiveness of chemical reduction method for the preparation of stable metal nanostructures colloidal solutions with technological applications.

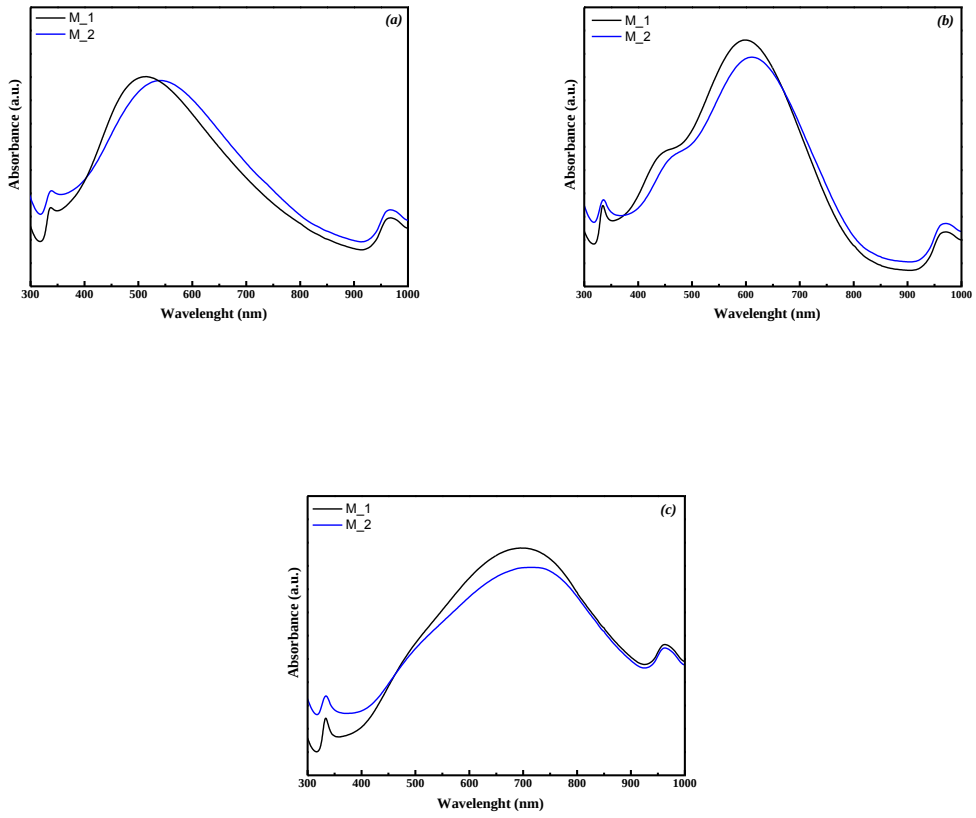

Figure 23. Stability analysis of silver nanoprisms solutions for three samples by Ultraviolet visible spectroscopy.

Finally, we propose one reaction mechanism for the anisotropic transition from silver nanoparticles to nanoprisms. Our results have revealed that silver nanoparticles or nanoprisms can be etched by several oxidizing agents under various reactions conditions. So as, the presence of hydrogen peroxide in combination with sodium citrate, polyvinylpyrrolidone (PVP), and sodium borohydride are important for the synthesis of silver nanoprisms.

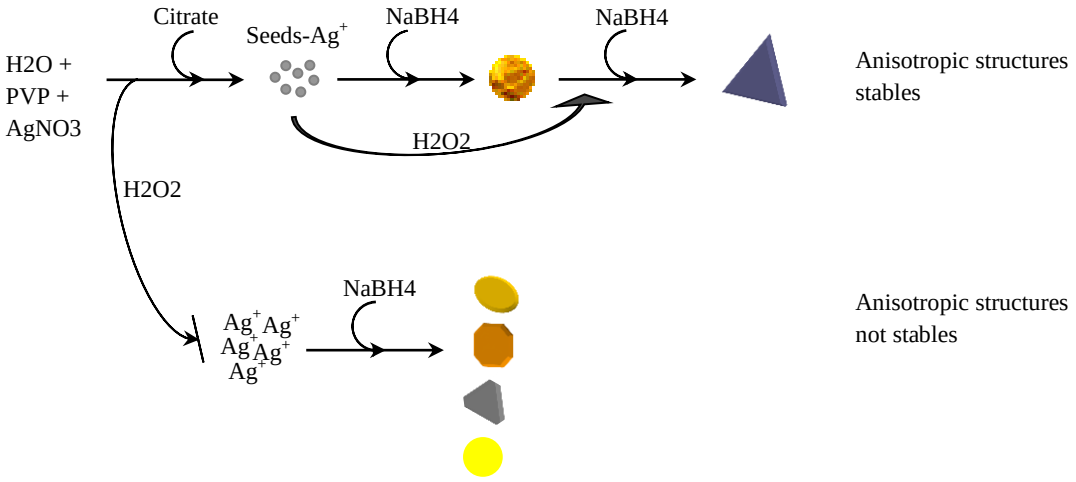

Figure 24. Reaction mechanism during the anisotropic transition of silver spherical nanoparticles to silver nanoprisms.

2.6. Dynamic Light Scattering Analysis (Photon correlation spectroscopy)

The samples were analyzed by Dynamic light scattering (DLS) to obtain the particle size distribution in the solutions. The results obtained are shown in the graphs of ***Figure 25***. These data represent the hydrodynamic diameter of the particle and not the real particle size. The hydrodynamic diameters is affected by the environment surrounding the particle and are calculated assuming isotropic spherical particle. Therefore, is important to determine by other characterization techniques (HRTEM, AFM) the real particle size. Meanwhile, for our study, we will have a representative data on the distribution size present in the solution show by the hydrodynamic size.

For the sample SS (with 0 µl of hydrogen peroxide and 0.4 mg of NaBH4) a hydrodynamic particle size of 66.1 nm is obtained, compared with the particle size observed by HRTEM of 20 nm. The thickness of the shell (40 nm) formed by the polymer that covers the particle is the difference between the two data obtained. However, for sample S1 and S3 (10 µl and 30 µl of hydrogen peroxide) three peaks of different diameters (r) are observed, as shown in the graph (*b*, and *c*). This result would indicate that the sodium citrate retains NaBH4 reduction effect, generating a distribution of particle sizes. This deduction is available only to particles, because of spherical geometry.

In the case of nanoprisms, the deduction of particle size by dynamic light scattering is more complicated, due to geometric anisotropy present in this structure. Therefore, we consider the values determined by dynamic light scattering as the approximate diameter (r) generated passing through the center to the ends of the prism. In the graphs (*d* - *f*), the 82% correspond to silver nanoprisms and the remainder to nanoparticles in growth. Also, we note that the nanoprisms percentage formed decreases with increasing hydrogen peroxide. In graph (*g*) a big peak (97%) is observed, indicating that we only have silver nanoparticles. We can deduce from the graphs that hydrogen peroxide increase have an oxidative effect on nanoprisms formed, reducing them to nanoparticles.

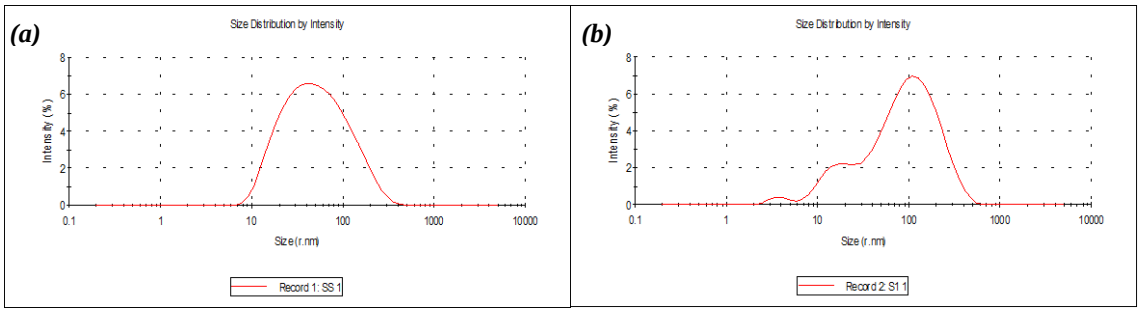

H_2O_2 = 0µL, r = 66.10nm (100%)

H_2O_2 = 10µL, r = 125.20nm (82.8%), 16.51nm (15.4%), 3.92nm (1.8%)

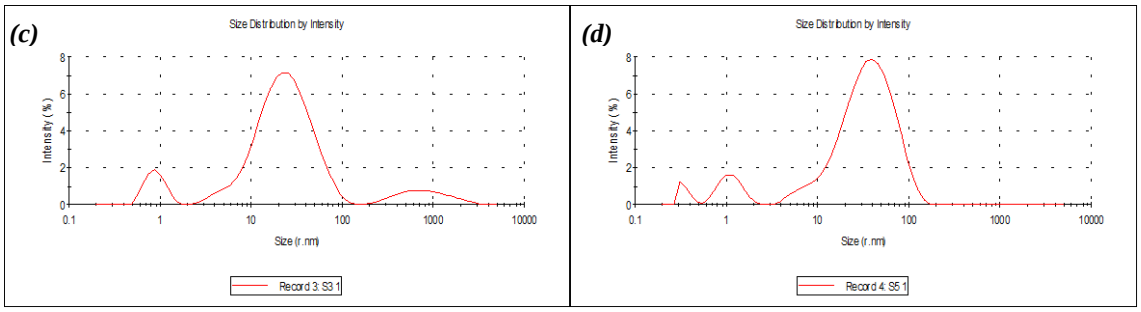

H_2O_2 = 30µL, r = 27.34nm (82.9%) 0.897nm (8.7%)

H_2O_2 = 70µL, r = 40.96nm (88.9%), 1.131nm (8.3%), 0.3558nm (2.8%)

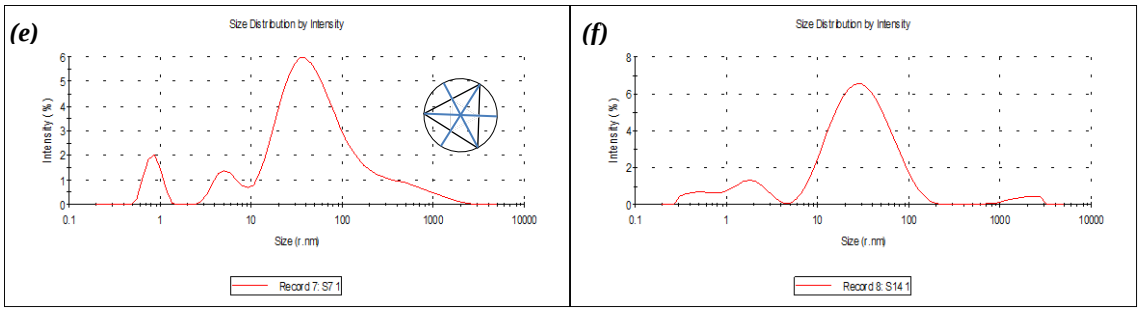

H_2O_2 = 100µL, r = 39.7nm (85%), 5.646nm (7.8%), 0.8512nm (7.2%)

H_2O_2 = 300µL, r = 36.82nm (82.9%), 1.766nm (10.2%), 0.5137nm (4.3%)

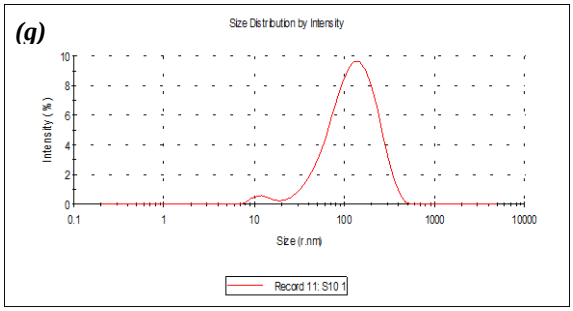

H_2O_2 = 1000µL, r = 141.7nm (97.6%), 12.4nm (2.4%)

Figure 25. Size distribution by Dynamic Light Scattering for different samples.

2.7. Summary

It is clear that nanoprisms can be formed under relatively mild reaction conditions, and that these prisms exhibit common optical and crystallographic features. There are still very few methods for controlling nanoprisms thickness, and the driving forces behind the growth of triangular nanoprisms are still not fully understood. A reduction method was developed for the synthesis of triangular silver nanoprisms. In this approach, a strong reductant (sodium borohydride), was employed to induce the reduction of silver nitrate and formation of small spherical silver nanoparticles at room temperature when was added immediately after of sodium citrate, and then the hydrogen peroxide was employed to induce the further oxidation of small particles into Ag^+ ions and their transformation into nanoprisms at room temperature.

We note that the sodium borohydride has a reduce effect on the silver; forming particles. When (SC + NaBH4) was added we observe formation of spherical particles with a uniform size distribution. Therefore, the silver nanoparticles growths are drastically reduce by sodium citrate.

Only silver nanoparticles were observed when hydrogen peroxide at a low concentration (10 µL) was added to the base solution (PVP + H2O + AgNO3 + SC) and the sodium borohydride concentration was increased. However, silver nanoprisms were obtained to a greater hydrogen peroxide concentration and a small range of sodium borohydride concentrations (0.4-0.8 mg). The increase of sodium borohydride in the solution caused the oxidative dissolution of the silver prisms to particles.

Smaller silver particles were produced when the sodium citrate and sodium borohydride were added to the solution. By the other hand, opposite effect was observed (large particles "excessive growth") when the sodium citrate was not added to the solution, so as in the solutions prepared with hydrogen peroxide plus sodium borohydride.

The concentration of two reductants ($NaBH_4$ and H_2O_2) was found to be critical in the formation of triangular silver nanoprisms. Such an approach provides a facile way to prepare silver nanoprisms capped only by PVP chains, which can be readily replaced by a variety of other ligands including biomolecules.

Silver nanoprisms solutions appeared blue-purple and showed an absorption maximum at longer wavelength. The oxidative effect was observed in solution with nanoparticles or nanoprisms. After added 2 ml of hydrogen peroxide to nanoparticles solution; the absorption maximum shifted from 421 to 397 nm; while the silver nanoprisms were dramatically reduced as shown in ***annex D***. With the increase of hydrogen peroxide concentration in the solution, the colour of the solution changed into to be colourless. These indicate that the corners of the silver nanoprisms are poorly capped by PVP. Due that the pH value decreases with the H2O2 increase; increasing the amount H^+ ions. So as the etchant ability to be stronger producing that truncation reaction occurs more quickly and oxidative dissolution of nanoprisms have place.

Hydrodynamic diameter analyses obtained by DLS indicate that the silver nanoparticles and nanoprisms are protected by a PVP-SC film with a large thickness. In the nanoprisms the thickness on the (111) plane is larger that on the (110) plane.

CHARTER III

FILMS

III. OVERVIEW

Nanocomposite polymeric films combine the attractive functional properties of nanoparticles with the advantages of polymers. [149][174][183] Due to the novel properties that are not present in the bulk, nanoparticles and nanostructured materials have received great attention in a wide variety of material science and engineering. A unique value of nanoparticles is their extremely high particle surface area; having many more sites for achieving property enhancements makes them ideal for a wide variety of applications as dispersions and coatings. Dispersive and coating applications of nanoparticles include optical, thermal, and diffusion barriers. Important technological advances have been achieved in the field of catalysis, [175] electrochemistry, [176] photoluminescence [177] and separation membranes. [178][179] In recent years, the development of functional nanoparticles and nanocomposite has attracted much attention because it allows the formation of nanostructures with well-defined physical properties. Also in the semiconductor industry, a monolayer or thin film coating of atoms or molecules is deposited on foils, metal sheets, or glass to enhance storage capacity and accelerate responses from the electronic component.

Among many inorganic nanoparticles, silver nanoparticles have been intensively studied because electrical, [180] mechanical, [181] and antibacterial properties [182] can be enhanced by adding nanoparticles to polymers. Nanocomposite films containing silver nanoparticles have potential as surface conductive polymeric tapes, and metal contacts for VLSI circuits [183]. These films are also candidates for integral capacitors because they are easy to process at low temperature and exhibit high dielectric constant.

In particular, they play important roles for the possible applications to catalysis, [184] surface-enhanced Raman spectroscopy (SERS) [185] and facilitated olefin transport [186]. Several methods to grow thin films of inorganic compound semiconductors are taking vital roles in the advancement of technologies. To obtain precision in the performance of thin film based devices, control over the film properties is necessary. Therefore, many sophisticated techniques namely, vacuum evaporation [187], sputtering [188], molecular beam epitaxy [189], laser assisted vacuum evaporation [190] etc. are being used. These processes are the energy intensive and involve high temperature. These sophisticated methods have merit in having control over film growth and consequently the properties of thin films. However, researchers also studied wet chemical processes from the economic considerations and some other advantages namely, simplicity and low temperature processing etc. Spin coating [191] is widely applied amongst many wet chemical processes namely chemical bath deposition [192], electrodeposition [193], Langmuir Blodgett technique [194], spray pyrolysis [195], liquid interface reaction technique [196], sol-gel process etc. [197]. This technology can prevent the agglomeration of nanoparticles and allow the nanocrystal to be uniformly dispersed, which results in the highly ordered arrays of functional nanostructures.

Polyvinyl alcohol (PVA) is a biodegradable and hydrophilic polymer, which has multiple uses in the preparation of plastics, textile industry and the pharmaceutical industry. In the pharmaceutical industry is used as an excipient, adhesive, film-forming and as matrix. The polyvinyl alcohol properties are influenced by their hydrolysis degree and molecular weight. Polyvinyl alcohol aqueous solutions can solubilize copper hydroxide (II) at pH> 6 via hydrophobic interactions[199].

Also, PVA-Cu(OH)2 composite intercalated with graphite oxide has been prepared [200]. Other inorganic compounds mixed with PVA are Fe2O3 [201], lithium and manganese oxide [202].

In this section, we prepared template film of silver nanoparticles and nanoprisms at solid state. Silver nanoparticles or nanoprisms were prepared previously using a polymer medium. Then, template films samples were prepared by spin coating technical and thermally treatment to eliminate polymer excess. The resultant films were characterized using UV-visible spectroscopy.

3.1. Spin Coating

Spin coating is a suitable technique for the preparation of periodic films on almost all flat materials. Spin coating has the following advantages: it requires a relatively short manufacturing time; it is cost effective; and, it allows for relatively large surface coverage [203] and [204]. Moreover, the adsorption and rearrangement of adsorbed materials and the elimination of weakly bonded materials can be achieved simultaneously in short processing times by using high spinning speeds [205]. Different types of solutions, such as those comprised of inorganic complex sols, organic/inorganic macromolecules, and colloidal nanoparticles, have been used as film deposition precursors [206][207][208][209]. However, the film deposition process described above can only be applied to precursors or colloids that are dispersed in either water or organic solvent. In addition, rinsing previously deposited films is a general feature of the repeated film deposition process in the absence of baking.

A typical process (***0***) involved four steps: *i) deposition*: depositing a small puddle of a metal silver nanoparticles polymeric solution onto the center of a substrate and then spinning the substrate at high speed (typically around 3000 rpm); *ii) spin-up*: centripetal acceleration will cause the polymeric solution to spread to, and eventually off, the edge of the substrate leaving a thin film of polymeric solution on the surface. *iii) spin-off*: final film thickness and other properties will depend of the viscosity, drying rate, percent solids, tension surface, final rotational speed, acceleration, and iv) evaporation: the drying rate of the polymeric solution during the spin process is defined by the volatility of the solvent used, as well as by the air surrounding the substrate during the spin process. The slower rate of drying offers the advantage of increased film thickness uniformity across the substrate.

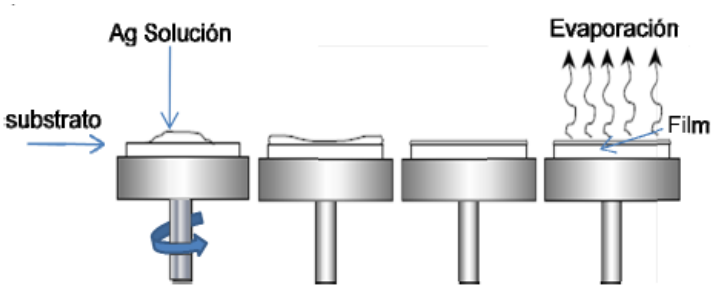

Figure 26. Spin coating method

3.2. Coatings preparations

Glass plates (1 x 3.5 cm) were cleaned by sonication with hexane, acetone, ethanol and deionized water for 15 min. each one. A clear viscous solution (6 to 24% w/v) of polyvinyl alcohol (PVA, medium molecular weight 57,000-66,000) was made using distilled water (90º C) as solvent and stirring for 2 hours. The polyvinyl alcohol (PVA) powder was added slowly to avoid its agglomerates. Finally, the spin-coating technique was used to deposit a uniform thin film of the polyvinyl alcohol polymer solution on glass substrate at 2,000 rpm for 10 sec. The layer was dried in a standard hot air-oven at 100º C. The use of polyvinyl alcohol solution is also crucial to obtain a uniform distribution of nanoparticles on the coatings. Then, 20 µL of the resulting solutions (***0***), silver spherical nanoparticles colloidal solution heated at 90º and 120º C were deposited onto standard microscope glass plates by spin coating using a two-step ramp at 2,000-1,000 rpm for 5 sec each one. After spin coating, the PVP/Ag nanoparticle composite films were dried in a standard hot air oven at 150º C for 60 sec. and then stored in Petri dish glasses for its analysis, this process is shown in the scheme in ***0***.

The spin coating speed determines the thickness of PVP/Ag composite layer and therefore the density of nanoparticles per unit area. The thermal processing is used to dry the solvent and promote adherence of the nanoparticles to the glass substrate. The optical spectra of the Ag-PVA films coated on glass substrates and Ag colloids were recorded on an UV-Vis Spectrophotometer Shimadzu UV-2101, in the range from 300 to 800 nm wavelength. The spectra were deconvoluted using Gaussian functions to extract the intensity, peak and line width of the plasmon absorption accurately.

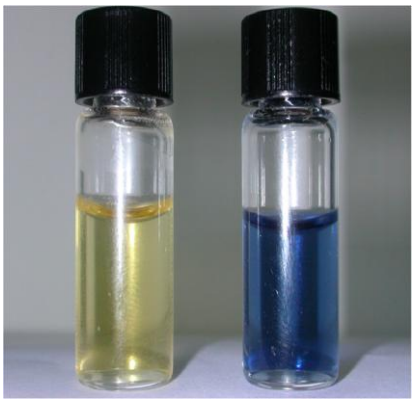

Figure 27. Optical photograph showing the clear color difference between the colloidal solutions of spherical silver nanoparticles (yellow) and triangular nanoprisms (blue) obtained at room temperature.

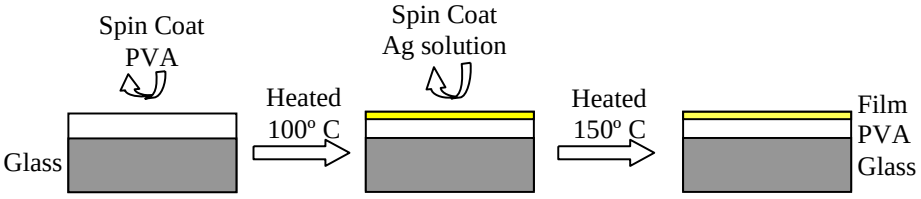

Figure 28. Silver nanostructures coatings process.

3.3. Results and discussion

By means of the chemical reduction method a spherical nanoparticles colloidal solution was obtained. The morphological study of the solutions by transmission electron microscopy (TEM) and high resolution transmission electron microscopy (HRTEM) to determine shape and size (***Figure 10***) clearly reveals that the presence of PVP during the reduction of silver ions results in the growth of isolated spherical nanoparticles and not agglomerates. The results of UV-Vis confirmed that shape and size did not change after one month of the colloid preparation. We confirmed that it is possible to obtain stable Ag spherical nanoparticles in colloids and films using a quite low concentration of PVP [149], much lower than the usual concentrations previously reported in the literature.

A rapid thermal processing is carried out after spin coating in order to eliminate the solvent and promote adherence of the metal nanoparticles to the glass substrate without nanoparticle growth or aggregation. The coated substrates acquire the color of the coating solution, and the color changes to a lighter color on the dried coatings after the thermal processing (***0***). The in-plane dipole surface plasmon band has been demonstrated to be a good indicator of silver nanoprism morphology [14]. Therefore we characterized the spin coated glass substrates by UV–Vis measurements in order to determine any change in the morphology of the silver nanoparticles. The ***0*** shows the UV–Vis spectra of coated glass substrates using silver nanoparticles and nanoprisms colloidal solutions. The glass is not transparent in the UV region below 300 nm, so only the region where the glass is transparent can be shown. The UV–Vis features remain very similar to the spectrum of the nanoprisms before spin coating deposition and the position of the in-plane dipole and quadrupole resonances do not change, revealing that there is little change in the morphology of the nanoprisms after deposition.

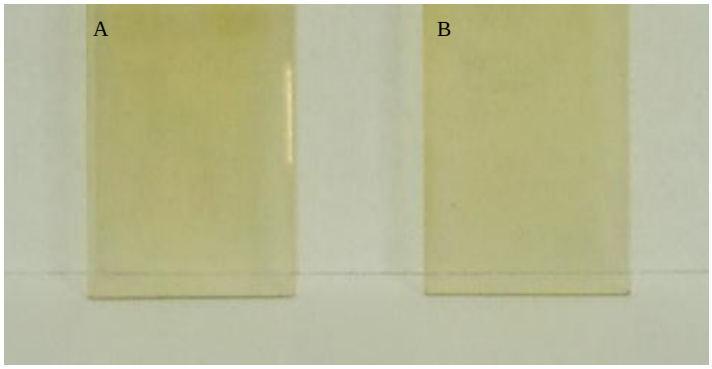

Figure 29. Digital photographs of the coloration and bleaching of spherical silver nanoparticles in 1, 2-propanediol [PVP: AgNO3, 0.5:1], (A) 90 ºC and (B) 120 ºC. Shadows and lighting gradients are responsible for the variations in brightness on the film surface as the films are smooth and uniform.

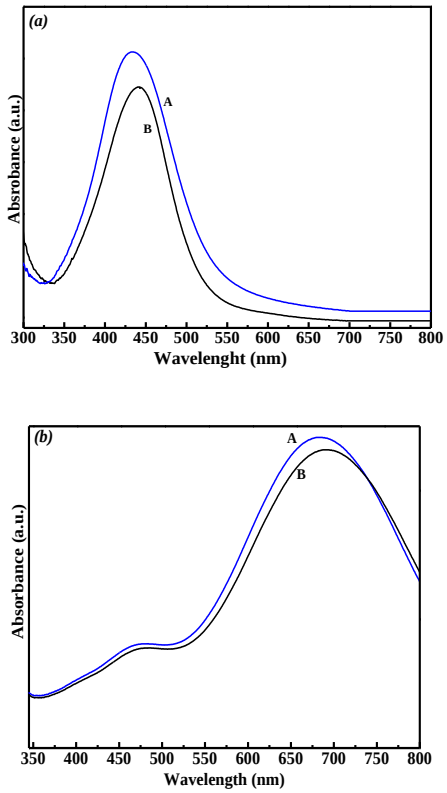

Figure 30. UV-Vis absorption spectra of optical glass substrates after spin coating with (right) colloidal spherical nanoparticles and (left) silver nanoprisms.

Absorption spectra of silver nanoparticle-coated glass substrates show a slight blue shift in the plasmon dipole wavelength compared with the colloidal suspension, which is likely due to the interaction between the silver nanoparticles and the glass surface and the interparticle reactions between the silver nanoparticles [211]. Silver nanoprisms-coated glass substrate appeared deep blue and showed an absorption maximum at 680 nm (shown in the ***0b***). The nanostructures (particle or prisms) immobilized on the substrate retain their original size and shape. So as, all prims lie face down (111) plane on the substrate reported in the literature [212].

The position of the surface plasmon absorption peak of spherical silver particles, separated by long distances, depends on the refractive index of the surrounding medium, particle size and adsorbed substances on their surfaces. If one considers that the ‘‘true’’ position of the surface plasmon band of spherical silver particles (particle diameter $\leq$ 10 nm) in water has been predicted to be 382±1 nm [[26]], the red shift observed for the absorption peak of silver particles in solid PVA must be due to the larger refractive index (η= 1.50) of this polymeric matrix. This experimental result agrees with theoretical predictions, which indicate that the position of the SPAB of silver particles embedded in solid Polymer shifts to longer wavelengths [213][214].

3.4. Summary

Stable colloids of Ag spherical nanoparticles were obtained in 1,2-propanediol using a simple wet-chemical route. As well as, silver spherical nanoparticles monolayer coatings were deposited on optical glass substrates by spin coating. The nanosized spheres (diameters below 20 nm) were obtained by chemical reduction of silver Ag^{+} ions in a solution of 1,2-propanodiol using PVP as stabilizer. The PVP modulates particle growth and shape through absorption onto the particle surface and stabilize the silver spherical nanoparticles in the colloidal solution. Use of 1,2-propanediol with a larger chain length leads to shaper and more symmetrical UV-Vis spectra. The presence of a single absorption peak (~ 410 nm) in the UV-Vis spectrum confirms the nanosized spheres formation for the solutions at room temperature, 60º, 90º and 120º C, showing an unimodal distribution of the particle size.

The solution can be deposited on PVA thin film. We observed a red shift of the absorption peak in the UV-Vis spectrum of the coatings, this shift toward higher wavelength and broadening is affected slightly by PVP-PVA absorbed on particle surface and particle growth (particle radius increases ~ 20 nm) occurred when the coatings were heated at 150º C.

Chapter IV

Composites materials synthesis

IV. OVERWIEW

4.1 Core-shell nanoparticles

Core–shell nanoparticles represent one of the most interesting areas of material science because of their unique combined and tailored properties for several applications. Silica is a good candidate to prepare core–shell nanoparticles and silica nanoparticles emerge particularly as a suitable matrix due to their surface functionality, thus allowing bio-conjugation to bio-activate molecules for objectives like monitoring and marking. Metal–silica core–shell particles have been prepared by the use of a silane coupling agent to provide the metal surface with silanol anchor groups [215]. Silica shells not only enhance the colloidal and chemical stability but also control the distance between core particles within assemblies through shell thickness [216]. Kobayashi et al. have reported more recently silica coating of silver nanoparticles via a modified Stöber [217] method using dimetilamine [218] or the adsorption of Sn^{2+} ions on the surface of the silica particles, so that Ag^{+} ions are reduced and simultaneously adsorbed on the surface, while Sn^{2+} oxidizes to Sn^{4+} [219]. Silver nanoshells have been prepared on silica nanoparticles which had been functionalized with 3-aminopropyltrimethoxysilane (APTMS) and a gold colloid [220]. Recently silver–silica core–shells have been also obtained via a wet chemical modified Stöber route by using N-[3-(trimethoxysilyl)dropyl]ethylene as a coupling agent [221]. Gedanken and co-workers have readily synthesized different metallic nanoparticles and core–shells with encapsulated metal by employing intense ultrasound irradiation without using coupling agents [222][223][224][225][226], including gold and silver nanoparticle shells on silica and titania [227][228][229][230]. We have previously used poly(vinylpyrrolidone) as both reducing agent and stabilizer of silver nanoparticles in ethanol and other polar solvents [231][149].

4.2 Composites materials

Transition metal oxides are a fascinating class of inorganic materials, exhibiting a wide variety of structures, properties, and phenomena. Associated with their complex structures, these materials show a variety of interesting properties: diverse electronic, magnetic, and optical properties. Metal oxides occur in nature as many minerals and are used in many applications such as pigments, catalysts, catalyst supports, ceramics, energy storage, magnetic data storage, sensors, and ferrofluids [232]. TiO2 nanoparticles are of particular interest inasmuch as they have been widely used in important technological applications. The dye-sensitized TiO2 solar cells are inexpensive and have high photon to electron conversion efficiency [233][234]. TiO2 is probably the most investigated photocatalyst system and has been found to be capable of decomposing a wide variety of organics [235]; it is becoming a promising material for lithium rechargeable batteries [236].

The main concern with Titania (TiO2) is that it adsorbs light in the near-Uv spectrum, that is, between 315 and 400nm, where the solar radiation at the surface of the earth arrives at very small intensities. Thus, a lot of effort has been made to sensitize titania in the visible spectrum by employing organic and inorganic sensitizers [237][238]. So, extensive efforts to dope titania with various metal or nonmetal dopants so that it would adsorb in the visible spectrum are being researched. Supporting TiO2 in small amounts on various porous materials such as SiO2 [239][240] or doping the TiO2 [241][242][243] has been used to increase the adsorption capacity of organic compounds, so as to improving surface characteristics (surface area and porosity), thermal stability, photo-catalytic efficiency and surface acidity of the composite. For example, Wilhelm and Stephan [244][245] synthesized silica-titania core-shell materials by heterocoagulation with pH adjustment and a fixed concentration of titania sol. So, Nakamura et al. [246][247] prepared closed-packed titania-coated silica spheres using a layer-by-layer templating method, involving a complex lamination of cationic polyelectrolytes and anionic titania sheets on silica spheres. Subsequently, Holgado et al. [248] deposited uniform titania coating on silica spheres arrays, obtained spheres agglomerated with different thickness. Other researchers have controlled the hydrolysis rate of titanium alkoxides to avoid agglomeration of the coated silica spheres [249][250].

Various wet chemical methods have been reported for the preparation of nano-sized TiO2 and has been classified as liquid process (sol-gel [251][252][253], solvothermal [254], hydrothermal [255][256][257]). From the above, Sol–gel route has been regarded as an excellent method to synthesize nano-sized metallic oxides and has been widely employed for the preparation of titanium dioxide nanoparticles. There are several parameters for controlling sol-gel process to prepare TiO2 nanoparticles with significant properties (precursor concentration, water: titanium molar ratio and pH of prepared solution).

In the present chapter, we show the result succeed in the direct synthesis of different silver nanoshells on silica spheres without using a coupling agent: continuous smooth layer, and silver nanoparticles. The preparation route is based on the complexation of silver ions in water/ethanol solutions containing ammonia, a modification from the Stöber method for preparation of homogeneous silica spheres at room temperature, using water/ethanol mixtures, tetraethyl-orthosilicate as Si-source and ammonia as a catalyst, combined with the deposition of silver from colloidal solutions in Methoxyethanol, using silver nitrate as Ag source. This work was realized in collaboration with a doctorate student.

So as to develop a new generation of materials in solution and nanometric size with photocatalytic activity in the visible range (nano-photocatalysts) to be characterized by UV-visible spectroscopy. The fundamental hypothesis is that inorganic materials (such as the TiO2) with photocatalytic activity in ultra-violet are capable of degrading from not selective form to toxic species present in our environment. The challenge is to overcome the problems derived only from the utilization of the Ultraviolet part of the solar spectrum and to extend the response towards the visible range. We herein, present a simple one step method for the preparation anatase-TiO2, TiO2-Ag and TiO2-SiO2-Ag nanocomposite aqueous solution, starting the hydrolysis of titanium (IV) isopropoxide (TTIP) in the presence of ethanol.

4.3 Experimental section

4.3.1. Synthesis of bare SiO2 particles

The method used to prepare bare silica nanoparticles is based on the Stöber method [217]. In one-pot process, we added the follow reagents: 1.115mL of tetraethyl-orthosilicate (TEOS) for synthesis (MERCK); 24.75mL of absolute ethanol (PANREAC); 5.0mL ammonia 20% (PANREAC); and 8mL of de-ionized water, all the reactants were mixed by stirring at 300 rpm with a magnetic stir bar. Technical details, operation procedures and instrumentations are not the subjects of discussion here. The intention of this chapter is to provide readers with the basic information on the fundamentals that the characterization methods are based on. For technique details we recommended to review the papers appendix.

4.3.2. Synthesis of SiO2@Ag core–shells particles

The method used to prepare the silver shell–silica core nanospheres is based on a Stöber synthesis modified with the addition of colloidal silver nanoparticles. In a single reaction vessel, we added the follow reagents: tetraethyl-orthosilicate (TEOS); absolute ethanol; ammonia 20%; de-ionized water and silver nanoparticles, mixed by stirring at 300 rpm at room temperature (22 ◦C). For the production of continuous smooth Ag shells on SiO2 core, after 30 min of starting the reaction, the stirring was stopped and the solution stored (***Figure 31a***). The pH and the stabilizers present in the silver colloid added as a second step of the synthesis dictates the morphology of the silver nanoshell as shown in the scheme in ***Figure 31b***.

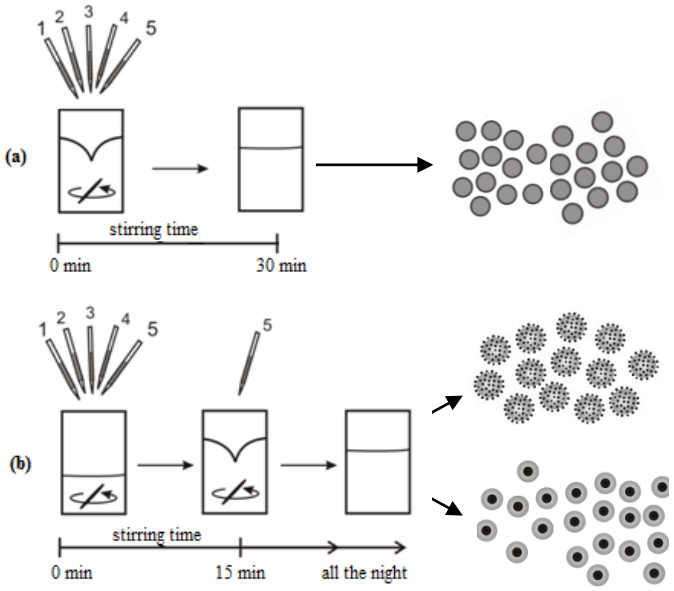

Figure 31. Deposition procedure of silver nanoparticles on the silica spheres: (a) continuous smooth layer, (b) SiO2@Ag and Ag core silica shell. (1) TEOS, (2) Ethanol, (3) ammonia, (4) water and (5) Ag nanoparticles.

4.3.3. Synthesis of TiO_2 and TiO_2-Ag composites in solution

Titanium (IV) isopropoxide (TTIP, purum, Fluka), used as precursor for TiO2 powder synthesis, NH4OH (20% aqueous solution, Panreac chemical), dimethyl-ammonium (DMA, 40% aqueous solution, Merck), ethanol 98%, water distilled, HCl (37% aqueous solution), and TEOS (Tetraehtylorthosilicate). All these products were used without further purification. TEM images of nanoparticles were taken with a Hitachi H-800MT microscopy and higher resolution structural characterization of the nanoparticles was carried out using a field emission transmission electron microscope (JEOL3000F) operated at accelerating voltage of 300 kV. SEM images and EDS spectrums of the nanoparticles were taken with a Hitachi S-4300 microscopy. X-ray powder diffraction (XRD) patterns were recorded using a Cu Kα radiation (λ ~1.5406 Å) in a Siemens D-500 operating at 40 kV. The optical properties were studied by UV–visible spectrophotometer (Model Shimadzu UV-2101Pc).

Anatase TiO_2 nanoparticles were synthesized via the Stöber method. Tetrabutyl orthotitanate was used as precursor in the presence of absolute ethanol, ammonia and water to produce one Titania sol. A typical synthesis procedure is as follows: Tetrabutyl orthotitanate (0.3 ml, 0.87 mmol), ethanol (20 ml) were added to 19.7 ml of water and ammonia (0.4 ml, 0.378 g, 0.02 mol) to adjust the pH at 10. The resulting solution was vigorous stirring during 2 h until a white TiO_2 precursor solution was obtained. The total amount of solution was kept at 40 ml, and different reaction medium (NH_4OH, HCl, HCl-NH_4OH and NH_4OH-HCl) were used to produce nanoparticles with chemically modified surface. The solid was washed several times with ethanol: water (1:1) and centrifuged at room temperature. The powder was heated from 500 to 800 ºC in air for 2 hours. The initial resulting powder was white and amorphous. After the heat treatment particles de TiO2 anatase were obtained.

The surface decoration of TiO2 particles with Ag nanoparticles was based on the traditional silver mirror reaction. The silver nanoparticles were deposited over TiO2 amorphous. Firstly, TiO2 powders were prepared using a sol-gel method. The synthesis process had been described previously. The material obtained without heating was mixed with various amount of silver nanoparticles prepared in 2-Methoxiethanol (*see synthesis process in chapter 1*). The solution was kept stirring for 30 min.

4.3.4. Synthesis of SiO_2-TiO_2-Ag nanocomposites

The formation of monodispersed silica particles was first carried out by the procedure based on the Stöber method described previously [258]. Briefly, tetraethylorthosilicate (TEOS); absolute ethanol; ammonia 20%; and de-ionized water were mixed by stirring during 20 minutes. Subsequently, direct coating of the thin titania shell on silica core was performed with continuous feeding via hydrolysis of tetra butylorthotitanate (TTIP) in ethanol solution and vigorous stirring during 2 h. The volume ratio of TTIP and ethanol used in the coating was 1:67. The SiO_2-TiO_2-Ag nanocomposites were prepared as follow: the material obtained without heating was mixed with various amounts of silver nanoparticles prepared in 2-Methoxiethanol. The solution was kept stirring for 30 min. The solvent was removed by centrifugation (8000 rpm, 10 min) and washed with water: ethanol ratio (1:1). The composites were redispersed in 3 ml of ethanol and left 2 h in an ultrasonic bath for eliminate agglomerate.

4.4 Result and Discussion

4.4.1. SiO2@Ag core–shells particles

The UV–visible absorption spectra of the silver nanoparticles solution and core-shell composites are presented in ***0***; they feature the band edge of silver nanoparticles (417 nm) [149] and SiO2@Ag particles. A weak band near to 420 nm corresponding to the signal of Ag nanoparticles is present in spectra of SiO2@Ag and Ag@SiO2. This weak signal can explain it in the fact that there is more quantity of silica than silver in the whole particle. These composites could be used in photocatalysis without the use of Ultraviolet light.

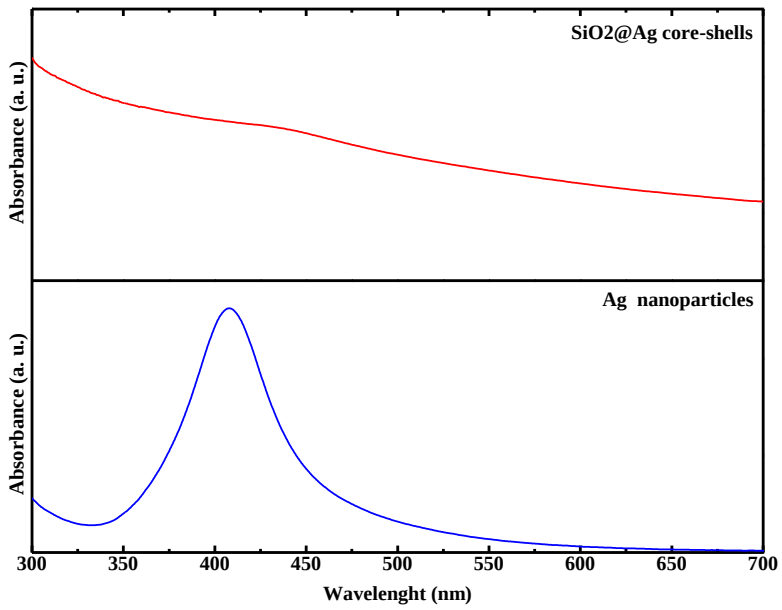

Figure 32. UV–vis spectra of silver nanoparticles, bare silica spheres and silver coated silica spheres.

TEM images of monodisperse spheres of bare silica particles with smooth surface and homogeneous size are shown in ***Figure 33a***. The measured average size of the bare silica spheres obtained without addition of silver NPs was 300 nm. The addition of ammonia (NH4OH) cause a rapid increase in the pH of the Ag nanoparticles solution, resulting in the deposition of silver onto the silica surface forming a silver shell, at the expense of the colloidal silver nanoparticles. Our observations agree well with those reported by Jackson and Halas [60], where gold decorated silica particles are mixed with a 0.15 mM solution of fresh hydrogen tetrachloroaurate trihydrate (HAuCl4) and stirred vigorously during the addition of ammonia. They observe "a minimal amount of silver colloid accompanying the formation of a continuous silver nanoshell in solution" and also "if small nanoparticles are formed in the solution, deposition of the nanoshell silver layer will continue at the expense of these particles". A rapid pH change appears to result in the preferential deposition onto a shell at the expense of preexisting colloidal silver. No aggregation was observed, and the reaction occurred rapidly, much less than 30 min were required to complete the reaction. Due to the high pH, the resulting silver coated silica particles are charge-stabilized in solution. TEM images at the same magnification after the rapid addition of silver are shown in ***Figure 33b***. This method produces smooth, complete silver nanoshells with a thickness of ~10 nm.

The use of silver colloids without trisodium citrate stabilizer resulted in nanoshells of 3–5 nm silver nanoparticles on silica spheres and in silver nanoparticles embedded in silica spheres (***Figure 33c, d***).

Methods derived from the original Stöber report are very widely known and used for the preparation of homogeneous silica spheres. It is well known the ability of amorphous silica to incorporate metal cations in its network [259]. The preparation of silver nanoparticles via the reduction of Ag+ ions in solution is also very well documented [231][149]. We have modified it in order to deposit silver nanoshells onto the silica spheres. The preparation of silica spheres in the submicron range containing silver nanoparticles inside has been reported by Shibata et al. using a sol–gel method [260]. More recently Kobayashi et al. have reported the silica coating of silver nanoparticles, Ag@SiO2, with a silver NP in the center, using a modified Stöber method adding dimethylamine (DMA) as a catalyst [217]. To our knowledge, we report here the first synthesis of silver nanoshell–silica core spheres with different morphologies using a very simple chemical route at room temperature based on the Stöber method without adding any coupling agent or catalyst and without the functionalization of the silica surface.

In order to ascertain the reaction mechanism, we have carried out the following control experiment: before the addition of Ag^+ containing solution, the silica spheres were separated from the liquid by centrifugation at 15,000rpm for 10min and washed in distilled water two times, in order to eliminate the ammonia in the solution. Water and ethanol in the same concentrations than the starting solution were added to the silica nanospheres and the synthesis followed as was described above. This change in the synthesis did not yield SiO2@Ag nanoparticles. Therefore ammonia must be present for the formation of both the silica core and the silver shell.

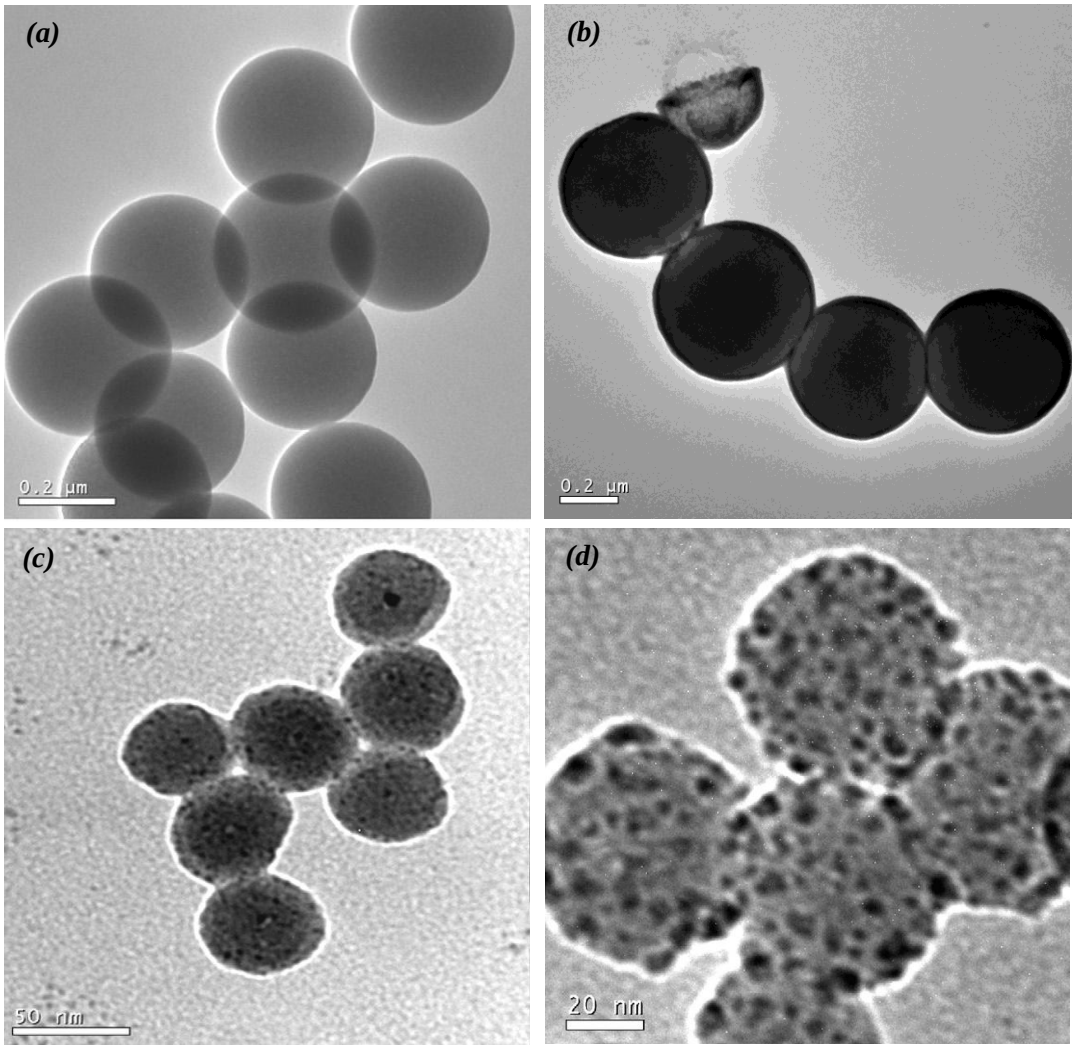

Figure 33. TEM micrographs showing: (a) bare silica spheres, (b) silver coated silica spheres, (c) Silver nanoparticles deposited on silica spheres and (d) magnification of Ag nanoparticles on silica spheres.

The formation of silanols on silica surface in water–ethanol mixtures, the formation of silver–ammonia complex and the reduction of silver ions by PVP and trisodium citrate, are well documented. It is possible that a moderately strong chemical bond between the siloxane oxygen and elemental Ag (Si–O–Ag_+) is formed. A theoretical investigation by Johnson and Pepper [261] showed that the formation of a direct and primarily covalent chemical bond between an elemental metal such as Fe, Ni, Cu, or Ag and oxygen anions on the surface of clean sapphire is favored. Recently, Murphy and coworkers have grown crystalline silver nanowires in water, in the absence of a surfactant or polymer to direct nanoparticle growth, and without externally added seed crystallites. They have proposed the reaction as one in which silver salt is reduced to silver metal, at 100 ◦C, by sodium citrate [262]. Our explanation involves the hydrolysis and condensation of TEOS for the formation of silica nanosized spheres, the incorporation of $[Ag(NH3)2]^{+}$ complexes in the surface of the silica rich in negatively charged silanol groups $Si–OH^{-}$, and the reduction and stabilization of silver by PVP and trisodium citrate, leading to the formation of the silver nanoshells. The reduction of silver on the nanometer scale is strongly dependent on the chemical stabilizers (sodium citrate and PVP) in the silver nanoparticle solution and the pH of the solution.

4.4.2. TiO2 composites

The XRD analysis was employed to characterize the crystallinity of the samples. First, XRD patterns of TiO2, and Ag nanoparticles covered with TiO2 composites are presented in *Error! Reference source not found.*. The results show that the main structural characteristic phases of TiO2 and all TiO2-covered composites is the pure anatase phase, which seems that the titania anatase phase structure remained in all cases. The highest anatase content was found in the material calcined at 600 ºC, beyond which it disordered ahead of the transformation to rutile. The second part of XRD analysis was performed in order to assess the crystallinity of the transition metal loaded onto TiO2, which showed that our samples exhibited peak from the transition metal; this is probably attributed to the high transition metal doping content. The pattern for Ag nanoparticles exhibited the diffraction peaks at 2θ= 38.1, 44.2, 64.4, and 77.5°, all of which coincided with those for Ag. Titania-coated Ag nanoparticles were found to keep the diffraction peaks characteristic of Ag crystal, whereas no peak assigned to titania crystal was detected, suggesting that the titania is amorphous.

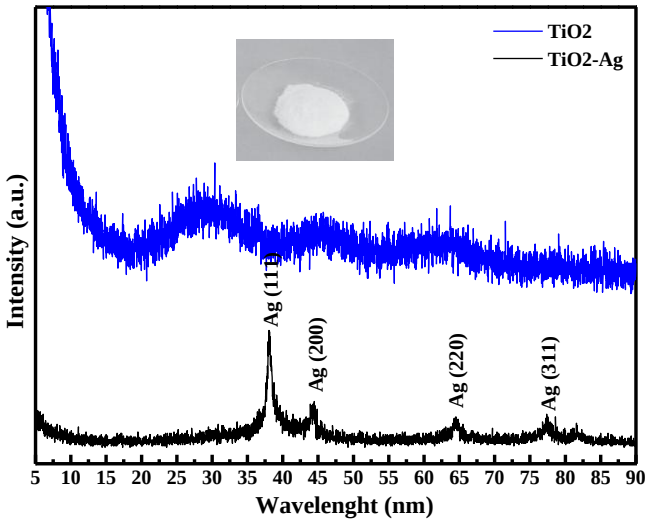

Figure 34. Wide-angle X-ray diffraction patterns of TiO2 and TiO2-Ag composites.

The UV-Vis absorption spectra of Titania, titania-silver and silica-titania-silver composites suspensions in the range 300–800 nm are shown in ***Figure 35***. The TiO2 exhibits absorption in the UV light range, while the TiO2-Ag and SiO2-Ag-TiO2 catalysts exhibit absorption in the visible light range. The strong absorption below a wavelength of 340 nm in all curves of graph ***(a)*** is associated with the optical band gap of TiO2. The syntheses of TiO2 in various medium (acid, base, acid-base or base-acid) have not effect over the absorption band of titania. In graph ***(b)***, a peak indicating the presence of a localized surface plasmon for the sample made of TiO2-Ag nanoparticles is observable at 440 nm. It is presumed that the silver nanoparticles were incorporated to titania matrix. In the sample of TiO2-Ag nanoparticles prepared in NH4OH-HCl medium a broad absorption band was observable.

Also, as shown in graph ***(c)*** of ***Figure 35***, the SiO2-Ag-TiO2 and SiO2-TiO2-Ag catalysts exhibit intense absorption band due to the silver nanoparticles around 440 nm, when the silver nanoparticles concentration was very high (3 ml). While the broad absorption band that appear about 450 nm, would indicate that the silver nanoparticles concentration is low or that the nanoparticles are immersed inside the titania matrix. In the case of SiO2-Ag-TiO2, the intensity of this broad absorption band is smaller than that of SiO2-TiO2-Ag, suggesting that the incorporation of the silver nanoparticles inside the titania matrix in the second case is lower than of SiO2-Ag-TiO2.

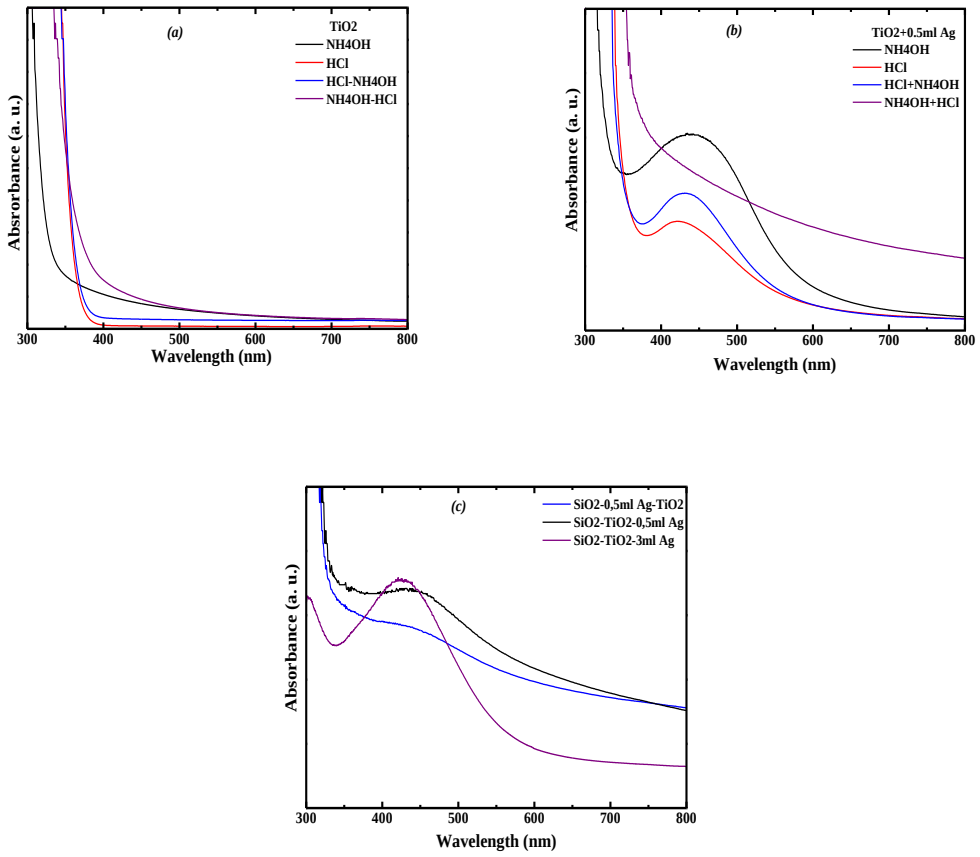

Figure 35. Optical studies by UV–vis spectrophotometer of (*a*) TiO_2 nanoparticles, (*b*) TiO_2/Ag composites (with 0.5 ml of Ag nanoparticles, using different reaction medium: NH_4OH, HCl, HCl-NH_4OH and NH_4OH-HCl), and (*c*) SiO2-TiO_2-Ag composites (with 3 ml of Ag nanoparticles).

The ***Figure 36*** shows the TEM image of the as-calcined TiO2 powder synthesized via different catalysis routes. Can be observed that the average size of the particle size after calcinations was larger than that of the without-treated particle and prepared in a basic medium. According to Song et al., it was found that TiO2 particles catalyzed by acid were more closely packed than those treated by base catalyst [263]. Also, the particles prepared in a base medium have more tendency to retain hydroxyls and water molecules. So as, the particles size after calcinations may be smaller than particles prepared in acid medium [264]. Therefore, we can considerate that a more closely packed structure of primary particles of TiO2 synthesized in acid medium could provide larger secondary particles during heat treatment. On the contrary, the TiO2 particles synthesized in base medium presented loosely packed during calcinations resulting relatively smaller secondary particle size. Then we can to assume than the TiO2 particles prepared by using basic catalyst would be desirable for preparing Anatase TiO2 powder. Because the small particles size and high anatase content are employs to fabricate highly efficient solar cell [233][265], photocatalytic membranes [266].

The sequence of application of these two types of catalysts is the key to success; the catalyst added at first stage affected mainly on the size of the primary particles, while the secondary catalyst determined the dispersion and final crystalline phase. Therefore, "acid and then base" treatment can be a far better route to provide optimum final powder than "base and then acid" sequence.

Figure 37(a) and ***(b)*** show the TEM micrographs representatives of the nanosized TiO2–Ag composites prepared with different catalyst and 0,5ml of silver-nanoparticles prepared above. For Titania matrix, the Ag deposits appeared as dark spots in the TEM images, identified by EDAX and UV-visible. The high atomic contrast of the image clearly shows than the particles are very uniform in size and randomly distributed on/inside the titania matrix. Higher magnification of the sample shows that the Ag nanoparticles were hemispherical in shape. Silver nanoparticles can be deposited on the TiO2 nanoparticle surface by either cation adsorption or anion adsorption to the TiO2 surface depending on the pH of the working solution. The TiO2 is an amphoteric oxide with an isoelectric point $IEP_{TiO2} = 6$ [267]. Therefore, in our case we prepare Titania solution using a catalyst solution as a pH higher than IEP_{TiO2}, producing surface species as $-O^-$, so the TiO2 surface is negatively charged and silver can be deposited on TiO2 by cation adsorption. When the solution pH was lower than IEP_{TiO2}, silver nanoparticles was not deposited on the TiO2 surface.

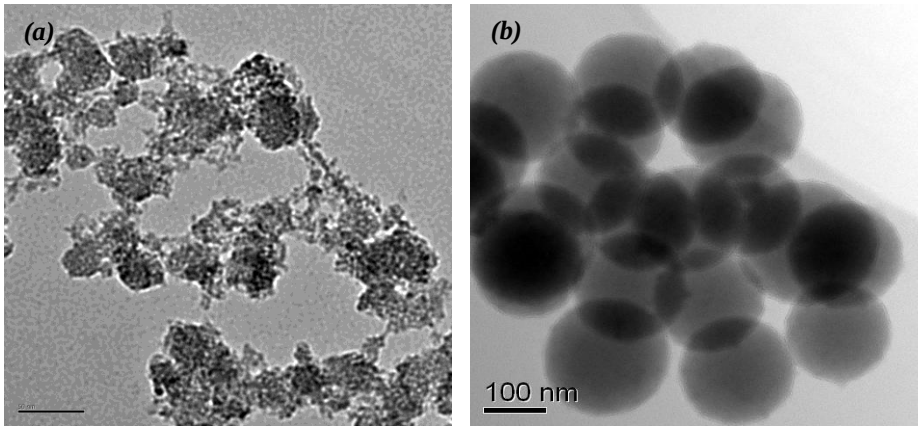

Figure 36.TEM images of TiO_2, a) as prepared, b) after thermal treatment at 600ºC for 2 h.

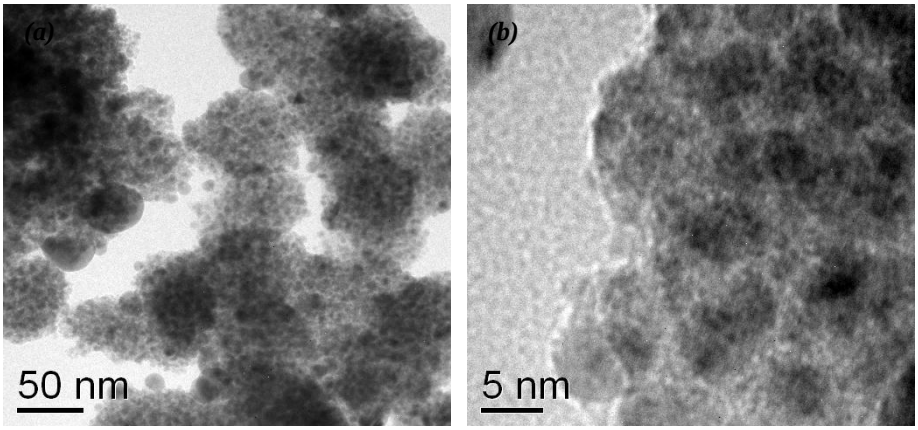

Figure 37. TEM images of TiO_2-Ag composites using a Titania colloidal solution.

TEM analysis images of both the SiO2-TiO2-Ag and SiO2-Ag-TiO2 composites showed in ***Figure 38*** reveal amorphous and crystalline structures for silica-titania and silver respectively. The results show that the particle size of Ag as-prepared is the smallest particle size. In the first system, SiO2@TiO2 core-shell nanoparticles were observed in the samples with any silver nanoparticles distributed on the SiO2@TiO2 nanoparticles surface ***(images a-c)***. The samples showed a Titania shell very homogenous on the silica surface. While the second system (SiO2-Ag-TiO2 composites), silica nanoparticles coated of silver crystalline and titania amorphous were observed in the samples. Also, a titania amorphous excess was detected (***images d-e***). A surface analysis was realized to one sample to determinate the chemical composition present on the surface of silica nanoparticles, as shown in the image (***f***).

Our approach is based on our previous work, in which silver nanoparticles were incorporated on silica microsphere through a sol–gel process [268]. The measured average size of the bare silica spheres obtained without addition of silver nanoparticles was from 270± 30 nm and Ag nanoparticles size are about 40 nm. The measurements shown that silica microspheres no were homogeneously impregnated with silver nanoparticles when the titania solution was added. This disproportion in both cases might be caused by the low presence of ammonia, indicating that ammonia plays a key role in the deposition of silver nanoparticles on silica surface. However, we think that a maximum capacity of highly dispersed TiO_2 species on silica could be reach by carefully controlling the above preparation variables. This maximum capacity will be correlating with the surface concentration of OH groups on silica, suggesting so a maximum coverage of titania species on the silica surface.

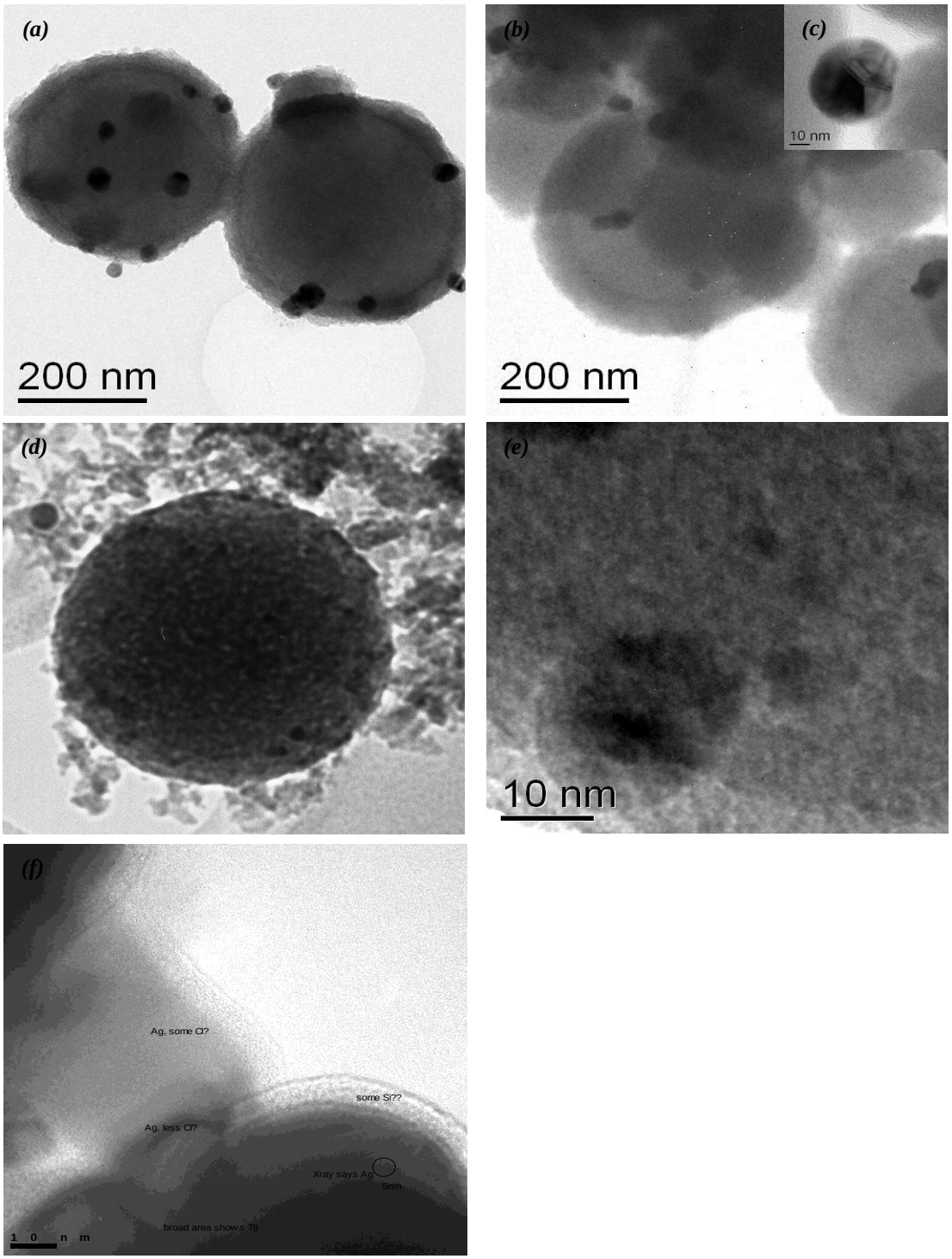

Figure 38. TEM images of SiO_2-TiO_2-Ag (*a-c*) and SiO_2-Ag-TiO_2 (*d-f*) nanocomposites as prepared.

Scanning electron microscopy (SEM) and Electron Diffraction Scattering (EDS) show that the morphology of the core microspheres (***Figure 39***) did not change during the deposition of titania, also rougher surfaces were observed for titania nanoparticles. As noted above, the crucial step for incorporating titania or silver nanoparticles into silica microspheres was the preparation of the started solution in ethanol and the ammonia concentration in the solution. EDS pattern of TiO2, TiO2–Ag and SiO2-TiO2–Ag composites in the HRTEM mode from a little area. The presence of X-ray lines associated with O Kα, Ag Kα, Ti Kα, and Si Kα is evident. Given that the Cu Kα line corresponds to the cupper grid used for TEM analysis, the results indicate that Si, Ti, O and Ag are the constitutive elements of the nanocomposites prepared by the sol–gel method.

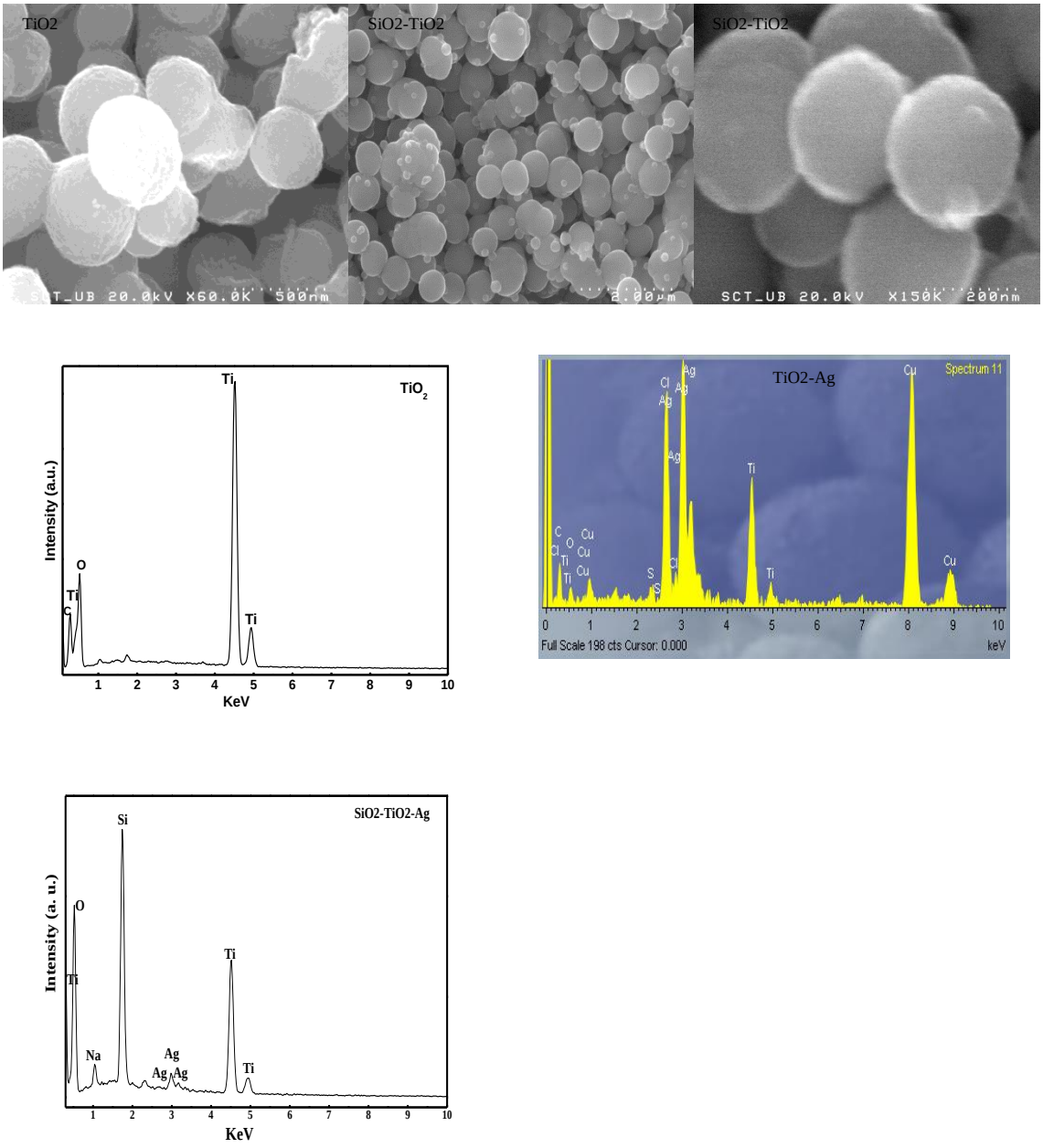

Figure 39. SEM images of TiO2 and SiO2-TiO2 nanoparticles calcined at 600ºC and EDS spectrums.

4.5 Summary

We have examined various design and synthesis strategies for the fabrication of nanostructured catalytic materials. Generally speaking, nanostructured parts as well as their organization methodologies are ready for direct usage or further assembly. However, a large research is needed, and this includes systematic investigations on multicomponent assemblies and resultant chemical-physical properties. While traditional methods will still dominate the industrial-scale catalyst processing at the actuality, we are beginning to see nanostructured catalytic materials in practical applications of chemical laboratory and chemical-sensing technology where the amount of catalysts required is small, and supported type catalysts may not be needed.

One hydrolysis of TTIP solution was used under acidic catalyst for preparing fine primary particles and then a basic catalyst was added into the solution to provide anatase TiO2 powder with a loosely packed structure. Moreover, TiO2-Ag nanocomposites were synthesized with a mixture of titania solution and silver nanoparticles as-prepared. Aggregation effects were observed as indicated by TEM imaging due to the formation of agglomerate of TiO2 amorphous. The high-resolution transmission electron micrographs showed that TiO2–Ag nanocomposites possessed a spherical morphology and narrow size distribution. Smooth titania shells on silica were obtained, but silver nanoparticles were not uniformly deposited on silica-titania particles. While, silver nanoparticles were observed inside of titania matrix when the silver colloidal was incorporated to the end.

The results of our study emphasize the role of Ag-deposits in enhancing photocatalytic activity of TiO2 under both UV and visible light as had been broadly reported at the literature. Since, the nanosized metallic silver particles on TiO2 surface enrich the accumulation of electrons, which act as electron traps and enhanced adsorption on their surface. So as better charge separation can be generate by TiO2-Ag and SiO2-TiO2-Ag composites compared to bare TiO2.

Annex E.

Precursors, reducing agents and polymeric stabilizers used in the metal nanoparticles synthesis

Precursores	***Formula***
Silver nitrate	$AgNO_3$
Agentes reductores	
Sodium citrate	$NH_40H + HCl$
Hydrogen peroxide	$C_6H_80_7$
	H_20_2
	$NaBH_4$
	NH_4OH
Estabilizadores poliméricos	
*Poly(*vinylpyrrolidone*), PVP*	
Polyvinylalcohol, PVA	
Ethylene glycol	

Chapter V

General Conclusion-Highlights

- We report a facile approach for the formation of colloidal silver nanoparticles with increased stability against aggregation (original result).

- The use of a chemical reduction route at room temperature in aqueous solution provides a high yield, technologically simple, low toxicity and time saving method for fabrication of well-defined silver nanoparticles and composite nanoparticles with well defined surface plasmon resonance properties and possible aplications in optical devices (original result).

- The long term stability of the obtained silver colloids was demonstrated for periods of time up to 5 years (original result), and the exposure to ambient laboratory light of the colloids did not result in any observable change or degradation of the optical properties, therefore the usability after prolnge stoage of the colloids is confirmed.

- Colloids heated up to 60º, 90º, and 120º C retained the nanoparticle shape and diameter over a long period even when submitted to direct sunlight.

- Unimodal distributions of silver spherical nanoparticles (diameters below 20 nm) were prepared in different solvents: 1, 2-pronanodiol, methoxyethanol, ethylenglycol. The presence of a single absorption peak centered at 410 nm corresponding to the dipole resonance in the UV-Vis spectrum confirms the nanosized spheres formation.

- Use of 1, 2-propanodiol with a larger chain length leads to sharper and more symmetrical plasmon resonance absortion spectra determined by UV-Vis measurements (original result).

- We demonstrated that the use of low concentrations of polyvinyl-pyrrolidone (PVP) results in colloidal solution stable against the formation of agglomerates (original result).

- The intensity and width of the surface plasmon resonance are determined by the nanoparticle morphology. We followed he formation and growth of anisotropic nanoparticles in the colloidal solutions through the evolution of the plasmon resonance absortion spectra.

- Anisotropic growth results in a multi-peak plasmon resonance spectra, with several overlapping features, which can be related to the main geometrical parameters of the anisotropic nanoparticle, once determined the nanoparticle shape (i. e. bi-dimensional prisms, rods. et..). Nanoparticle growth results in the blue shift of the main resonance peak, typically also increasing its full width half maximum.

- Lon time stable Ag colloids of nanosized triangular prisms were prepared in water at room temperature in the presence of PVP and H_2O_2 as stabilizer and growth directing agents.

- The Uv-Vis spectra of colloidal silver nanoprisms display a main feature, the in-plane (590 nm) plasmon resonance, and secondary out-of-plane (410 nm) dipole plasmon resonance and out-of-plane (340 nm) quadrupole plasmon resonance peaks which indicate the morphology of the nanoprisms in the colloid.

- The limits of hydrogen peroxide concentrations leading to the formation of silver nanoprisms were determined (orginal result), both n the absence and in the presence of sodim citrate (original result).

- It was determined the role of sodium citrate as an aid to preferentially stabilize spherical nanoparticales, hinderin the growth of anisotropic silver bodies (original result).

- Monolayer coatings of silver nanoparticles embedded in PVP on optical glass substrates were deposited by spin coating (original result).

- One rapid thermal process promote adherence of the nanoparticles on the substrate., conferring excellent stability to the silver nanoparticle coatings, exposed at sunlight, as demonstrated by UV–Vis spectral measurement and also by the appearance to the eye (original result).

- Silver-silica spheres with muffin cokie morphology of silver nanoparticles embeded in silica matrix were prepared in a simple single pot reaction at room temperature. (original result).

- Silver nanoshell–silica core spheres with different morphologies have been prepared, using a very simple chemical route at room temperature without adding any coupling agent or catalyst and without the functionalization of the silica surface (original result).

- Silver nanoparticle were deposited on the silica surface of monodisperse spheres of bare silica particles with smooth surface and homogeneous size prepared by a modified Stöber method. The use of ammonia in the reaction caused a rapid increase in the pH and the rapid deposition of silver.

- Ammonia addition can lead to different morphologies of the deposited silver from a continuous silver nanolayer coating of a few nm, to nanoshells of 3–5 nm silver nanoparticles, to spike-like silver protuberances (original result).

- Bare anatase TiO_2 nanospheres were prepared using an acid and basic media. as substrate for silver deposition

- TiO_2@Ag nanosized composites with morphology of silver nanoparticles embeded in amorphous titania matrix were prepared in a simple single pot reaction at room temperature (original result).

- SiO_2@TiO_2@Ag nanosized composites with morphology of silver nanoparticles embeded in amorphous titania matrix were prepared in a simple single pot reaction at room temperature (original result).

- SiO_2@Ag@TiO_2 composites were obtained by the sequential deposition of silver and then amorphous TiO_2 layers on bare silica nanoparticles (original result).

- The composite nanoparticles in the SiO_2-Ag, TiO_2-Ag and ternary system display-clear plasmon resonance absortion spectra typical of metallic nanoparticles. They can be dried up as a powder, stored for long time and redispersed a colloid maintaning intact its optical properties, demonstrating that Tthe silver clusters are protected from agglomeration, and oxidation by the oxide matrix.

Bibliography

[1]. C. B. Murray, D. J. Norris, and M. G. Bawendi, J. Am. Chem. Soc., 115, 8706, (1993)
[2]. A. Esumi, A. Suzuki, N. Aihara, K. Uswi, and K. Torigoe., Langmuir, 14, 3157, (1998)
[3]. M. Faraday, Philos. Trans. R. Soc., London, 147, 145, (1857)
[4]. J. Turkevich; G. Kim, Science, 169, 873, (1970)
[5]. N. Malikova, I. Pastoriza-Santos, M. Schierhorn, N. A. Kotov, L. M. Liz-Marzán, Langmuir, 18, 3694, (2002)
[6]. J. E. Millstone, S. Park, K. L. Shuford, L. Qin, G. C. Schatz, C. A. Mirkin, J. Am. Chem. Soc., 127, 5312, (2005)
[7]. F. Kim, S. Connor, H. Song, T. Kuykendall, P. Yang, Angew. Chem. Int. Ed., 43, 3673, (2004)
[8]. S. S. Shankar, A. Rai, B. Ankamwar, A. Singh, A. Ahmad, M. Sastry, Nat. Mater., 3, 482, (2004)
[9]. I. Pastoriza-Santos, L. M. Liz-Marzán, Nano Lett., 2, 903, (2002)
[10]. S. Chen, D. L. Carroll, Nano Lett., 2(9), 1003, (2002)
[11]. S. Chen, D. L. Carroll, J. Phys. Chem. B, 108, 5500, (2004)
[12]. N. Okada, Y. Hamanaka, A. Nakamura, I. Pastoriza-Santos, L. M. Liz-Marzán, J. Phys. Chem. B, 108, 8751, (2004)
[13]. G. S. Métraux, C. A. Mirkin, Adv. Mater., 17, 412, (2005)
[14]. R. Jin, Y. W. Cao, C. A. Mirkin, K. L. Kelly, G. C. Schazt, J. G. Zheng, Science, 294, 1901, (2001)
[15]. A. Callegari, D. Tonti, M. Chergui, Nano Lett., 3, 1565, (2003)
[16]. R. Jin, C. Y. Cao, E. Hao, G. Métraux, G. C. Schazt, C. A. Mirkin, Nature, 425, 487, (2003)
[17]. M. Maillard, P. Huang, L. E. Brus, Nano Lett., 3, 1611, (2003)
[18]. Y. Sun, B. Mayers, Y. Xia, Nano Lett., 3(5), 675, (2003)
[19]. Y. Sun, Y. Xia, Adv. Mater., 15, 695, (2003)
[20]. L. N. Lewis, Chem. Rev., 93, 2693, (1993)
[21]. J. S. Bradley, In clusters and colloids, From theory to applications; Schmind, G. Ed. VCH: Weinheim, 459, (1994)
[22]. S. Berciaud, L. Cognet, P. Tamarat and B. Lounis, Nano Lett., 5, 515, (2005)
[23]. M. A. El-Sayed,Acc. Chem. Res., 34, 257, (2001)
[24]. K. L. Kelly, E. Coronado,L.L. Zhao, and G.C. Schatz, J. Phys. Chem. B, 107, 668, (2003)
[25]. R. C. Jin,Y. W. Cao,C. A. Mirkin,K. L. Kelly,G. C. Schatz, and J. G. Zheng, Science, 294 1901, (2001)
[26]. P. Mulvaney, , Langmuir, 12, 788, (1996)
[27]. P. A. Kossyrev,A. Yin,S.G. Cloutier,D.A. Cardimona,D. Huang,P.M. Alsing, and J.M. Xu, Nano Lett., 5, 1978, (2005)
[28]. A. Manna, T. Imae, M. Iida, N. Hisamatsu, Langmuir, 17, 6000, (2001)
[29]. M. Gutierrez, A. Henglein, J. Phys. Chem., 97, 11368, (1993)
[30]. A. D. McFarland, R.P. Van Duyne, Nano Lett, 3(8), 1057, (2003)
[31]. A. Henglein, Chem. Mater., 10, 444, (1998)
[32]. T. Linnert, P. Mulvaney, A. Henglein, J. Phys. Chem., 67, 679, (1993)
[33]. A. J. Haes, S. Zou, G.C. Schatz, R.P. Van Duyne, J. Phys. Chem. B, 108, 109, (2004)
[34]. D. D. Evanoff Jr, R.L. White, G. Chumanov, J. Phys. Chem. B, 108, 1522, (2004)
[35]. S. Kapoor, Langmuir, 14, 1021, (1998)

[36]. S. Mandal, A. Gole, N. Lala, R. Gonnade, V. Ganvir, M. Sastry, Langmuir, 17, 6262, (2001)
[37]. J. Zheng, M.S. Stevenson, R.S. Hikida, O.G. Van Patten, J. Phys. Chem. B, 106, 1252, (2002)
[38]. U. Kreibig and M.Vollmer, Optical Properties of Metal Clusters, Springer-Verlag, Berlin, (1996)
[39]. J. P. Kottmann; O. J. F.Martin; D. R.Smith; S.Schultz, Chem. Phys. Lett., 341, 1, (2001)
[40]. W. H.Yang; G. C. Schatz; R. P.Van Duyne, J. Chem. Phys., 103, 869, (1995)
[41]. S. He, J. Yao, P. Jiang, D. Shi, H. Zhang, S. Xie, S. Pang,H. Gao, Langmuir, 17, 1571, (2001)
[42]. M. Zheng, M. Gu, Y. Jin, G. Jin, Mater. Res. Bull., 36, 853, (2001)
[43]. M. Kowshik, S. Ashtaputre, S. Kharrazi, W. Vogel, J. Urban, S.K. Kulkarni, K.M. Paknikar, Nanotechnol., 14, 95, (2003)
[44]. P. Y. Silvert, R. Herrera-Urbina, K. Tekaia-Elhsissen, J. Mater. Chem., 7(2), 293,(1997)
[45]. A. Taleb, C. Petit, M.P. Pileni, J. Phys. Chem. B, 102, 2214, (1997)
[46]. J. P. Wilcoxon, J.E. Martin, P. Provencio, J. Chem. Phys., 115(2), 998,(2001)
[47]. W. Wang, S. Efrima, O. Regev, Langmuir, 14, 602, (1998)
[48]. G. Carotenuto, G.P. Pepe, L. Nicolais, Eur. Phys. J. B, 116, 11, (2000)
[49]. G. Rodriguez-Gattorno, D. Díaz, L. Rendón, G.O. Hernández-Segura, J. Phys. Chem. B, 106, 2482,(2002)
[50]. C. Faure, A. Derre, W. Neri, J. Phys. Chem. B, 107, 4738, (2003)
[51]. I. Pastoriza-Santos, L. M. Liz-Marzán, Langmuir, 15, 948,(1999)
[52]. A. Callegari, D. Tonti, M. Chergui, Nano Lett, 3(11),1611,(2003)
[53]. Y. Sun, Y. Xia. Science, 298, 2176, (2002)
[54]. D. Zhang, L. Qi, J. Ma, N. Cheng, Chem. Mater., 13, 2753, (2001)
[55]. Y. Zhou, S.H. Yu, X.P. Cui, C.Y. Wang, Z.Y. Chen, Chem. Mater., 11, 545,(1999)
[56]. Y. J. Han, J.M. Kin, G.D. Stucky, Chem. Mater., 12, 2068, (2000)
[57]. E. Hao, K.L. Kelly, J.T. Hupp, G.C. Schats, J. Am. Chem. Soc., 124, 1518, (2002)
[58]. S. Chen, Z. Fan, D.L. Carroll, J. Phys. Chem. B, 106, 10778,(2002)
[59]. M. Maillard, S. Gieorgio, M.P. Pileni, J. Phys. Chem. B, 107,2466,(2003)
[60]. J. B. Jackson, N.J. Halas, J. Phys. Chem. B, 105, 2743, (2001)
[61]. Y. Yin, Y. Lu, Y. Sun, Y. Xia, Nano Lett., 2(4), 427, (2002)
[62]. G. S. Métraux, Y.C. Cao, R. Jin. C.A. Mirkin, Nano Lett., 3(4), 519,(2003)
[63]. J. T. G. Overbeek, In Colloidal Dispersions, J. W. Goodwin (ed.), Royal Society of Chemistry, London, p. 1, (1981)
[64]. J. S. Bradley, Clusters and Colloids. From Theory to Applications (Ed.: G. Schmid), VCH, Weinheim, 469-473, (1994)
[65]. G. D. Parfitt, in Dispersion of Powders in Liquids with Special Reference to Pigments, ed. G.D. Parfitt, Applied Science, London, p.1, (1981)
[66]. H. Hirai; Y.Nakao; N.Toshima; K. Adachi, Chem. Lett., 905, (1976)
[67]. I. Pastoriza-Santos and L. M. Marzán, Langmuir, 18, 2888, (2002)
[68]. Z. S. Pillai and P. V. Kamat; J. Phys. Chem. B.,108, 945, (2004)
[69]. J. Liu; R.Xu; A. E.Kaifer, Langmuir, 14, 7337, (1998)
[70]. R. M. Crooks; M.Zhao, L. Sun; V.Chechik, L. K.Yeung, Acc. Chem. Res.,34, 181, (2001)

[71]. B. Bönnemann, and M. Richards, R., Microreview, Eur. J. Inorg. Chem., 2455, (2001)
[72]. J. S. Bradley, Clusters and Colloids. From Theory to Applications, (Ed.: G. Schmid), VCH, Weinheim, 523, (1994)
[73]. M. T. Reetz;W. Helbig, J. Am. Chem. Soc., 116, 7401, (1994)
[74]. M. T. Reetz; M. Winter; R.Breinbauer; T.Them-Albrecht; W.Vogel, J. Chem. Eur., 7, 1084, (2001)
[75]. H. Hirai, Y. Nakao, and N. Toshima, J. Macromol. Sci. Chem., A12, 1117, (1978)
[76]. R. Tausch-Treml, A. Henglein, J. Lilie, Ber. Bunsenges. Phys. Chem., 82, 1335, (1978)
[77]. H. Bönnemann, R. M. Richards, Eur. J. Inorg. Chem., 245, 522, 480, (2001)
[78]. R. A. Salkar, P. Jeevanandam, S.T. Aruna, Y. Koltypin and A. Gedanken, J. Muter. Chem., 9, 1333, (1999)
[79]. M. Gutierrez and A. Henglein, J. Phys. Chem., 91, 6687, (1987)
[80]. T. Fujimoto; S.Terauchi; H.Umehara; I.Kojima; Henderson, Chem. Mater., 13, 1057, (2001)
[81]. K. Philippot; B. C. R.Chaudret, Chimie, 6, 1019, (2003)
[82]. K. Pelzer; O.Vidoni; K.Philippot; B.Chaudret, Adv. Funct. Mat., 13, 2, 1, (2003)
[83]. O. Vidoni; K.Philippot; C.Amiens; B.Chaudret; O. Balmes; J.O. Malm; J.O.Bovin; F.Senocq; M.J. Casanove, Angew. Chem. Int. Ed., 38, 24, 3736, (1999)
[84]. C. Pan; K. Pelzer; K. Philippot; B. Chaudret; F. Dassenoy; P. Lecante; M. J. Casanove, J. Am. Chem. Soc., 123, 31, 7584, (2001)
[85]. K. Pelzer; B. Laleu; F. Lefebvre; K. Philippot; B. Chaudret; J.P. Candy; J.M. Basset, Chem. Mater., 16, 4937, (2004)
[86]. V. Hulea; D. Brunel; A. Galameau; K. Philippot; B. Chaudret; P.J. Kooyman; F. Fajula, Microporous and Mesoporous Materials, 79, 185, (2005)
[87]. K. Pelzer; K.Philippot; B. Chaudret, Anorg. Allg. Chem., 629, 1217, (2003)
[88]. F. Dassenoy; K. Philippot; T.O. Ely; C. Amiens; P. Lecante; E. Snoeck; A. Mosset; M.J. Casanove; B. Chaudret, New J. Chem., 703,(1998)
[89]. E. Ramirez; S. Jansat; K. Philippot; P. Lecante; M. Gomez; A.M. Masdeu-Bultó; B. Chaudret, J. Organomet. Chem., 689, 4601, (2004)
[90]. F. Dassenoy; M.J. Casanove; P. Lecante; M. Verelst; E. Snoeck; A. Mosset; T.O. Ely; C. Amiens; B. Chaudret, J. Chem. Phys., 112, 8137, (2000)
[91]. K. Soulantica; A. Maisonnat; F. Senocq; M.J. Fromen; M.J. Casanove; B. Chaudret, Angew. Chem., Int. Ed., 40, 2983, (2001)
[92]. T. O. Ely; C. Pan; C. Amiens; B.Chaudret; F. Dassenoy; P. Lecante; M.J. Casanove; A. Mosset; M. Respaud; J.M. Broto; J. Chem. Phys. B, 104, 695, (2000)
[93]. F. Dassenoy; M. J. Casanove; P. Lecante; C. Pan; K. Philippot; C. Amiens; B. Chaudret, Phys. Rev. B, 63, 235407, (2001)
[94]. M. J. Hampden-Smith; T. T. Kodas; A. Ludviksson, Chemical Vapor Deposition, Chemistry of Advanced Materials. An Overview, Interrante, L. V.; Hampden-Smith, M. J. Ed.; Wiley-VCH: New York, capitol 5, 143-206, (1998)
[95]. M. T. Reetz and W. Helbig, J. Am. Chem. Soc., 116, 7401, (1994)
[96]. J. A. Becker, R. Schafer, R. Festag, W. Ruland, J.H. Wendorff, J. Pebler, S.A. Quaiser, W. Helbig, and M.T. Reetz, J. Chem. Phys., 103, 2520, (1995)
[97]. D. Cullity and S.R. Stock, Elements of X-ray Diffraction, 3rd edition, Prentice Hall, Upper Saddle River, NJ, (2001)

[98]. L. H. Schwartz, J. B. Cohen, Diffraction from Materials, Springer-Verlag, Berlim, (1987)
[99]. D. Chescoe; P. J. Goodhew; The Operation of the Transmission Electron Microscope. Oxford University Press, Royal Microscopical Society, New York, (1984)
[100]. B. E. P. Beeston; R. W.Horne; R.Markham, Electron Diffraction and Optical Diffraction Techniques. Practical methods in Electron Microscopy, Ed. Glauert, A. N., North Holland, Amsterdam, (1972)
[101]. M. R. Gallego, La Difracción de los Rayos X. Alhambra, Madrid, (1982)
[102]. W. Cai, H. Hofmeister, T. Rainer, Physica E, 11, 339, (2001)
[103]. W. C. Bell, M.L. Myrick, J. Colloid Interf. Sci., 242, 300, (2001)
[104]. G. Schider, J.R. Krenn, W. Gotschy, B. Lamprecht, H. Ditlbacher, A. Leitner, J. Appl. Phys., 90, 3825, (2001)
[105]. J. J. Mock, M. Barbic, D.R. Smith, D.A. Schultz, S. Schultz, J. Chem. Phys., 116, 6755, (2002)
[106]. Y. Liu, C. Liu, L. Chen, Z. Zhang, J. Colloid Interf. Sci., 257, 188, (2003)
[107]. B. J. Berne; R.Pecora, Dynamic Light Scattering; John Wiley: New York, (1975)
[108]. K. Schatztel, J. Mod. Opt., 38, 1849, (1991)
[109]. C. Urban; P.Schurtenberger,J. Colloid Interface Sci., 207(1), 150–158, (1998)
[110]. I. Block; F. Scheffold, Rev. Sci. Instruments, 81, 123107, (2010)
[111]. A. Henglein, J. Phys. Chem., 97, 5457, (1993)
[112]. M. Kerker, The Scattering of Light and Other Electromagnetic Radiation, Academic Press, New York, (1969)
[113]. C. F. Bohren and D.R. Huffman, Adsorption and Scattering of Light by Small Particles, Wiley, New York, (1983)
[114]. U. Kreibeg and M. Vollmer, Optical Properties of Metal Clusters, Vol. 25, Springer-Verlag, Berlin, (1995)
[115]. S. Link and M.A. El-Sayed, Int. Rev. Phys. Chem., 19,409, (2000)
[116]. N. R. Jana, L.Gearheart, C.J.Murphy, J. Phys. Chem. B, 105, 4065,(2001)
[117]. C. J. Johnson, E. Dujardin, S.A. Davis, C.J. Murphy, S. Mann, J. Mater. Chem., 12, 1765, (2002)
[118]. B. Nikoobakht, M. A. El-Sayed, J. Phys. Chem., 107, 3372, (2003)
[119]. A. M. Schwartzberg, T.Y. Oshiro, J.Z. Zhang, T. Huser, C.E. Talley, Anal. Chem., 78, 4732, (2006)
[120]. W. P. Halperin, Rev. Mod. Phys., 58, 533, (1986)
[121]. A. C. Templeton, W. P. Wuelfing, R. W. Murray, Acc. Chem. Res., 33, 27, (2000)
[122]. M. A. El-Sayed, Acc. Chem. Res., 34, 257, (2001)
[123]. D. M. K. Lam, B. W. Rossiter, Sci. Am., 265, 80, (1991)
[124]. S. R. Nicewarner-Pen˜a et al., Science, 294, 137, (2001)
[125]. J. J. Storhoff; R. Elghanian; R.W. Mucic; C.A. Mirkin; R.L.Letsinger, J. Am. Chem. Soc., 120, 1959, (1998)
[126]. K. Glynou; P.C. Loannou; T.K. Christopoulos; V.Syriopoulou, Anal Chem., 75, 4155, (2003)
[127]. M. Q. Zhu; L.Q. Wang; J. Exarhou; A. Li, J. Am. Chem. Soc., 126, 2656, (2004)
[128]. H. Q. Zhao; L. Lin; J.R. Lin; J.A. Tang; M.X. Duan; L. Jiang, J. Nanopart. Res., 3, 321, (2001)
[129]. S. A. Maier et al., Adv. Mater., 13, 1501, (2001)
[130]. P. V. Kamat, J. Phys. Chem. B, 106, 7729, (2002)
[131]. S. Nie, S. R. Emory, Science, 275, 1102, (1997)

[132]. L. A. Dick, A. D. McFarland, C. L. Haynes, R. P. Van Duyne, J. Phys. Chem. B, 106, 853, (2002)
[133]. M. P. Pileni, Adv. Funct. Mater., 11, 323, (2001)
[134]. L.M. Liz-Marzán; P. Mulvaney, New J. Chem., 1285, (1998)
[135]. M. P. Pileni, New J. Chem., 22, 693, (1998)
[136]. G. Schmid, M. Bäumle, M. Bayer, Angew. Chem. Int. Ed., 39, 182, (2000)
[137]. J. J. Pietron; J.F. Hicks; R.W. Murray, J. Am. Chem. Soc., 121, 5565, (1999)
[138]. G. M. Chow and K.E. Gonsalves, Nanotechnology, Molecularly Designed Materials, Ed.ACS Symposium series 622, Am. Chem. Soc., Washington DC., (1996)
[139]. M. M. Maye; Y. Lou; C. J. Zhong, Langmuir, 16, 7520, (2000)
[140]. M. Zhao; R. M. Crooks, Adv. Mat., 11, 217, (1999)
[141]. R. F. Service, Science, 285, 682, (1999)
[142]. M. Watanabe; S. Motto, J. Electroanal. Chem., 60, 267, 273,(1975)
[143]. J. O'M. Bockris; H. Wroblowa, J. Electroanal. Chem., 7, 428, (1964)
[144]. D. J. Aiken; R. G. Finke, J. Mol. Catal. A, 145, 1-44, (1999)
[145]. H. Bönnemann; R.M. Richards, Eur. J. Inorg. Chem., 2455, (2001)
[146]. A. Roucoux; J. Schulz; H. Patin, Chem. Rev., 102, 3757, (2002)
[147]. A. Grijalva, R. Urbina, J. Silva, M. Borja, F. Barraza and A. Amarillas, Physica E, 27, 104,(2005)
[148]. A. Grijalva, R. Urbina, J. Silva, M. Borja, F. Barraza, A. Amarillas, Physica E, 25, 438, (2005)
[149]. M. Popa, T. Pradell, D. Crespo, J. M. Calderón Moreno, Colloids and Surfaces A, Physicochem. Eng. Aspects,303, 184, (2007)
[150]. A. L. González and C. Noguez. Optical properties of silver nanoparticles. Physica Status Solidi C, 4(11), 4118, (2007)
[151]. W. R. Glomm, J. Dispersion Sci. Technol., 26, 389, (2005)
[152]. E. Hao, G. C. Schatz, J. T. Hupp, J. Fluoresc., 14, 331, (2004)
[153]. K. L. Kelly, E. Coronado, L. L. Zhao, G. C. Schatz, J. Phys. Chem. B, 107, 668, (2003)
[154]. V. Germain, A. Brioude, D. Ingert, M. P. Pileni, J. Chem. Phys., 122, 124, 707, (2005)
[155]. A. Brioude, M. P. Pileni, J. Phys. Chem. B, 22, 32, (2006)
[156]. L. M. Liz-Marzán, Langmuir, 109, 21 159, (2005)
[157]. I. O. Sosa, C. Noguez, R. Barrera, J. Phys. Chem. B, 107, 6269, (2003)
[158]. M. Maillard, S. Gieorgio, M. P. Pileni, Adv. Mater., 14, 1084, (2002)
[159]. C. Salzemann, J. Urban, I. Lisiecki, M. P. Pileni, Adv. Funct. Mater., 15, 1277, (2005)
[160]. B. Nikoobakht, M. A. El-Sayed, Chem. Mater., 15, 1957, (2003)
[161]. Y. Xia, P. D. Yang, Y.G. Sun, Y.Y. Wu, B. Mayers, B. Gates, Y.D. Yin, F. Kim, Y.Q. Yan, Adv. Mater., 15, 353, (2003)
[162]. J. Pérez-Juste, L. M. Liz-Marzán, S. Carnie, D. Y. C. Chan, P. Mulvaney, Adv. Funct. Mater., 14, 571, (2004)
[163]. N. R. Jana, L. Gearheart, C. J. Murphy, Chem. Commun., 617, (2001)
[164]. X. Dong, X. Ji, J. Jing, M. Li, J. Li, and W. Yang, J. Phys. Chem. C, 114, 2070, (2010)
[165]. C. Xue, G.S. Métraux, J. E. Millstone, and C. A. Mirkin, J. Am. Chem. Soc., 130, 8337, (2008)
[166]. A. J. Haes, J. Zhao, S. Zou, C. S. Own, L. D. Marks, G. C. Schatz, R. P. Van Duyne, J. Phys. Chem. B, 109, 11 158, (2005)

[167]. X. Zhang, E. M. Hicks, J. Zhao, G. C. Schatz, R. P. Van Duyne, Nano Lett., 5, 1503, (2005)
[168]. S. Kramer, R.R. Fuierer, C.B. Gorman, Chem. Rev., 103, 4367, (2003)
[169]. C. L. Haynes, R.P. Van Duyne, J. Phys. Chem. B, 105, 5599, (2001)
[170]. W. Y. Huang, W. Qian, M.A. El-Sayed, J. Phys. Chem. B, 109, 18881, (2005)
[171]. Y. Xiong, I. Washio, J. Chen, M. Sadilek, Y. Xia, Angew. Chem. Int. Ed., 46, 4917, (2007)
[172]. P. Fayet, F. Granzer, G. Hegenbart, E. Meisar, B. Pischel, L. Waste, Phys. Rev. Lett., 55, 3002, (1985)
[173]. V. Germain, J. Li, D. Ingert, Z. L. Wang, M. P. Pileni, J. Phys. Chem. B, 107, 8717, (2003)
[174]. J. M. Calderon-Moreno, E. R. Camargo, Catalysis Today, 78, 539, (2003)
[175]. W. Yan, V. Petkov, S.M Mahurin, S.H. Overbury, S. Dai, Catalysis Commun., 6, 404, (2005)
[176]. J. Wang, G. D. Liu, M. H. Engelhard, Y.H. Lin, Analytical Chem.,78, 6974, (2006)
[177]. A. H. Yuwono, Y. Zhang, J. Wang, X. H. Zhang, H. M. Fan, Chem. Mater., 18, 5876, (2006)
[178]. S. B. Hamouda, Q. T. Nguyen, D. Langevin, C. Chappey, S. Roudesli, React. Funct. Polym., 67, 893, (2007)
[179]. B. Alexandre, S. Marais, D. Langevin, P. Médéric, T. Aubry, Desalination,199, 164, (2006)
[180]. A. Heilmann, A. Kiesow, M. Gruner, U. Kreibig, Thin Solid Films, 344, 175, (1999)
[181]. D. K. Chae, S.G. Oh, B.C. Kim, J. Polym. Sci. B: Polym. Phys., 42, 790, (2004)
[182]. S. T. Dubas, P. Kumlangdudsana, P. Potiyaraj, Colloids Surfaces A: Physico-chem. Eng. Aspects., 289, 105, (2006)
[183]. R. D. Deshmukh, R. J. Composto, Chem. Mater., 19, 745, (2007)
[184]. Y. Shiraishi, N. Toshima, J. Mol. Catal. A: Chem., 141, 187, (1999)
[185]. L. Rivas, S. Sanchez-Cortes, J.V. Garcia-Ramos, G. Morcillo, Langmuir, 17, 574, (2001)
[186]. Y. S. Kang, S.W. Kang, H.S. Kim, J.H. Kim, J. Won, C.K. Kim, Adv. Mater., 19, 475, (2007)
[187]. N. Romeo, G. Sberveglieri and L. Tarricane, Appl Phys. Lett., 32, 807, (1978)
[188]. D. B. Fraser and H. Melchior, J. Applied Phys., 43, 3120, (1972)
[189]. S. Fujita, Y. Kawakami and S. Fujita, J. Cryst. Growth, 164, 196, (1996)
[190]. P. C. Dorsey, P. Lubitz, D. B. Chirisey and J. S. Horwitz, J. Appl. Phys., 79, 6338, (1996)
[191]. F. Cheng, Z. Peng, C. Liao, Z. Xu, S. Gao, C. Yan, D. Wang and J. Wang, Solid State Commun., 107, 471, (1998)
[192]. N. R. Pawaskar, C. A. Menezes and A. P. B. Sinha, J. Electrochem. Soc., 124, 743, (1977)
[193]. H. S. Potdar, R. I. Hegade, S. Badrinarayan and N. R. Pawaskar, Solar Energy Mater, 6, 183, (1982)
[194]. D. T. Amm, D. J. Johnson, T. Laursen and S. K. Gupta, Applied Phys. Lett., 61, 522, (1992)
[195]. I. S. Mulla, H. S. Soni, V. J. Rao and A. P. B. Sinha, J. Mater Sci., 21, 1288, (1986)
[196]. S. D. Sathaye, K. R. Patil, D. V. Paranjape, A. Mitra, S. W. Awate and A. B. Mandale, Langmuir, 16, 3487, (2000)

[197]. S. Sakka, "Science in Sol-Gel Method" Chapter 6,Agune, Tokyo, (1998)
[198]. J. Livage, M. Henry and C. Sanchez, Progress Solid State Chem., 8, 259, (1988)
[199]. H. Yokoi, S. Kawata, M. Iwaizumi, J. Am. Chem. Soc., 108, 3358, (1986)
[200]. Y. Matsuo, K. Hatase, Y. Sugie, Chem. Mater., 10, 2266, (1998)
[201]. A. Novakova, E. Smirnov, T. Gendler, J. Magn. Mater., 300, 354, (2006)
[202]. C. H. Lu, S. Saha, J. Sol-Gel Sc. Techn., 20, 27, (2001)
[203]. T. Ogi, L.B. Modesto-Lopez, F. Iskandar and K. Okuyama, Colloids Surf., A, 297, 71, (2007)
[204]. T. Komikado, A. Inoue, K. Masuda, T. Ando and S. Umegaki, Thin Solid Films, 515, 3887, (2007)
[205]. H. C. Lee, T. W. Lee, T.H. Kim and O.O. Park, Thin Solid Films, 458, 9, (2004)
[206]. H. Y. Fan, K. Yang, D.M. Boye, T. Sigmon, K.J. Malloy, H.F. Xu, G.P. Lopez and C.J. Brinker, Science, 304, 567, (2004)
[207]. R. S. Krishnan, M. E. Mackay, P.M. Duxbury, A. Pastor, C.J. Hawker, B. Van Horn, S. Asokan and M.S. Wong, Nano Lett., **7**, 484, (2007)
[208]. D. M. DeLongchamp, M. Kastantin and P.T. Hammond, Chem. Mater., 15, 1575, (2003)
[209]. S. Mintova and T. Bein, Adv. Mater., 13, 1880, (2001)
[210]. R. C. Jin, Y.W. Cao, C.A. Mirkin, K.L. Kelly, G.C. Schatz, J.G. Zheng, Science, 294,1901, (2001)
[211]. C. Xue; Z. Li and C. A. Mirkin, Small, 1, 513, (2005)
[212]. Y. Cheng, C. Wang, Z. Ma, and Z. Su, Nanotechnology, 18, 325602, (2007)
[213]. A. Gautam, S. Ram, Materials Chemistry and Physics, 119, 266, (2010)
[214]. A. Slistan-Grijalva, R. Herrera-Urbina, J.F. Rivas-Silva, M. Avalos Borja, F.F. Castillón-Barraza, A. Posada-Amarillas, Physica E, 27, 104, (2005)
[215]. L. Marzán, M. Giersig, P. Mulvaney, Langmuir, 12,4329, (1996)
[216]. L. Marzán, P. Mulvaney, J. Phys. Chem. B, 107, 7312, (2003)
[217]. W. Stöber, A. Fink, E. Bohn, J. Colloids Interface Sci., 26,62, (1968)
[218]. Y. Kobayashi, H. Katakami, E. Mine, D. Nagao, M. Konno, L. Marzán, Colloids Interface Sci., 283,392, (2005)
[219]. Y. Kobayashi, V. Salgueirino-Maceira, L. Marzán, Chem. Mater., 13, 1630, (2001)
[220]. J. B. Jackson, N. J. Halas, J. Phys. Chem. B, 105, 2743, (2001)
[221]. X. Ye, Y. Zhou, J. Chen, Y. Sun, Appl. Surf. Sci., 253, 6264, (2007)
[222]. L. H. Qiu, V.G. Pol, J.M. Calderon-Moreno, A. Gedanken, Ultrason. Sono-chem., 12, 243, (2005)
[223]. V. G. Pol, M. Motiei, A. Gedanken, J. M. Calderon-Moreno, Y. Mastai, Chem. Mater., 15,1378, (2003)
[224]. Q. L. Li, H.L. Li, V.G. Pol, I. Bruckental, Y. Koltypin, I.Nowik, J.M. Calderón-Moreno, A. Gedanken, New J. Chem., 27, 1194, (2003)
[225]. H. L. Li, R.H. Wang, Q. Hong, L.W. Chen, Z.Y. Zhong, Y. Koltypin, J.M. Cal-derón- Moreno, A. Gedanken, Langmuir, 20, 8352, (2004)
[226]. V. G. Pol, S.V. Pol, Y. Gofer, J.M. Calderón Moreno, A. Gedanken, J. Mater. Chem., 14, 966, (2004)
[227]. V. G. Pol, D.N. Srivastava, O. Palchik, V. Palchik, M.A. Slifkin, A.M. Weiss, A. Gedanken, Langmuir, 18(8), 3352, (2002)
[228]. V. G. Pol, J.M. Calderón-Moreno, A. Gedanken, Chem. Mater., 15(5), 1111, (2003)
[229]. V. G. Pol, G. Wildermuth, J. Felsche, A. Gedanken, J.M. Calderón-Moreno, J. Nanosci. Nanotechnol., 5(6), 975, (2005)

[230]. D. Chen, L. Li, J. Liu, S. Qi, F. Tang, X. Ren, W. Wu, J. Ren, L. Zhang, Colloids Interface Sci., 308, 351, (2007)
[231]. V. Torres, M. Popa, D. Crespo, J.M. Calderon-Moreno, Microelectron. Eng., 84,1665, (2007)
[232]. C. N. R.Rao; B.Raveau, Transition metal oxides; VCH: New York, (1995)
[233]. B. O'Regan; M. Grätzel, Nature, 353, 737, (1991)
[234]. A. Hagfeldt; M. Grätzel, Acc. Chem. Res., 33, 269, (2000)
[235]. M. R. Hoffmann; S. T. Martin; W. Choi; D. W. Bahnemann, Chem. Rev., 95, 69, (1995)
[236]. S. Y. Huang; L. Kavan; I. Exnar; M. Grätzel, J. Electrochem. Soc.,142, 142, (1995)
[237]. R. W. Fessenden and P. V. Kamat, J. Phys. Chem., 99, 12902, (1995),
[238]. T. Wu, G. Liu, J. Zhao, H. Hidaka, and N. Serpone, J. Phys. Chem. B, 102, 5845, (1998)
[239]. M. M. Mohamed, T. M. Salama, T. Yamaguchi, Colloids and Surfaces A: Physicochem.Eng. Aspects, 207, 25, (2002)
[240]. S. H. Lim, N. Phonthammachai, S. S. Pramana, and T. J. White, Langmuir, 24, 6226, (2008)
[241]. N. N. Martínez, G. A. M. Castañón, A. A. Piña, F. M. Gutierrez, J. R. M. Mendoza and F. Ruiz; Nanotechnology, 19, 8, (2008)
[242]. J. Chen, M. Yao, and X. Wang, J. Nanopart. Res., 10, 163, (2008)
[243]. G. Fu, P. S. Vary, and C. T. Lin, J. Phys. Chem. B, 109, 8889, (2005)
[244]. P. Wilhelm, and D. Stephan, J. Colloid Interface Sci., 293, 88, (2006)
[245]. P. Wilhelm, and D. Stephan, J. Photochem. Photobiol. A, 185, 19, (2007)
[246]. H. Nakamura, M. Ishii, A. Tsukigase, M. Harada, H. Nakano, Langmuir, 22, 1268, (2006)
[247]. H. Nakamura, M. Ishii, A. Tsukigase, M. Harada, H. Nakano, Langmuir, 21, 8918, (2005)
[248]. M. Holgado, A. Cintas, M. Ibisate, C. J. Serna, C. López, F. Meseguer, J. Colloid Interface Sci., 229, 6, (2000)
[249]. H. Tang, C. H. Yu, W. Oduoro, H. He, and S. C. Tsang, Langmuir Letters, 24, 5, 1587, (2008)
[250]. Y. Q. Li, S. Y. Fu, Y. Yang, Y. W. Mai, Chem. Mater., 20, 2637, (2008)
[251]. T. Trung, W. J. Cho, C. S. Ha, Mater. Lett., 57, 2746, (2003)
[252]. T. Sugimoto, X. Zhou, A. Muramatsu, J. Colloid Interface Sci., 252, 339, (2002)
[253]. P. Arnal, R.J.P. Corriu, D. Leclercq, P.H. Mutin, A. Vioux, Chem. Mater., 9, 694, (1997)
[254]. C. S. Kim, B. K. Moon, J. H. Park, S. T. Chung, S. M. Son, J. Cryst. Growth, 254, 405, (2003)
[255]. A. M. Ruiz, G. Sakai, A. Cornet, K. Shimanoe, J. R. Morante, N. Yamazoe, Sens. Actuators B: Chem., 103, 312, (2004)
[256]. J. N. Nian, H. Teng, J. Phys. Chem. B, 110, 4193, (2006)
[257]. Y. V. Kolenko, B. R. Churagulov, M. Kunst, L. Mazerolles, C. Colbeau-Justin, Appl. Catal. B: Environ., 54, 51, (2004)
[258]. J. C. Flores, Victor Torres, Monica Popa, Daniel Crespo and Jose M. Calderón-Moreno, Colloids and Surfaces A: Physicochemical Eng. Aspects, 330, 86-90, (2008)
[259]. M. Popa, J.M. Calderon-Moreno, L. Popescu, R. Torecillas, M. Kakihana, J. Non-Cryst. Solids, 297, 290, (2002)

[260]. S. Shibata, K. Aoki, T. Yano, M. Yamane, J. Sol–Gel Sci. Technol., 11, 279, (1998)
[261]. K. H. Johnson, S.V. Pepper, J. Appl. Phys., 53, 6634, (1982)
[262]. K. K. Caswell, C.M. Bender, C.J. Murphy, Nano Lett., 3 667, (2003)
[263]. K. C. Song and S.E. Pratsinis, J. American Ceram. Soc., 84, 92, (2001)
[264]. Y. C. Lee, Y. J. Jung, P. Y. Park and K. H. Ko, J. of Sol-Gel Sci. and Tech., 30, 21, (2004)
[265]. C. J. Barbe, F. Arendse, P. Comte, M. Jirousek, F. Lenzmann, V. Shklover, and M. Gratzel, J. Am. Ceram. Soc., 80(12), 3157, (1997)
[266]. A. Sclafani, L. Palmisano, and E. Davi, J. Photochem. Photobio. A: Chem., 56, 113, (1991)
[267]. R. Zanella; S.Giorgio; R. C.Henry; C.Louis, J. Phys. Chem. B, 106, 7634, (2002)
[268]. J. C. Flores, V. Torres, M. Popa, D. Crespo, J.M. Calderón-Moreno, Journal of Non-Crystalline Solids, 354, 5435, (2008)
[269]. C. M. Ho, S. K. W. Yau, C.N. Lok, M.H. So, and C.M. Che, J. Chem. Asian, 5, 285, (2010)